LASER MACHINING OF CERAMICS AND METALS; DEVELOPMENT OF A LASER LATHE

by

James Frederic Bredt

SUBMITTED IN PARTIAL FULFILLMENT
OF THE REQUIREMENTS OF THE
DEGREE OF

MASTER OF SCIENCE
IN MECHANICAL ENGINEERING

at the

MASSACHUSETTES INSTITUTE OF TECHNOLOGY

February, 1987

The author hereby grants to M.I.T. permission to reproduce and to distribute copies of the thesis document in whole or in part.

Signature of Author...
Department of Mechanical Engingeering
January 15, 1986

Certified by..
Professor George Chryssolouris
Thesis Supervisor

Accepted by...
Professor Ain A. Sonin, Chairman
Departmental Commitee on Graduate Students
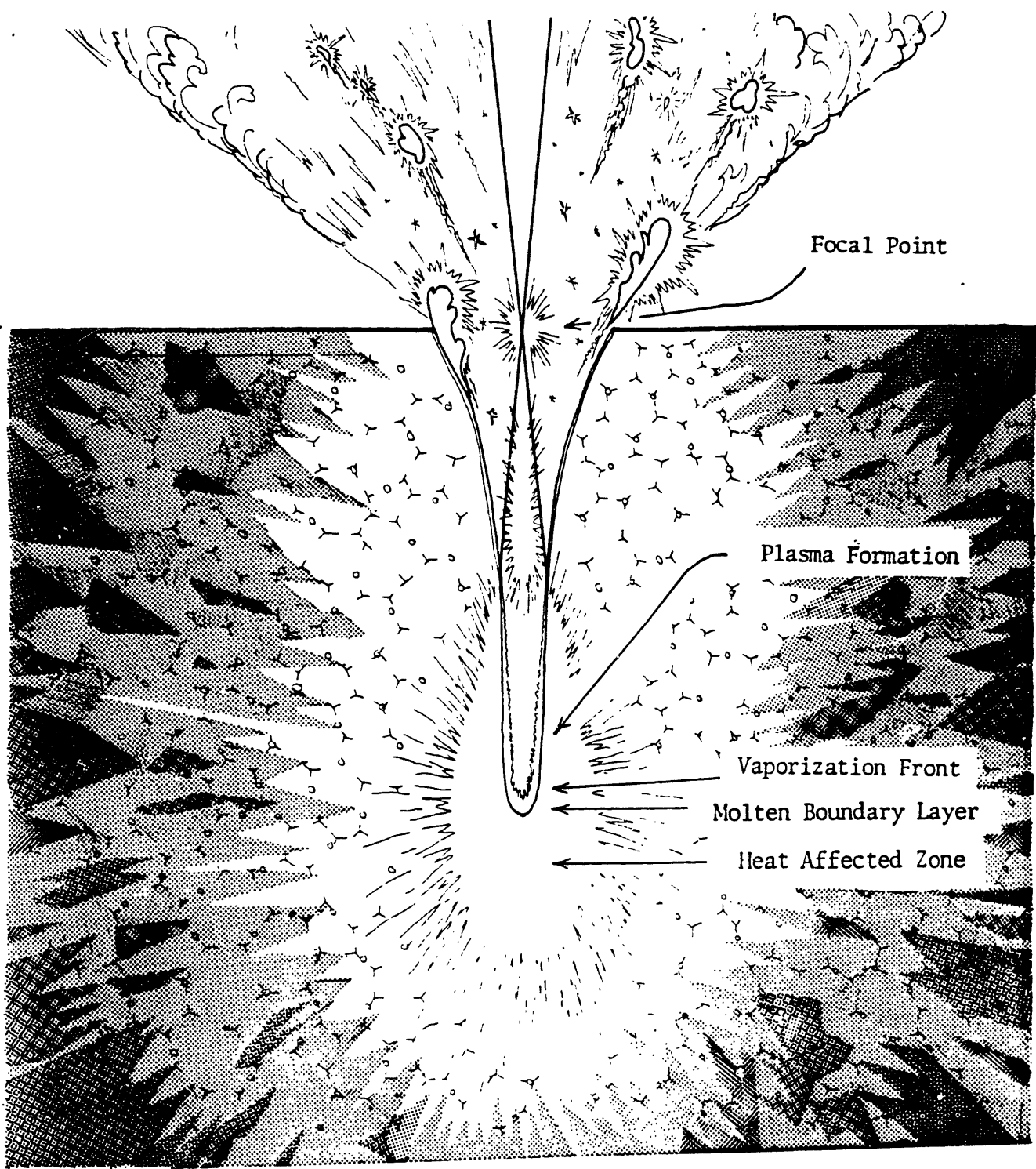
Focal Point

Plasma Formation

Vaporization Front

Molten Boundary Layer

Heat Affected Zone

Table of Contents

1 Abstract

A new machine tool concept has been developed at the MIT Laboratory for Manufacturing and Productivity. The cutting tool consists of a pair of converging laser beams which section large pieces of material from the workpiece. Since material is removed from the workpiece with is substantially unheated by the laser, the energy efficiency of the process is increased by a factor of ten to one hundred beyond what is obtainable by direct laser ablation. A prototype laser lathe was constructed based upon this concept.

The purpose of this thesis is to address the phenomenon of laser cutting of various engineering materials to optimize this cutting tool. An extensive experimental program culminated in the design of a laser cutting tool especially suited to this concept. Various analytical models from the literature dealing with various aspects of laser materials processing were used to derive an approximate analytical model for laser blind cutting.

It was concluded from this research that the converging beam laser cutting tool is a feasible concept, and is particularly well suited to materials which are mechanically very hard and difficult to machine using conventional methods. Data is reported for cutting of alumina, silicon carbide, silicon nitride, mild steel, AMS 5613 stainless steel, 303 stainless steel, invar, inconel, monel, nickel, titanium and molybdenum.

2 . List of Figures

oxidizing asist gas.

Figure 34. Cut profiles in mild steel comparing differences between argon, oxygen, and compressed air assist gases. Conditions for all three: P = 1000 W, V = 10 cm/sec, d = 0.016 cm, n = 50 passes.

Figure 35. D/d vs. ED/d for mild steel at various powers. Conditions: V = 10 cm/sec, d = 0.016 cm, Assist = Air, 100 psi.

Figure 36. D/d vs. ED/d for mild steel at various powers. Conditions: V = 5 cm/sec, d = 0.016 cm, Assist = Air, 100 psi.

Figure 37. D/d vs. ED/d for mild steel at various powers. Conditions: V = 2 cm/sec, d = 0.016 cm, Assist = Air, 100 psi.

Figure 38. D/d vs. ED/d for 303 stainless steel at various surface speeds. Conditions: P = 1000 W, d = .016 cm, Assist = Argon, 500 psi.

Figure 39. D/d vs. Surface speed for 303 stainless steel for various energy densities. Conditions: P = 1000 W, d = .016 cm, Assist = Argon, 500 psi.

Figure 40. Experimental configuration for calorimetry tests performed of August 1, 1986.

Figure 41. Temperature rise, Δ T, vs. Laser energy, P x t, in 50 g mild steel specimens. Conditions: P = 1000 W, V = 10 cm/sec, d = .016 cm, Assist = Argon, 500 psi.

3 . Nomenclature

α_λ = Absorbtion coefficient for radiation $[cm^{-1}]$

a_0 = Diameter of the unfocused laser output beam

$\alpha = \frac{k}{\rho C_p}$; Thermal diffusivity

α_θ = Coefficient of thermal expansion

$ci(x)$ = cosine integral function $= -\int_x^\infty \frac{cos(t)}{t} \partial t$

d = Focused spot size

D = Depth of kerf

$\partial(\ )$ = Differential operator

d_{eff} = Effective spot diameter a depth D below focal point

δ = Depth of absorbing region below momentary laser ablation surface

ΔD = Increase in depth of cut on a given laser scan

ΔED = Increment of energy applied per unit area of laser trace

E = Young's modulus

$ED = \frac{P\tau}{\pi r^2}$ = Energy Density in stationary frame

$ED = \frac{nP}{dV}$ = Energy density in moving frame

ε = Strain component

ε_λ = Surface emissivity

f = Focal length of the objective lens.

$g = g(z)$ = Radius of hole at depth z

$H = \rho \, C_p \left(T_s - T_0 \right) + L$ = Enthalpy of removal by laser ablation for a given material

h = Thickness of a volume element in a finite-difference model.

η = Cutting efficiency factor $= \frac{HD}{ED}$

i, j, k = Unit vectors in x, y, and z directions, respectively

$J(\xi, y)$ = Power density of focused spot

J_0 = Laser intensity at the center of the focal point

J_{eff} = Effective power density resolved at the bottom of a deep kerf.

$k(T)$ = Thermal conductivity

K_0 = Modified Bessel function of second kind of order zero

L_m = Latent heat of fusion

L_v = Latent heat of vaporization

MRR_k = Kerf material removal rate

MRR_r = Ring material removal rate

MRR_m = Material removal rate for milling

MRR_{total} = Material removal rate for an entire machining job

n = Number of laser scans to form kerf

P = Laser power

$Q(x,t)$ = Heating at depth x in medium

q = Number of rings cut during operation

$r = \sqrt{x^2 + y^2 + z^2}$

$\rho C_p(T)$ = Density x Specific heat = Specific heat/unit volume

R_i = Outer radius of ring being cut

R = Surface reflectivity

r_0 = Radius of the focal point

R_o = Initial radius of the workpiece

R_x = Average radius of the kerf

s = Thickness of liquid film

$S(r,\phi,z)$ = Heat function, $\int_{T_0}^{T(r(\phi,z)} k(T)\, \partial T$

$s(\xi,y)$ = Ablation surface beneath laser spot

$s_+(y)$ = Cold kerf surface in advance of laser spot

$s_-(y)$ = Cold kerf surface behind laser spot

$si(x)$ = sine integral function = $-\int_x^\infty \frac{sin(t)}{t}\, \partial t$

σ = Stress component

σ_λ = Stefan-Boltzmann coefficient

$T = T(\xi,y,z)$ = Temperature distribution

t_i = Time to form a ring in a turning operation

$T_{i,j}$ = Temperature of the i,j-th element in numerical calculation

T_m = Melting temperature

T_0 = Initial ambient temperature

$T_{s(\xi,y)}$ = The temperature at the ablation surface or any isothermal surface given

by $s(\xi, y)$

T_v = Vaporization temperature

Δt = Time increment of a numerical calculation

τ = Laser intertaction time over a given stationary spot on the workpiece

V = Velocity of the medium with respect to the laser spot

V_i = Volume of a given ring $= 2\pi D_a D_r \left(R_i - \frac{D_r}{2} \right)$

w = Width of kerf

$\xi = x - Vt$; Quasi-stationary frame.

y_i = Depth of the i-th element below the instantaneous ablation front.

y_w = Half-width of weld

z = Depth of penetration

Z = Position of the ablation front in one-dimensional frame.

z_w = Depth of weld

1. INTRODUCTION

Since the invention of the laser in 1960, it has found increasing use in materials processing. This versatile tool is used for welding, cutting, heat treating, crystal growing, material synthesis, and cladding. The development of high power systems over the last decade has improved the laser's ability to perform relatively large scale machining operations. The introduction of new materials such as composites and synthetic ceramics to many industrial applications requires the development of a machining tool which can be used in manufacturing with these materials. The laser offers great potential for machining advanced materials, particularly ceramics, because of its properties as a material removal tool.

1.1 A Laser Cutting Tool

Since the laser heats the workpiece with a focused beam of light, there is no tool wear, and the lack of contact forces eliminates machine tool deflections and vibrations. The lack of inertia or forces in the laser beam means that it is easily adaptible to automation. Despite these advantages, the laser has been severely limited as a material removal tool because of the poor energy efficiency of the process, and the difficulty of producing three dimensional shapes.

In order to overcome this difficulty, a new laser machining method has been developed by Cryssolouris et. al. (1986) which uses two intersecting laser beams to cut a three dimensional shape by sectioning large chips from the workpiece, thereby increasing the energy efficiency of the process by a few orders of magnitude. This cutting tool has been used as the basis for designing a lathe. The difference between turning with this laser cutting tool and turning with a conventional cutting tool are illustrated in figure [1].

Two laser beams are dircted along two different axes of the workpiece producing two converging cuts. When the cuts intersect, a solid portion of the worpkiece is removed. When this cutting tool is used in a lathe, the workpiece is attatched to a lathe spindle, and the chip produced is a solid ring of material. After one ring is cut, a new surface is exposed in which new laser cuts may be made to cut a new ring. The desired contour
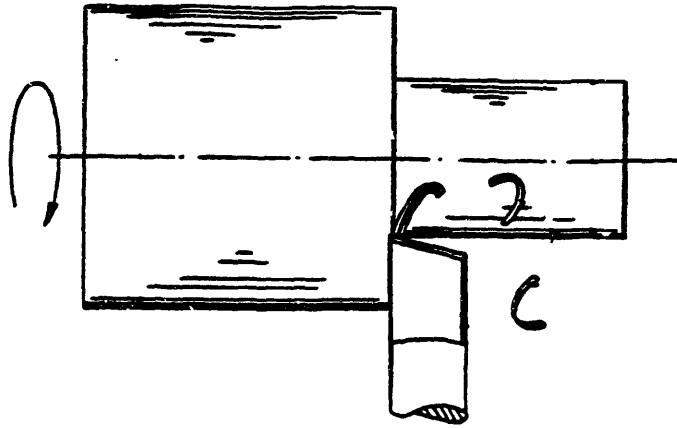
a.) Conventional Turning
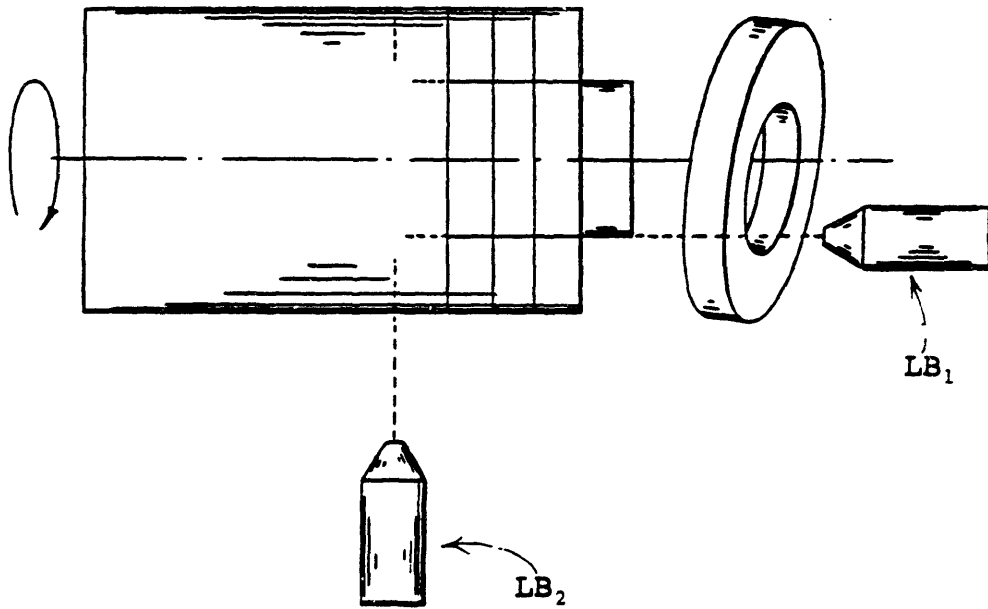
b.) Laser Turning

Figure 1. Comparison Between Conventional and Laser Turning.

is produced by the successive removal of rings. The same cutting tool may be used for milling, as shown in figure [2]. Figure [3] shows how this concept may be used for threading.

LB$_1$: Laser Beam 1
LB$_2$: Laser Beam 2
s : Material Feed Rate
d : Depth of Cut
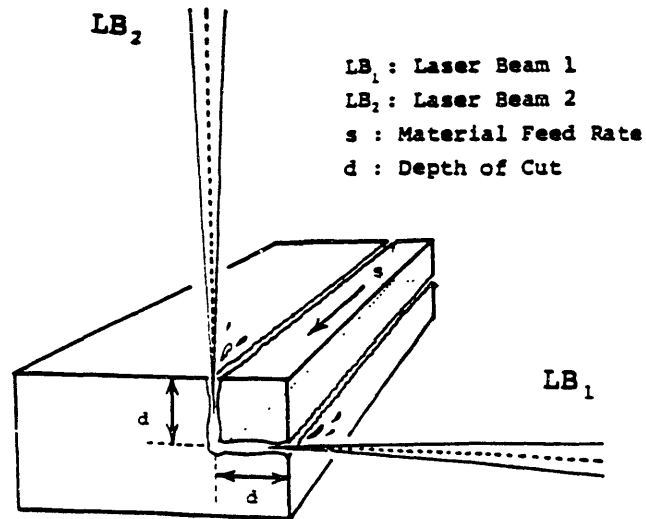
Figure 2. Laser beam configuration for milling.
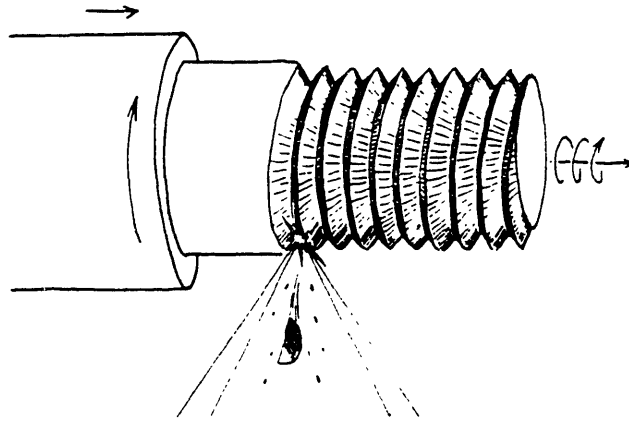
Figure 3. Thread cutting using intersecting laser beams.

Using this concept, large volumes of material can be removed by dissipating energy only in the deep, narrow kerfs. In this way, the energy efficiency as well as the material removal rate of the cutting tool is ten to one hundred times higher than conventional laser machining methods, in which material is removed from the workpiece only in molten or vaporized form.

Conventional laser cutting involves the cutting of sheets, usually steel. Very complex two-dimensional shapes can be cut relatively quickly from sheets up to 3/8 in. thick. In this process, the laser is used first to drill a hole entirely through the workpiece, and then the laser is translated along the surface of the sheet until the shape is cut. These cuts are extremely reliable, although the accuracy of the cut is limited due to the width of the kerf. Laser cut kerfs are typically .01 to .02 inches (200 to 500 μm) across, and the dimensional tolerance is on that scale, in spite of the fact that the positioning systems used to produce the cuts typically have accuracies on the order of .0001 in.

Three different forms of laser cutting have been distinguished by virtue of differences in material removal:

In laser sublimation cutting, the focused beam heats the material to its evaporation temperature and a jet of inert gas can be used to carry the vapor out of the cut. Three materials which have been found to behave in this way are acrylic, silicon nitride, and quartz.

In laser fusion cutting, a stronger inert gas jet is used to blow molten material out of the kerf. The material in the kerf must be heated only above its melting point; however, this form of cutting is generally more difficult than sublimation cutting because molten material has a tendency to resolidify within the kerf. Materials which have been found to behave in this way are metals and most ceramics, as well as fiber-resin and metal-matrix composites.

Laser gas cutting uses a chemically active gas which reacts exothermally with the material as soon as the ignition temperature is reached. Material removal during reactive gas assisted laser cutting takes place by the ejection of molten material and by

evaporation. Ferrous alloys and resin-based composites can be cut using this method.

The laser cutting tool studied in this thesis is different from conventional cutting processes by virtue of is ability to cut three dimensional forms from a large workpiece. To do this, the tool must make cuts which do not entirely penetrate the workpiece. These cuts are referred to as "blind" cuts and the difference between them and conventional "through" cuts is illustrated in figure [4]. In through cutting, the thickness of the workpiece is the depth of cut. The laser penetrates the workpiece, and material is removed from the leading edge of the kerf and thrown out the bottom of the sheet by a vertical gas jet. In blind cutting, material is removed from two fronts: a cutting front along the leading edge of the kerf, and a drilling front on the bottom of the kerf. Material removed from these two fronts must exit the workpiece from the top of the kerf. As a result, blind cutting is difficult to accomplish using a conventional gas jet configuration. A specialized cutting head is required, and part of this thesis was the design of a cutting head for blind cutting.

1.2 The Laser Machining Process

A description of the physics of lasers is beyond the scope of this thesis. The lasers used for macromachining applications fall into a few small categories, and their design has been optimized to the point where the laser unit can be simply regarded as a tool with certain functional properties.

A laser is a device which generates a beam of light by a process called stimulated emission. The light emitted by a laser is coherent. This means that the light waves in the beam all travel in one direction and in phase with one another. The light in a laser beam is usually monochromatic, or at least restricted to a small number of narrow lines.

The light from a laser is not emitted by a hot body. The type of emission is similar to a radio antenna; energy is fed into the antenna and emitted as radiation without having been converted to heat. The emission is characteristic of the properties of the antenna, and the concept of black-body temperature does not apply. A laser is capable of heating a body to any temperature without limit. For this reason, they are used to heat plasmas in fusion experiments.
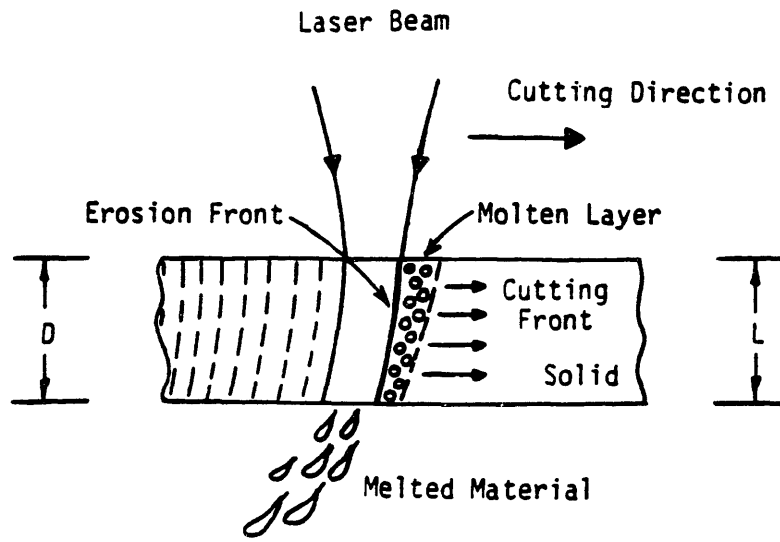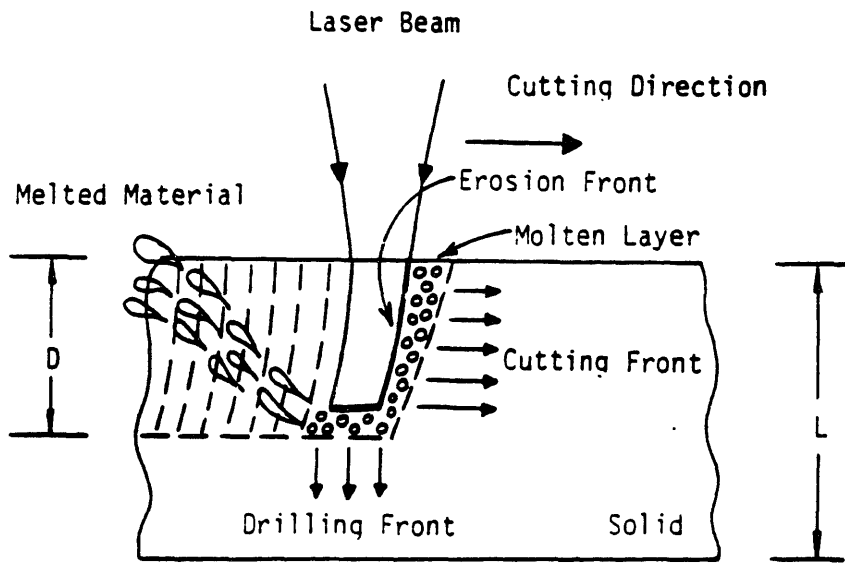
Figure 4. Comparison between "through" and "blind" cutting

The coherence of a laser beam allows it to be focused by a lens to a spot size which is limited only by the wavelength of the light. In ordinary machining operations, a 1000 watt laser can be focused to a spot 0.007 in. across. In laser drilling, pulses of 50 kW peak power are directed to the spot. This concentration of power is enough to vaporize any material. Different materials processing operations are performed with different magnitues of laser intensity. The approximate ranges of laser power and interaction times are shown in figure [5]
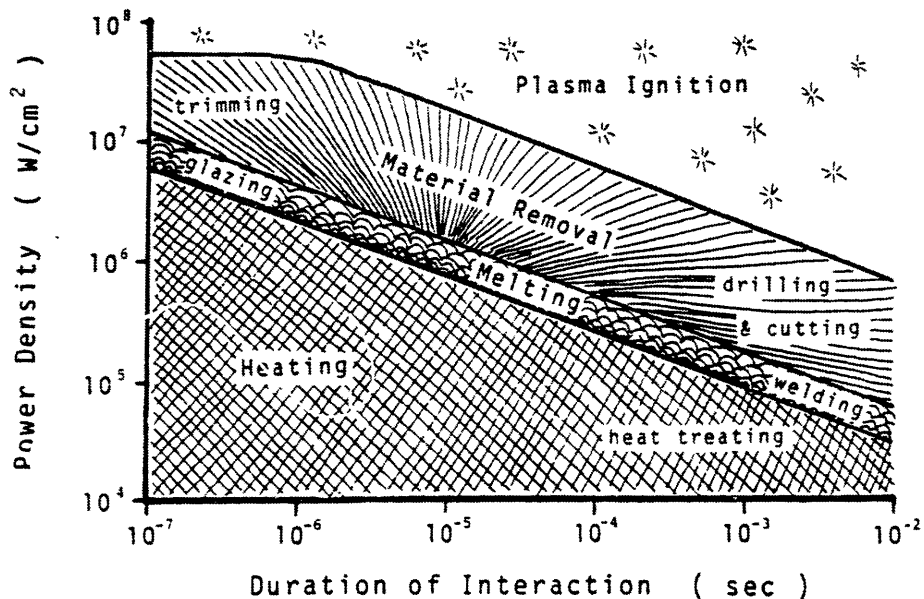
Figure 5. Power densities and interaction times for various types of laser machining.

The lasers which are used for large-scale materials processing operations fall into two major categories: gas lasers and solid-state lasers. These lasers must have a relatively high output power; a 100-watt laser is considered very modest for machining, and a laser with a kilowatt output is common.

The dominant gas laser used in the industry is the CO_2 laser. This laser uses a high-voltage gas discharge in a resonant cavity to produce infrared light with a wavelength of 10.6μm. This laser is capable of producing a continuous output beam, called "continuous-wave" (CW), as well as a pulsed output. A typical CO_2 laser used in industrial applications has an output power of 500 to 1500 W, and lasers as powerful as

25 kW are in use. About 5 - 8 % of the electric power consumed by a CO_2 laser is converted into laser light, making CO_2 lasers the most efficient lasers in the industry. This thesis focused exclusively on optimizing blind cutting with CO_2 lasers.

Solid-state lasers produce laser light from a ceramic body which is illuminated by a gas-discharge strobe light. Lasers of this type are ruby lasers, YAG (yttrium aluminum garnet), and rare-earth-doped glass lasers. These lasers all emit infrared light of a shorter wavelength than CO_2 lasers. YAG lasers, the most widely used type in industry, have an output of 1.06μm. Solid-state lasers are only capable of emitting short pulses of light. The average power of solid-state lasers rarely exceeds 250 watts, but because the energy is delivered in very short bursts, the instantaneous power can be as high as 50 kW during a millisecond pulse. They are used extensively for cutting and welding of metals, particularly steels. Solid-state lasers are much smaller than typical gas lasers, and because of this short cavity length, the diameter of the focused spot is usually larger that what can be obtained with a CO_2 laser.

The CO_2 laser was chosen for study because of its high output power, and the option of choosing between pulsed and continuous operation. In the theoretical model developed in this thesis, CW operation is addressed because it is simpler. It was decided that a thorough understanding of CW cutting was a necessary starting point for an understanding of cutting in general. The experimental program used CW operation almost exclusively to develop this understanding.

In this research project, a theoretical model was developed in conjunction with an experimental program to optimize the cutting tool. To perform machining operations with the laser lathe, it is necessary to know in advance how deep a cut will be, in order to place the two cuts in such a way that they will intersect at the proper point inside the workpiece. The theoretical model developed in this thesis is incapable of predicting cut depths accurately, its purpose is to provide insight into the physics of the process. In addiditon to the approximate nature of the model, it was discovered that laser blind cuts can vary in depth by as much as 30% at different points in the same cut. It is not known whether this difference is due to fluctuations in laser power or to chaotic behavior of the absorbing surface in the kerf.

Regardless of the cause of the fluctuations in depth of cut, their existence requires that the laser lathe incorporate some form of closed-loop control to regulate the depth of cut. The development of a sensor for such a control system is not addressed in this thesis; it is addressed briefly in the Master's thesis of Stefanos N. Kordas (MIT Mech. E. 1986), in the context of the same research project.

2. MODELLING OF LASER CUTTING

Laser cutting is one of the major applications of lasers as material removal tools. The study and modelling of the laser cutting process first requires a good understanding of the classical heat transfer problem of material heating by moving heat sources. Much of the relevant work has been done for the laser welding process.

Rosenthal (1946) gave a comprehensive treatment of moving point sources for modelling arc welding on workpieces with various boundary conditions. The equation he gave of a moving point source on a semi-infinite plate is reproduced in many later articles dealing with lasers. Although Rosenthal owes much of his formulation to Carslaw, his treatment is much more approachable for the engineer.

Carslaw and Jaeger (1959) published an overwhelming collection of analytical solutions to heat conduction problems. For the moving heat source problems, they relied upon Fourier series methods, and generally obtained expressions for both transient and quasi-stationary heating in terms of infinite series. Their treatments have been elaborated upon by several workers to describe laser welding, cutting, and heat treating.

In Rosenthal's paper, transient phenomena are neglected, and attention is focused upon the "quasi-stationary" state. Briefly, the quasi-stationary state refers to the temperature distribution surrounding a moving heat source which exists after all transient effects have completely dissipated. In moving heat source problems, this temperature distribution is stationary with respect to the heat source, and translates with respect to the medium.

Beginning with the classical heat conduction equation

$$\alpha \left(\frac{\partial^2 T}{\partial x^2} + \frac{\partial^2 T}{\partial y^2} + \frac{\partial^2 T}{\partial z^2} \right) = \frac{\partial T}{\partial t}$$

1

which applies to a stationary medium, one can change to a moving reference frame with a change of variable. The heat source is assumed to translate at a steady velocity

V in the positive x direction, and a new coordinate is introduced which corresponds to the distance of a given point in front of or behind the instantaneous location of the source:

$$\xi = x - Vt$$

<div align="right">2</div>

Substituting into the heat equation, one obtains

$$\alpha \left(\frac{\partial^2 T}{\partial x^2} + \frac{\partial^2 T}{\partial y^2} + \frac{\partial^2 T}{\partial z^2} \right) = \frac{\partial T}{\partial t} - V \frac{\partial T}{\partial \xi} .$$

<div align="right">3</div>

The quasi-stationary state is the solution of this equation in which the temperature distribution in the moving frame does not change over time. In other words, $\frac{\partial T}{\partial t} = 0$ and the quasi-stationary heat equation is obtained:

$$\alpha \left(\frac{\partial^2 T}{\partial \xi^2} + \frac{\partial^2 T}{\partial y^2} + \frac{\partial^2 T}{\partial z^2} \right) = -V \frac{\partial T}{\partial \xi} .$$

<div align="right">4</div>

What remains to complete an analytic model is to select the correct boundary conditions and find a solution to this equation which satisfies them. Solutions to this problem are harmonic functions and except in particularly simple cases, they are usually expressed in terms of either Bessel functions or Fourier series, occasionally both at once.

Although Carslaw is the primary source of Rosenthal's methods, and is much more thorough in their derivations, Rosenthal solves a collection of moving source problems in a very condensed package which is much easier to digest.

Rosenthal simplifies the problem by creating a new temperature variable Φ such that

$$T = T_0 + exp \left(\frac{-V\xi}{2\alpha} \right) \Phi(\xi, y, z)$$

<div align="right">5</div>

With this change of variables, he obtains the heat equation in a very simple and elegant form:

$$\nabla^2(\Phi) - \left(\frac{V}{2\alpha}\right)^2(\Phi) = 0$$

6

Rosenthal proceeds to solve one-, two-, and three-dimensional problems in which the heat source moves across the medium at a constant velocity. The one-dimensional solution is an exponential function which solves the one-dimensional form of the above heat equation:

$$T - T_0 = \frac{Q}{V\rho C_p} exp\left(\frac{-V\xi}{2\alpha}\right) \quad for \quad \xi > 0$$

$$= \frac{Q}{V\rho C_p} \quad for \quad \xi < 0.$$

7

For the two-dimensional problem, Rosenthal uses the cylindrical form of the heat conduction equation

$$\frac{\partial^2}{\partial r^2}(\Phi) + \frac{1}{r}\frac{\partial}{\partial r}(\Phi) - \left(\frac{V}{2\alpha}\right)^2(\Phi) = 0$$

8

where:

$$r = \sqrt{\xi^2 + y^2}$$

The solution of this equation for a moving point source in two dimensions is

$$T(\xi, y, z) - T_0 = \frac{P}{2\pi k_\alpha} K_0\left(\frac{Vr}{2\alpha}\right) exp\left(-\frac{V\xi}{2\alpha}\right)$$

9

K_0 is the modified Bessel function of the second kind of zeroth order. This solution

applies to the cutting of thin sheets when surface losses are neglected, and to deep penetration welding and blind cutting when the laser forms a cylindrical cavity which penetrates vertically into the workpiece.

The three-dimensional solution, which applies to a moving point source absorbed on the surface of a semi-infinite slab, is solved in spherical coordinates beginning with the corresponding form of the heat equation:

$$\frac{\partial^2}{\partial r^2}(r\Phi) - \left(\frac{V}{2\alpha}\right)^2 (r\Phi) = 0$$

10

where: $r = \sqrt{\xi^2 + y^2 + z^2}$

and the solution for a semi-infinite slab is

$$T(\xi, y, z) - T_0 = \frac{P}{2\pi k}\exp\left(-\frac{V(\xi + r)}{\alpha}\right)$$

11

Other solutions obtained by Rosenthal deal with surface losses due to convection and plates of finite thickness using the method of images.

In 1956 Masters calculated heat transfer during ablation of a one-dimensional medium with a change of state. The purpose of this paper was to aid in the design of reentry vehicles, and it has been successfully applied to laser processing of materials, primarily drilling.

Masters divides the problem into two cases which correspond to the upper and lower bounds to the velocity of the ablation front. In the first case, the material removal is assumed to occur at the instant of melting while in the second case, a molten boundary layer is assumed to exist and material is removed at a temperature higher than the melting point.

Masters avoids the change of variable presented by Rosenthal by stating that the moving heat wave in the medium satisfies both the one-dimensional heat equation

$$\alpha \frac{\partial^2 T}{\partial x^2} = \frac{dT}{dt}$$

12

and the one-dimensional wave equation

$$V^2 \frac{\partial^2 T}{\partial x^2} = \frac{d^2 T}{dt^2} \ .$$

13

The result is identical with Rosenthal's because any function

$$T = f(x - Vt)$$

14

satisfies the one-dimensional wave equation automatically. The solutions of equation 13 are exponential functions. In the solid material in front of the melting surface, the temperature is given by

$$T = T_m \exp\left(-\frac{V(x - Vt)}{\alpha} \right)$$

15

which is identical to the solution obtained by Rosenthal. At the melting boundary, a discontinuity occurs in the slope of the temperature profile corresponding to the absorbtion of latent heat. If the thermal conductivity of the medium is assumed to stay constant, the change in temperature gradient is given by

$$\left(\frac{\partial T}{\partial \xi} \right)_{\xi-} - \left(\frac{\partial T}{\partial \xi} \right)_{\xi+} = \Delta \frac{\partial T}{\partial \xi} = \frac{V L_m}{k}$$

16

where:

L_m = Latent heat of fusion

k = Thermal conductivity

and the temperature in the liquid boundary is given by a combination of exponentials that provides a new temperature gradient at the melting front:

$$T = \frac{Q}{V \rho C_p} exp\left(-\frac{Vs}{\alpha}\right)\left[exp\left(-\frac{V(x-Vt)}{\alpha}\right)-1\right]$$

17

where:

s = Thickness of liquid film.

Masters obtains the following for an upper bound of the melting velocity:

$$V \leq \frac{Q}{\rho C_p T_m + L}$$

18

in the case where liquid is removed immediately upon melting, and he obtains

$$V \leq \frac{Q}{\rho C_p T_m + L}\left(\frac{T_m + L/C_p}{T_s + L/C_p}\right)$$

19

in the case where material is removed at an elevated temperature

where:

T_s = Temperature at the absorbing surface. $T_s > T_m$

The upper bound to the melting velocity corresponds to the quasi-stationary conditions. Assuming the medium begins at a uniform temperature, the velocity of the ablation front will necessarily be slower than this upper bound until the quasi-stationary condition is obtained.

Hablanian (1962) performed a dimensional analysis upon the parameters associated with single-pass welding of metals. He derived two dimensionless parameters between which he found a correlation that applies to laser, electron beam, and plasma-jet welding. This analysis has not been mentioned by any workers outside MIT. The two

dimensionless groups that Hablanian found are:

$$\frac{Vd}{\alpha} \quad \text{and} \quad \frac{zT_m k}{P}$$

20

Hablanian used data for a variety of metals (aluminum, stainless steel, beryilium, titanium, and zirconium) from electron beam welding. Plotting the data logarithmically, he found the values for the dimensionless groups to lie near to a line with the generic formula

$$\frac{zT_m k}{P} = C \left(\frac{Vd}{\alpha}\right)^{1/2}$$

21

where C is a constant with a value of approximately 0.09.

Hella (1974) used Hablanian's correlation as a model for laser welding, although the agreement of his data is unconvincing.

Babenko and Tychinskii (1973) used a formulation similar to Rosenthal's to calculate the dimensions of a weld pool in a plate surrounding a moving point source which is absorbed at the surface. The temperature distribution surrounding a moving Gaussian heat source was derived by Cline and Anthony (1971) to calculate heating and cooling rates in the metal in the vicinity of a laser weld. They went on to derive a model for depth of penetration of the laser beam and fluid flow during welding.

The penetration of a laser beam into a target has been studied extensively for modelling laser drilling. Ready (1965) calculated the temperature rise in a one-dimensional slab heated by a laser pulse. He models the heating of the target by considering the absorbtion of radiation by a partially transmissive medium:

$$Q(x,t) = J(t) a_\lambda \exp\left(\frac{-x}{\delta}\right)$$

22

where:

$Q(x,t)$ = Heating at depth x in medium

$J(t)$ = Power density of incident laser

α_λ = Absorbtion coefficient

δ = Depth of absorbing region below momentary surface

Ready uses this expression as the heating function in the heat equation

$$\alpha \, \frac{\partial^2 T}{\partial x^2} + \frac{1}{\rho C_p} Q(x,t) = \frac{\partial T}{\partial t}$$

23

and arrives at a voluminous exact solution for the temperature as a function of time in the one-dimensional medium. His paper concludes with an approximate expression which corresponds to a simple heat balance between energy applied to the medium and heat dissipated by evaporation:

$$D = \frac{ED}{\rho \, (L + CT_v)}$$

24

where:

$$ED = \frac{P\tau}{\pi r^2} = \text{Energy Density in stationary frame.}$$

This equation predicts depths of drilled holes when drilling occurs with negligible heat dissipation in the medium. Ready applies this relation to laser drilling of metals and nonmetals at power densities between 10^7 and 10^9 W/cm^2. For purposes of comparison, the cuts performed in this research project were on the order of 10^5 to 10^7 W/cm^2.

One-dimensional heat-transfer calculations similar to Masters' have been used to model ablation of material from a stationary target in laser drilling. Dabby and Paek (1972) solved the problem for a partially transmissive medium, and Warren and Sparks (1979) included variable absorbance.

Dabby and Paek model the heating of the medium in a translucent target in much the same way Ready did; and they arrive at a one-dimensional form of the heat conduction equation with prescribed heating conditions:

$$\rho C_p \frac{\partial T}{\partial t} = a_\lambda I \exp\left(-a_\lambda (z-Z)\right) + K \frac{\partial^2 T}{\partial z^2} \quad z > Z$$

25

where:

z = Depth in workpiece

Z = Position of the ablation front in one-dimensional frame.

After changing variables into a dimensionless reference frame,

$$\frac{\partial \theta}{\partial \tau} - u \frac{\partial \theta}{\partial s} - \frac{\partial^2 \theta}{\partial s^2} = \frac{B}{\lambda} \exp(-Bs)$$

26

and:

$$u = \lambda \frac{\partial \theta}{\partial s}\Big|_{s=0}$$

27

where:

$$\theta = \frac{T}{T_v}$$

$$s = \frac{I C_p}{k L_v} (z-Z)$$

$$u = \frac{\rho L_v}{I} \frac{\partial Z}{\partial t}$$

$$\tau = \frac{I^2 C_p}{\rho k L_v^2} t$$

$$\lambda = \frac{C_p T_v}{L_v}$$

$$B = \frac{kdL_v}{TC_p}$$

d = diameter of laser spot

T_v = Vaporization temperature

I = Laser power

k = Thermal conductivity

L_v = Latent heat of vaporization.

They solve this problem using Laplace transforms and obtain expressions for the temperature distribution as a function of time in the moving reference frame. The equations for the temperature distributions are too voluminous to reproduce here, so several of their conclusions will be discussed instead.

The velocity of the ablation surface starts out at u = 0. At τ = 0 the ablation surface accelerates very quickly between τ = 0 and τ = 1. After this, the acceleration diminishes until the normalized velocity obtains its asymptotic limit. The conditions at this limiting ablation speed are identical to Rosenthal's "quasi-stationary" state, and are equal to

$$u_\infty = \frac{1}{1+\lambda}$$

Dabby and Paek also conclude that the temperature gradient in the target can become inverted during drilling. They predict temperatures as high as twice the vaporization temperature inside an alumina target which is ablating at its vaporization point. This is due to the transmission of radiation into the medium before absorbtion. Since the radiation propagates at the speed of light, it will always superheat the medium no matter how fast the ablation front is progressing. Thus, they predict explosive vaporization of material from a laser drilled hole, a phenomenon which has been observed experimentally and is called "laser-supported detonation".

Wagner (1974) used finite differences to calculate drilling velocities in aluminum

oxide. He uses a one-dimensional model which takes into account the transmittance in alumina of the infrared laser radiation. He rejects Dabby and Paek's conclusion that superheating can occur below the ablation surface. Wagner assumes that vaporization occurs reversibly in the medium, with the absorbtion of the latent heat of vaporization at the vaporization temperature, in spite of the exceedingly rapid heating rate which can lead to superheating. He claims that radiation pressure accounts for the acceleration of molten material out of the hole.

While the precise mechanism of material removal from a hole in laser drilling is largely irrelevant to the subject of this thesis, the numerical technique which Wagner uses is illuminating. He divides his one-dimensional medium into a number of slices of finite width, and uses a one-dimensional difference form of the heat equation

$$\rho\, C_p \Delta T_i \;=\; \left(\tfrac{\Delta t}{h}\right)\!\left(\;\tfrac{k}{h}(T_{i-1}-2T_i+T_{i+1}) \;+\; d(1-R_\lambda)J_0 a_\lambda exp(-a_\lambda y_i)\;\right)$$

29

where:

$\rho\, C_p$ = Density x Specific heat = Specific heat/Unit volume, J/°C-cm³

T_i = Temperature of the i-th element

Δt = Time increment of the numerical calculation

k = Thermal conductivity

h = Thickness of a single element

R_λ = Surface reflectivity

J_0 = Incident laser intensity

α_λ = Absorbtion coefficient [cm^{-1}]

y_i = Depth of the i-th element below the instantaneous ablation front.

Although the finite difference approach is less precise and more prone to instability

than the so-called finite element method, it gives much greater flexibility in dealing with phase transformations and latent heat. Wagner creates an auxiliary variable P_i which records for each element the quantity of latent heat absorbed. Heating at the melting point can be followed by exchanging ΔP_i for $\rho C_p \Delta T_i$ in the difference equation until P_i equals the latent heat of fusion. At this point, the element is assumed to be melted, and the temperature begins to rise again, with a different coefficient of specific heat. Again, when the vaporization point is reached, the heating is isothermal and added to P_i until a quantity equal to the latent heat of vaporization is transferred, at which point the element is deleted from the scheme. Thermal radiation can also be accounted for by simply subtracting the quantity

$$\left(\tfrac{\Delta t}{d}\right) \varepsilon_l \sigma_l \left(T_i^4 - T_{amb}^4\right)$$

<div align="right">30</div>

where:

ε_l = Surface emissivity

σ_l = Stefan-Boltzmann coefficient

from the right side of the difference equation for the element which happens to be at the momentary ablation surface.

The flexibility of the finite difference approach makes it possible to deal with phase changes and complicated motion of the heat source. This flexibility is not obtained without substantial cost, however. Finite difference models are prone to numerical instabilities which can occur because the heat transferred during a given time increment is assumed linear over that interval. This is only approximately correct if the temperature change during the time increment is insignificant compared to the temperature difference between each element. If very small dimensions of the elements are desired, then the time increments must be exceedingly small. The number of iterations necessary to find the temperature distribution at a particular time could easily be in the millions for a respectably large field. When iteration cycles of this magnitude are used,

there is an additional problem of truncation errors in the computer. Since the computer rounds off any real number it stores, the cumulative error in the answer after several million iterations can easily be the same order of magnitude as the answer itself, making the results all but meaningless.

Wagner does not mention any difficulties he may have had in executing his scheme. A finite difference model was developed, similar in approach to Wagner's, using a two-dimensinal field. It will be discussed in a later chapter.

Paek and Gagliano (1972) adopted a more analytical approach to find the thermal stresses surrounding a vertically descending disc heat source. They begin the paper by deriving analytically the temperature distribution in a slab of finite thickness using the method of images, as described exhaustively by Carslaw.

Next they evaluate the thermal stresses induced in an elastic medium by this temperature field. Beginning with the stress-strain relations

$$\varepsilon_r = \frac{1}{E}\left(\sigma_r - v(\sigma_\theta + \sigma_z) \right) + \alpha_\theta T$$

31

$$\varepsilon_\theta = \frac{1}{E}\left(\sigma_\theta - v(\sigma_r + \sigma_z) \right) + \alpha_\theta T$$

32

$$\varepsilon_z = \frac{1}{E}\left(\sigma_z - v(\sigma_\theta + \sigma_r) \right) + \alpha_\theta T$$

33

where:

ε = Strain component

σ = Stress component

E = Young's modulus

α_θ = Coefficient of thermal expansion

$T = T(r,\theta,z)$ = Temperature

they proceed to define the stress function:

$$\sigma_r = \frac{\Psi}{r}$$

34

$$\sigma_\theta = \frac{\partial}{\partial r}(\Psi).$$

35

Assuming plane strain:

$$\sigma_z = \nu\left(\sigma_r + \sigma_\theta\right) - \alpha E T$$

36

and rotational symmetry:

$$r\frac{\partial}{\partial r}(\varepsilon_\theta) + \varepsilon_\theta - \varepsilon_r = 0.$$

37

They obtain the following differential equation for the stress function:

$$\frac{\partial^2}{\partial r^2}(\Psi) + \frac{1}{r}\frac{\partial}{\partial r}(\Psi) - \frac{\Psi}{r^2} = -\frac{\alpha E}{1-\nu}\frac{\partial T}{\partial r}.$$

38

The temperature distribution which they obtained in the first part of their paper is coupled into the equation as a forcing function. By integrating, and evaluating the constants of integration, they obtain an equation for Ψ:

$$\Psi = -\frac{\alpha E}{1-\nu}\frac{1}{r}\int_g^r Tr\,\partial r$$

39

where:

$g = g(z)$ = Radius of hole at depth z .

From this expression, they arrive at expressions for the stress components in cylindrical coordinates. The reason they perform this derivation is to predict the occurance of thermal cracking in brittle media, so the tangential component of the stress is of chief interest:

$$\sigma = -\frac{\alpha E}{1-v} \frac{1}{r^2} \int_g^r Tr \, \partial r - Tr^2 .$$

40

When they apply the temperature distribution derived in the first part of the paper, they show that the hydrostatic compressive stress which exists in the hot center of the drilling region is, quite understandably, surrounded by a region of tensile hoop stress. For alumina drilled by ruby laser with a pulse length of 1.38 ms, the tangential stress reaches 20 kg/mm^2. This is high enough to cause cracking if there is a large enough flaw in the tensile region, and in the last part of the paper, they attempt to verify their findings experimentally by drilling several holes in alumina wafers at different distances from each other, and from a free edge. They finish by concluding that thermal stresses are not significant for the laser parameters they used.

In laser cutting, the penetration of the laser beam into the workpiece is an essential feature of the process. A vertical cavity is formed which translates laterally through the workpiece. Swift-Hook and Gick (1973) adapted a solution of Carslaw and Jaeger's to model the propagation of the melting front surrounding a vertical beam-penetration cavity in laser welding. This is the earliest paper in which the existence of such a cavity is discussed. By assuming the heat source to be a vertical line source of negligible diameter, and by accomodating variation of thermal properties into a heat function, they derive the following expression:

$$S(r,\phi,z) = \frac{P}{2\pi z} K_0\left(\frac{Vr}{2\alpha} \right) exp\left(-\frac{Vr}{2\alpha} cos\phi \right)$$

41

where:

$S(r,\phi,z)$ = Heat function, $\int_{T_0}^{T(r(\phi,z)} k(T)\, \partial T$

$k(T)$ = Thermal conductivity

T_0 = Ambient temperature

P = Laser Power

z = Depth of laser-supported cavity

V = Translation speed in direction $\phi=0$

$\alpha = \frac{k}{\rho C_p}$; Thermal diffusivity

The heat function $S(r,\phi,z)$ is created to accomodate variations in the thermal conductivity of the medium with temperature. It differs from another function, the heat content (or enthalpy) H:

$$H = \text{Enthalpy} = \int_{T_0}^{T(r,\phi,z)} \rho C_p(T)\, \partial T$$

42

so
$$\frac{S}{H} = \alpha.$$

43

Using the heat function S, the heat diffusion equation becomes

$$\nabla^2 S = \alpha \nabla S.$$

44

Swift-Hook and Gick then create a new heat function which is a normalized power input per unit depth:

$$X(r,\phi) = \frac{P}{zS(r,\phi)} .$$

45

Next, they calculate the expected width of a weld by considering a melting isotherm

whose half-width y is expressed in radial coordinates:

$$y = r \sin(\phi)$$

<div align="right">46</div>

which has a maximum value when

$$0 = \frac{\partial y}{\partial \phi} + \frac{\partial y}{\partial r}\frac{\partial r}{\partial \phi}$$

<div align="right">47</div>

Next they define a normalized width variable Y:

$$Y = \frac{2Vy}{\alpha}$$

<div align="right">48</div>

since an isotherm is a line of constant X, the following is also true at the maximum melting width:

$$0 = \frac{\partial X}{\partial \phi} + \frac{\partial X}{\partial r}\frac{\partial r}{\partial \phi}$$

<div align="right">49</div>

By substituting the analytic solutions for the temperature distribution, they obtain the following relations:

$$Y = \frac{2Vr}{\alpha}\sqrt{1 - \left[K_0^2 / K_0'^2 \right]\left(\frac{Vr}{2\alpha} \right)}$$

<div align="right">50</div>

for the normalized maximum weld width, and

$$X = \frac{2\pi}{K_0\left(\frac{Vr}{2\alpha} \right)}\, exp\left[\frac{2Vr}{\alpha}\left[K_0^2 / K_0'^2 \right]\left(\frac{Vr}{2\alpha} \right) \right]$$

<div align="right">51</div>

for the normalized beam power per unit depth. Both of these equations are functions of the dimensionless variable

$$\left(\frac{Vr}{2\alpha} \right)$$

which could in principle be eliminated between them. This can be done numerically, however, Swift-Hook and Gick find analytical solutions for these quantities for the upper and lower asymptotic limits of the variable

$$\left(\frac{Vr}{2\alpha} \right)$$

by substituting approximate forms of the modified Bessel function K_0.

• As the argument increases at high translation speeds, low thermal diffusivity, and larger distances from the source,

$$K_0\left(\frac{Vr}{2\alpha} \right) = \left(\frac{\pi\alpha}{Vr} \right)^{1/2} exp\left(-\frac{Vr}{2\alpha} \right)$$

52

with

$$\frac{-K_0}{K'_0} \approx 1 - \left(\frac{Vr}{\alpha} \right).$$

53

The solutions for the weld width and power/unit depth are:

$$Y \approx 4\left(\frac{Vr}{2\alpha} \right)^{1/2} = \text{weld width}$$

54

and

$$X \approx 4\left(\frac{4\pi e Vr}{\alpha} \right)^{1/2}$$

55

so $Y \approx 0.483 X$

56

This function predicts a linear relation between the volume of the weld and the quantity of energy applied:

$$2 y z V H \approx 0.48 P$$

where:

V = Translation speed

z_w = Depth of weld

y_w = Half-width of weld

P = Laser power

and the depth and width of the weld both increase as the square root of the energy density.

This is a very important result because it predicts nearly the correlation which Hablanian found in 1962 for laser welding, equation [21]. The assumption which must be made for this relationship to hold are the following:

1. The absorbing region of the workpiece must be a vertical cylindrical cavity which is much taller than the spot diameter. This allows the neglection temperature gradients in the vertical direction to obtain the two-dimensional solution for the temperature distribution.

2. The translation speed must be sufficiently large compared to the thermal diffusivity.

3. A direct consequence of 1. and 2. is that the laser power must be sufficiently large at the high translation speed to maintain the vertical cavity. Mathematically,

$$\frac{J}{VH} = \frac{ED}{Hd} \gg 1$$

where:

$$J = \frac{P}{\pi(d/4)^2} = \text{Power density}$$

$$H = \rho \, C_p \left(T_s - T_0 \right) = \text{Enthalpy of removal}$$

T_s = Temperature at which material is removed

$ED = \frac{P}{dV}$ = Energy density of a single laser scan

d = Focused spot size.

• The second asymptotic limit proposed by Swift-Hook and Gick occurs at low translation speeds, high thermal diffusivity, and at distances close to the heat source:

$$K_0 \left(\frac{Vr}{2\alpha} \right) \approx -0.577 + \ln \left(\frac{4\alpha}{Vr} \right)$$

59

so

$$Y \approx \frac{2Vr}{\alpha}$$

60

$$\text{and} \quad X \approx \frac{2\pi}{-0.577 + \ln(\alpha/Vr)} \approx \frac{P}{\alpha Hz}$$

Using these two asymptotic limits to the behavior of a weld at high and low translation speeds, Swift-Hook and Gick assume a smooth transition in the intermediate range and compare their predictions with data for electron beam and laser welding. They find a good correlation in the range of 1.5 to 22.5 kw and speeds of 4 to 40 mm/sec for welds 5 to 40 mm deep. Tests done with laser power of 250 W gave poor correlation.

The work of Swift-Hook and Gick is applicable to the subject of deep blind cutting, particularly for single pass cuts at low surface speeds. The fact that the molten material is removed from the kerf before it can resolidify perturbs the temperature distribution in the region behind the laser spot where material next to the kerf is cooling. The heating region in front of the laser spot is relatively unperturbed, so their solution should approximate the heating region better than the cooling region.

Gonsalves and Duley (1972) modelled laser cutting of thin sheets using a two-dimensional model of heat conduction from a moving point source. They derived an expression for a critical cutting speed above which a cut does not penetrate through the

sheet. Bunting and Cornfield (1975) modified this concept to a diffuse vertical line source. They derived a general theory of thermal sheet cutting by considering a variety of techniques such as laser, electron beam, and plasma jet cutting.

Klemens (1976) modelled deep-penetration welding and calculated the depth of peneteration by estimating the heat dissipation per unit depth of the vartical cavity. Cline and Anthony [1977] modelled depth of penetration by considering the pressure distribution of vapor within the cavity.

Souecker et al. have analyzed the mechanism of material removal in cutting across relatively thick workpieces by considering the erosion front which occurs at a nearly vertical plane at the momentary end of cut. It is assumed that the material is removed by ejection at the lower surface of the workpiece due to friction of the melt with the cutting gas flow and by evaporation at the erosion front.

Decker roughly estimates the maximum cutting speed for a given thickness assuming high cutting speeds, narrow kerfs, and low pressure assist gas.

Copley et al. employed a continuous wave CO_2 laser to shape metallic and ceramic materials by grooving and threading turning cylindrical workpieces. Although this work deals with the formation of grooves on ceramic materials and metals, its emphasis has been more experimental, and a theoretical model of the process has not been attempted.

Recently, a thermal analysis by Modest and Abakians [1986] has resulted in the formulation of the governing equations for heat conduction at a moving isothermal ablation surface under a scanning laser spot. Their treatment applies to laser blind cutting in a single scan over a semi-infinie solid. In the following chapter, their approach is adapted to the modelling of laser blind cutting in multiple scans over a pre-existing kerf.

In general, research work in laser cutting, whether experimental or theoretical, assumes a given depth of cut, usually identical to the workpiece thickness, and attempts to determine a cutting speed which optimizes a particular criterion, such as cutting rate

or surface quality. In "blind" cutting, however, the depth is not a set parameter, but a critical variable which also must be optimized with respect to a given criterion.

3. ANALYTICAL MODEL FOR LASER BLIND CUTTING

3.1 . Governing Equation

To develop a model for multiple pass laser blind cutting, it is necessary to consider the heat conduction from a moving heat source in a pre-existing kerf. It is assumed that the kerf can be formed through several previous laser scans, and each subsequent scan increases the depth of the kerf by removing material from the bottom and sides of the pre-existing kerf. A model for evaporative laser cutting has been developed by Modest and Abakians [1986] which applies to the formation of a kerf with a laser scanning in a single pass. They formulated the governing equation for heat conduction from an ablation surface beneath a moving gaussian laser spot, and obtained numerical solutions for the cut profile. While their approach was successful for a single pass kerf, their method becomes unwieldy when the problem of a pre-existing kerf is addressed. The boudary conditions of the equation change from one pass to the next and a new analytical solution must be found for every laser scan.

An analytical is presented here which attempts to solve the multiple pass problem with an approximate analytical solution. The governing equation derived below is the same as that which Modest and Abakians found, and the general form of the equation is preserved as long as possible before approximations must be made regarding the steady-state temperature profile.

Figure [6] illustrates the coordinate system used in this derivation. A semi-infinite medium is bounded by the x-y plane. In addition, a kerf runs across the medium along the x-axis and has a profile given by the general formula :

1. $z = s(\xi, y)$ under the laser spot   61

2. $z = s_+(y)$ in advance of the laser spot   62

3. $z = s_-(y)$ behind the laser spot   63

Laser Beam

$J(\xi,y)$

$s_+(y)$

$s_-(y)$

$s(\xi,y)$

z

y

ξ

V
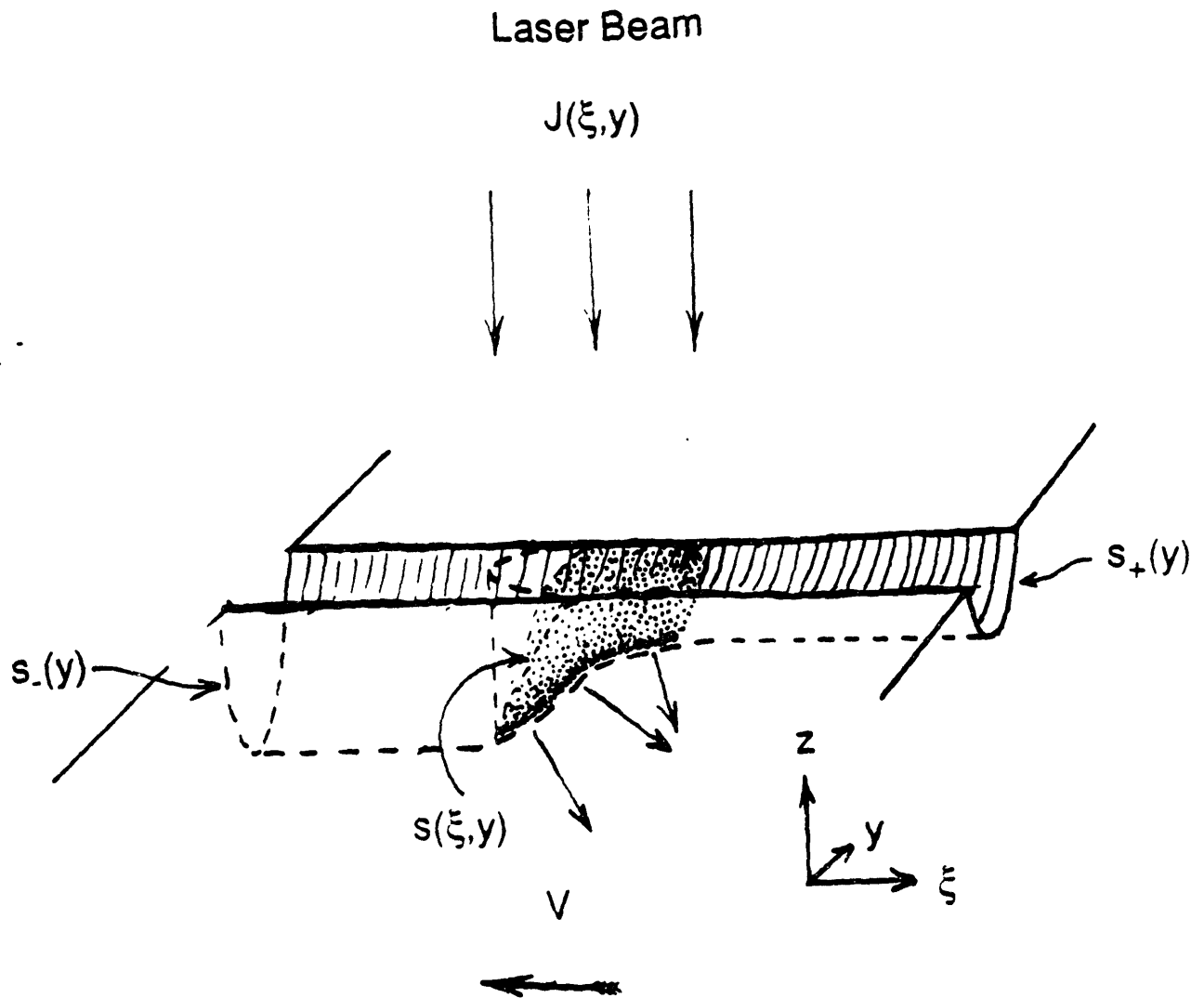
Figure 6. Diagram of ablation surface during kerf formation in laser blind cutting.

The laser beam has an intensity profile $J(\xi,y)$ and projects downward into the kerf. The beam is assumed stationary and the medium translates in the negative x-direction with a velocity V. Furthermore, the quasi-stationary condition developed by Rosenthal exists and therefore, the corresponding form of the heat conduction equation applies:

$$k \left(\frac{\partial^2 T}{\partial \xi^2} + \frac{\partial^2 T}{\partial y^2} + \frac{\partial^2 T}{\partial z^2} \right) = -V \rho C_p \frac{\partial T}{\partial \xi}$$

$$64$$

where $\xi = x - Vt$; Quasi-stationary frame.

The ablation surface under the laser spot is assumed to be isothermal. Also, reflections from the ablation surface are neglected, as are cooling effects due to assist gas used to scour molten material from the kerf. Considering a differential volume element which contains a portion of the ablation surface, shown in figure [7], the following heat balance can be written:

$$0 = J \partial \xi \partial y + k \frac{\partial T}{\partial \xi} \left(\partial y \partial z - 1/2 \frac{\partial s}{\partial y} \partial y^2 \right)$$

$$+ k \frac{\partial T}{\partial y} \left(\partial \xi \partial z - 1/2 \frac{\partial s}{\partial \xi} \partial \xi^2 \right)$$

$$- k \frac{\partial T}{\partial z} \left(\partial \xi \partial y \right)$$

$$- k \left(\frac{\partial T}{\partial \xi} + \frac{\partial^2 T}{\partial \xi^2} \partial \xi \right) \left(\partial y \partial z - 1/2 \frac{\partial s}{\partial y} \partial y^2 - \frac{\partial s}{\partial \xi} \partial \xi^2 \right)$$

$$- k \left(\frac{\partial T}{\partial y} + \frac{\partial^2 T}{\partial y^2} \partial y \right) \left(\partial \xi \partial z - 1/2 \frac{\partial s}{\partial \xi} \partial \xi^2 - \frac{\partial s}{\partial y} \partial y^2 \right)$$

$$- VL \frac{\partial s}{\partial \xi} \partial \xi^2 .$$

$$65$$

where:

$J(\xi,y)$ = Laser intensity

$T(\xi,y,z)$ = Temperature distribution inside the medium
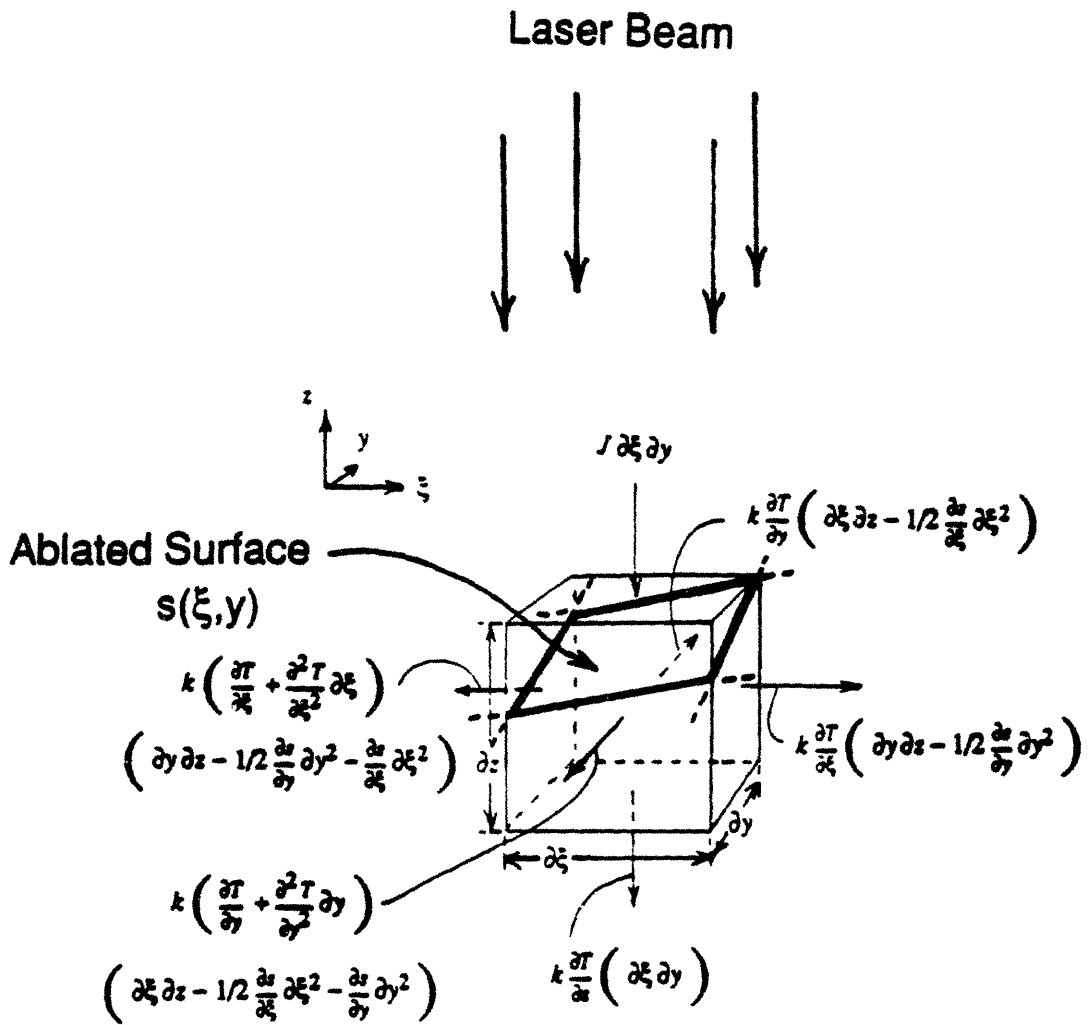
Figure 7. Heat flow conditions at a laser-ablated surface.

$\frac{\partial T}{\partial x_i}$ = Temperature gradient resolved at the ablation surface $s(\xi, y)$.

V = Velocity of the medium with respect to the laser spot

L = Latent heat of phase change at ablation surface.

The volume element is assumed to be cubic, that is, the magnitudes of the differential elements $\partial\xi$, ∂y, and ∂z are equivalent. Therefore, all the differentials

$$\partial\xi^2 = \partial y^2 = \partial z^2 = \partial\xi\partial y = \partial\xi\partial z = \partial y\partial z$$

66

are equivalent in magnitude and may be cancelled from the equation. Collecting terms, one obtains

$$0 = J + k\left(\frac{\partial T}{\partial\xi}\frac{\partial s}{\partial\xi} - \frac{\partial^2 T}{\partial\xi^2}\partial\xi\left(1 - 1/2\frac{\partial s}{\partial y} - \frac{\partial s}{\partial\xi}\right)\right)$$

$$+ k\left(\frac{\partial T}{\partial y}\frac{\partial s}{\partial y} - \frac{\partial^2 T}{\partial y^2}\partial y\left(1 - 1/2\frac{\partial s}{\partial\xi} - \frac{\partial s}{\partial y}\right)\right)$$

$$- k\frac{\partial T}{\partial z} - VL\frac{\partial s}{\partial\xi}.$$

67

The terms which are multiplied by $\partial\xi$ and ∂y are insignificant, and can be ignored. The governing equation for an isothermal ablation surface thus simplifies to

$$0 = J + k\left(\frac{\partial T}{\partial\xi}\frac{\partial s}{\partial\xi} + \frac{\partial T}{\partial y}\frac{\partial s}{\partial y} - \frac{\partial T}{\partial z}\right) - VL\frac{\partial s}{\partial\xi}.$$

68

Since the ablation surface is isothermal, the temperature gradient at the surface is parallel to the surface normal {n}. Vector algebra gives the temperature gradients in cartesian coordinates:

$$\left| \frac{\partial T}{\partial n} \right| = \sqrt{ \left(\frac{\partial T}{\partial \xi} \right)^2 + \left(\frac{\partial T}{\partial y} \right)^2 + \left(\frac{\partial T}{\partial z} \right)^2 }$$

69

$$\frac{\partial T}{\partial \xi} \partial \xi = \frac{\partial T}{\partial y} \partial y = -\frac{\partial T}{\partial z} \partial z$$

70

where:

n = Unit normal vector to the surface $s(\xi, y)$

From these identities, the temperature gradients in the cartesian coordinates can be related to one another:

$$\frac{\partial T}{\partial y} = \frac{\partial T}{\partial \xi} \frac{\left(\frac{\partial s}{\partial y} \right)}{\left(\frac{\partial s}{\partial \xi} \right)} \quad \text{and} \quad \frac{\partial T}{\partial z} = \frac{-\left(\frac{\partial T}{\partial \xi} \right)}{\left(\frac{\partial s}{\partial \xi} \right)} .$$

71

Substituting these expressions into the governing equation, the following general equation is obtained:

$$0 = J + k \frac{\partial T/\partial \xi}{\partial s/\partial \xi} \left(\left(\frac{\partial s}{\partial \xi} \right)^2 + \left(\frac{\partial s}{\partial y} \right)^2 + 1 \right) - VL \frac{\partial s}{\partial \xi}.$$

72

or,

$$0 = J + k \frac{\partial T}{\partial n} \sqrt{ \left(\frac{\partial T}{\partial \xi} \right)^2 + \left(\frac{\partial T}{\partial y} \right)^2 + 1 } - VL \frac{\partial s}{\partial \xi}.$$

73

The second form of this equation is essentially identical to the one obtained by Modest and Abakians, neglecting the term which accounts for convective cooling due to

a gas jet. Although a gas jet is always present in laser blind cutting, its cooling effect renders the analytic solution to the heat conduction problem unwieldy, and since a simple, approximate solution is desired, this effect is ignored for the moment.

Using the first form of the governing equation, the shape of the ablation surface is related to $\frac{\partial T}{\partial \xi}$ evaluated at the surface. To evaluate this temperature gradient, one returns to the quasi-stationary heat equation

$$k \left(\frac{\partial^2 T}{\partial \xi^2} + \frac{\partial^2 T}{\partial y^2} + \frac{\partial^2 T}{\partial z^2} \right) = -V \rho C_p \frac{\partial T}{\partial \xi}.$$

74

Consider a control volume which begins at the ablation surface and extends arbitrarily far in the positive x-direction. The cross-section of the volume is ∂y by ∂z and is shown schematically in figure [8], neglecting insignificant higher-order terms at the outset. The heat conduction equation applies to any differential element of this control volume, and the heating of the entire volume is found by integrating the above equation from the ablation surface in the x-direction until the temperature of the medium is the ambient temperature and all thermal gradients are arbitrarily small.

$$k \int_{s(\xi,y)}^{+\infty} \left(\frac{\partial^2 T}{\partial \xi^2} + \frac{\partial^2 T}{\partial y^2} + \frac{\partial^2 T}{\partial z^2} \right) \partial \xi = -V \rho C_p \int_{s(\xi,y)}^{+\infty} \frac{\partial T}{\partial \xi} \partial \xi$$

75

The reason that the x-direction is chosen for integration is because the component of heat conducted in that direction contribures directly to the cutting process. A certain amount of the heat which is conducted in the y- and z-directions escapes from the vicinity of the kerf and contributes to bulk heating of the workpiece. The goal in this analysis is to obtain a method for evaluating the heat lost by lateral conduction.

Part of the equation can be evaluated exactly without making any assumptions about the temperature distribution:

$$k \int_{s(\xi,y)}^{+\infty} \frac{\partial^2 T}{\partial \xi^2} \partial \xi = \frac{\partial T}{\partial \xi}\bigg|_{s(\xi,y)}$$
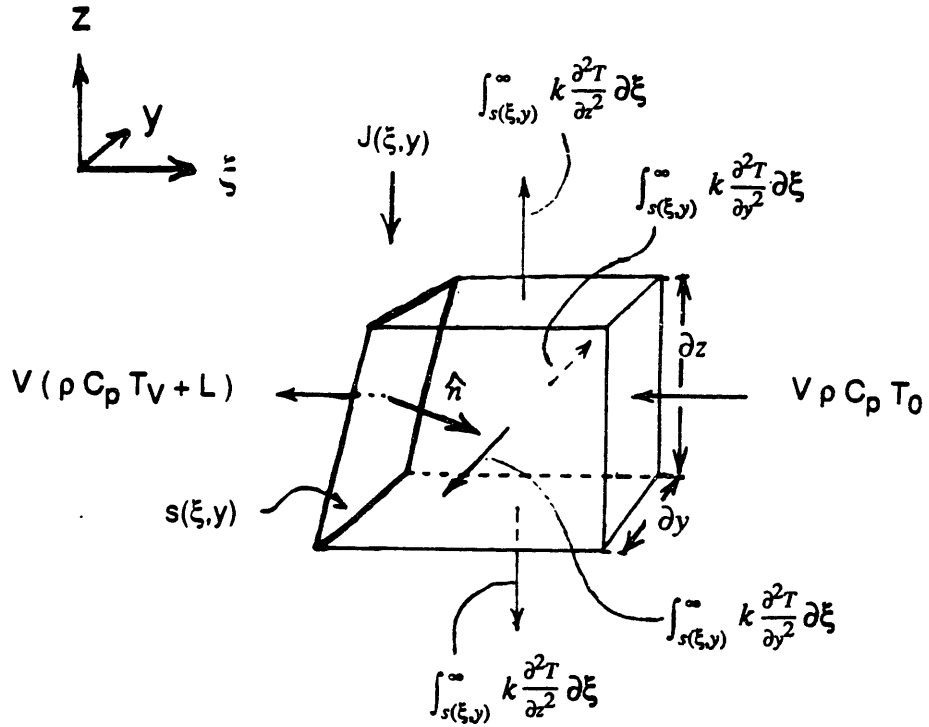
Figure 8. Differential control volume for evaluating heat conduction from ablation surface.

and

$$k \int_{s(\xi,y)}^{+\infty} \frac{\partial T}{\partial \xi} \partial \xi = T_{s(\xi,y)} - T_0.$$

76

where:

$T_{s(\xi,y)}$ = The temperature at the ablation surface or any isothermal surface given by $s(\xi,y)$

T_0 = Ambient temperature of the medium.

The remainder of the integral cannot be evaluated without obtaining an analytic solution for the temperature distribution, which is a function of $s(\xi,y)$, the function which we hope to determine. Since the purpose of the modelling work is to obtain an approximate analytic expression, the different conditions which apply to laser cutting will be examined and these integrals evaluated approximately to obtain solutions which are simple enough to provide insight into the physics of the process.

3.2 High-speed Behavior

The first condition to be addressed pertains to laser cutting when a very fast translation speed is used. The precise assumption is found by considering the quantity

$$\frac{k}{V \rho C_p} = \frac{\alpha}{V}.$$

77

This quantity has the dimensions of distance and expresses the extent of the heat wave which travels in front of the ablation surface in the material. If this distance is very much smaller than the diameter of the laser spot, the heat which is conducted in advance of the laser spot remains very close to the ablation surface, and the isotherms

in the medium can be assumed to be parallel to the ablation surface. The condition

$$\frac{Vd}{\alpha} \gg 1$$

<div align="right">78</div>

is obtained with very large translation speeds, low thermal conductivity, high density, high specific heat, and large spot size. For aluminum oxide using a spot size of .013 cm, this condition is obtained at speeds higher than approximately 10 cm/sec. For steel using the same spot size, the speed must be greater than approximately 100 cm/sec.

This is the condition that Klemens [1976] referred to as "adiabatic". When it is applied to this problem, the following substitutions can be made:

$$\frac{\partial^2 T}{\partial y^2} = \frac{\left(\frac{\partial s}{\partial y}\right)^2}{\left(\frac{\partial s}{\partial \xi}\right)^2} \frac{\partial^2 T}{\partial \xi^2}$$

$$\frac{\partial^2 T}{\partial z^2} = \frac{\frac{\partial^2 T}{\partial \xi^2}}{\left(\frac{\partial s}{\partial \xi}\right)^2}$$

<div align="right">79</div>

Substituting these into the integrated heat equation, we obtain

$$\left[1 + \frac{\left(\frac{\partial s}{\partial y}\right)^2}{\left(\frac{\partial s}{\partial \xi}\right)^2} + \frac{1}{\left(\frac{\partial s}{\partial \xi}\right)^2} \right] k \left(\frac{\partial T}{\partial \xi}\right)_{s(\xi,y)} = -V\rho C_p (T_s - T_0)$$

<div align="right">80</div>

or,

$$-k \frac{\partial T}{\partial \xi} = \frac{V\rho C_p (T_s - T_0) \left(\frac{\partial s}{\partial \xi}\right)^2}{\left(\left(\frac{\partial s}{\partial \xi}\right)^2 + \left(\frac{\partial s}{\partial y}\right)^2 + 1\right)} .$$

<div align="right">81</div>

When this is substituted into the governing equation [72], the quite simple expression is obtained:

$$0 = J - V\rho C_p(T_s-T_0)\frac{\partial s}{\partial \xi} - VL\frac{\partial s}{\partial \xi}$$

<div align="right">82</div>

or,

$$\frac{J}{VH} = \frac{\partial s}{\partial \xi}$$

<div align="right">83</div>

where:

$$H = \rho C_p(T_s-T_0) + L$$

The change in depth of the kerf between s_+ (y) in front of the laser beam and s_- (y) behind the laser beam is found by integrating $\frac{\partial s}{\partial \xi}$ across the spot:

$$s_-(y) - s_+(y) = \int_{+\infty}^{-\infty} \frac{\partial s}{\partial \xi} \partial \xi$$

<div align="right">84</div>

$$= \frac{1}{VH} \int_{+\infty}^{-\infty} J(\xi,y)\, \partial \xi \ .$$

<div align="right">85</div>

This is to say that the cut profile under these conditions should exactly mimic the energy density profile. When this solution is carried into multiple passes of the laser, this model predicts a linear increase in depth of cut with energy density.

In order to simplify the following discussion, the following quantities are introduced. The depth of kerf, D, corresponds to the maximum value of s(y). Since the process developed in this thesis depends on the production of intersecting kerfs, the depth kerf is of much greater importance than any other feature of the kerf profile. Similarly, the change of depth on a given laser scan will be denoted by the quantity ΔD. Rigorously, these quantities are defined as

$$D = s_+(0) \quad \text{and} \quad \Delta D = s_-(0) - s_+(0) \ .$$

<div align="right">86</div>

The "energy density" is here defined as the integral

$$\Delta ED = \tfrac{1}{v} \int_{-\infty}^{+\infty} J(\xi,0)\, \partial\xi.$$

87

When a gaussian power distribution is considered, the energy density is related to the average laser power by an algebraic formula.

The intensity of the beam is given by the formula

$$J(\xi,y) = J_0 \exp\left(-\frac{\xi^2+y^2}{r_0^2} \right)$$

88

where

J_0 = Laser intensity at the center of the focal point

r_0 = Radius of the focal point

The so-called radius of a gaussian distribution is the distance from the center of the distribution to the point at which the intensity has dropped to $1/e$ times the intensity at the center. The average power of the laser beam is found by integrating the power density over x and y:

$$P = \int_{-\infty}^{+\infty}\int_{-\infty}^{+\infty} J_0 \exp\left(-\frac{\xi^2+y^2}{r_0^2} \right) \partial\xi\, \partial y.$$

89

When the appropriate identities are substituted, we find that:

$$J_0 = \frac{P}{\pi r_0^2}.$$

90

The energy density, which has been defined as the power density integrated only over ξ is given by:

$$\Delta ED = \tfrac{1}{v}\int_{-\infty}^{+\infty} J(\xi,0)\, \partial\xi$$

$$= \tfrac{1}{v}\int_{-\infty}^{+\infty} J_0 \exp\left(-\frac{\xi^2+y^2}{r_0^2} \right) \partial\xi .$$

$$= \frac{J_0}{V} \frac{\sqrt{\pi}}{2} r_0 \left(2 \, erf(\infty) \right)$$

$$= \frac{P}{Vd} \frac{2}{\sqrt{\pi}} .$$

91

where:

d = Spot diameter = $2r_0$.

The simplified variables can be substituted into the expression which was derived for the formation of a kerf at high translation speeds:

$$\Delta D = \frac{1}{V^2 H} \int_{-\infty}^{+\infty} J(\xi, y) \, \partial \xi$$

$$= \frac{\Delta ED}{H}$$

$$= \frac{2}{\sqrt{\pi}} \frac{P}{V d H}$$

92

Since a kerf made with multiple passes of the laser begins at zero depth and increases with each subsequent pass, the depth of cut after n passes of the laser is given by:

$$D_n = \sum_{i=1}^{n} \Delta D_n$$

93

And the cumulative energy density used to produce the cut is:

$$ED_n = \sum_{i=1}^{n} \Delta ED$$

$$= n \Delta ED$$

$$= \frac{2}{\sqrt{\pi}} \frac{nP}{dV} .$$

94

While ED is a quantity which increases monotonously in a stepwise manner over time,

the depth of cut may not.

3.3 Approximate Analyitcal Low-Speed Solutions

To obtain approximate solutions which apply to various heat source geometries, it will be helpful to reformulate the heat balance given in equation 75 using the simplified variables. Consider a control volume, similar to figure 8, which begins at the ablation surface $s(\xi,y)$ and extends arbitrarily far in front of the laser spot. The boundaries of this control volume are determined by the function $s_-(y)$ which corresponds to the contour of the kerf which will be formed when the laser scans over a particular point. For the sake of simplicity, the kerf will be assumed rectangular with a depth D and a width $d = 2r_0$. The laser beam penetrates vertically into the workpiece and melts material to a depth $D + \Delta D$ inside the kerf. The molten material does not accumulate on the workpiece; rather, it is assumed that a gas stream accelerates it out of the kerf before the melted material flows behind the spot. This configuration is illustrated in figure [9]. It is assumed that the laser power is entirely absorbed by the surface $s(\xi,y)$, which constitutes the rear boundary of the control volume.
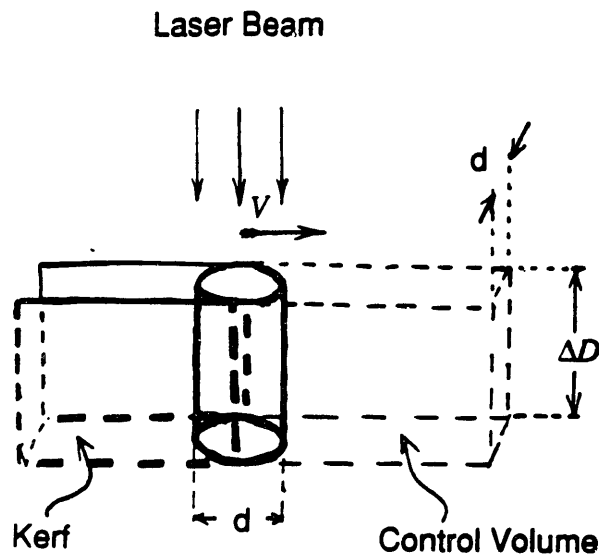
Figure 9. Control volume for approximating heat conduction from a cylindrical ablation surface during laser machining.

The laser must heat the material contained within this control volume to the average temperature at which it is removed from the workpiece. In addition, the laser must supply the heat which is conducted out through the walls of the future kerf into the bulk of the workpiece as a result of the impressed temperature field. This leads to the following heat balance:

$$P = Vd\Delta D \rho C_p(T_{s(\xi,y)} - T_0) + k \int_0^\infty 2\Delta D \left(\frac{\partial T}{\partial y} \right)_{y=d/2} + d \left(\frac{\partial T}{\partial z} \right)_{z=\Delta D} \partial\xi$$

95

It should be noted that when a strong gas nozzle is used to clear molten material from the kerf, the absorbing surface may be assumed to be at the vaporization temperature, and material is removed from the workpiece from a molten boundary layer which exists between the vaporized surface and the melting isotherm. The average temperature of

material removal may be assumed to be

$$T_s = \frac{T_v + T_m}{2}$$

96

The temperature field in the vicinity of the kerf is assumed to be a function of the geometry of the heat source resolved on s(ξ,y) and the translation speed of the workpiece. It has been shown that the quantity

$$\frac{\Delta E D}{H d} = \frac{J}{V H}$$

97

where:

J = Average power density

$H = \rho C_p (T_{s(\xi,y)} - T_0) + L$ = Enthalpy of removal

L = Latent heat melting and/or vaporization

corresponds to the "steepness" of the absorbing surface under the laser spot which is bounded by the inequality

$$\frac{\Delta D}{d} \approx \frac{\partial s}{\partial \xi} \leq \frac{J}{V H}.$$

98

3.4 One-Dimensional solution

The heat source has dimensions of approximately d x d in the ξ-y plane and the extension of the heat source in the z-direction is ΔD. If ΔD is small with respect to d, the spot diameter, the heat source will be concentrated on a nearly level surface (figure [10]) To a first approximation, heat will be conducted vertically into the workpiece. This condition is obtained when

$$\frac{J}{V H} \ll 1.$$

$$J(\xi, y)$$
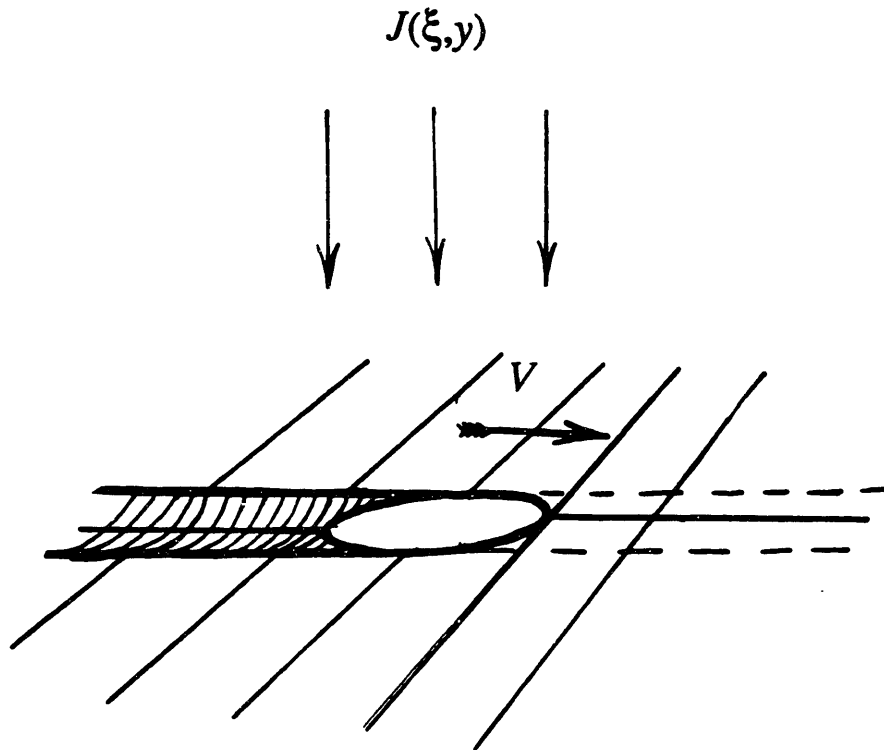
Figure 10. Diagram of kerf formation for small J/VH.

Heat is conducted into the workpiece vertically, and some heat escapes from the ablation surface. To approach this problem, Masters' one-dimensional treatment of a moving ablation front can be used.

The ablation surface is stationary with respect to the laser spot. With respect to a reference point on the workpiece, the ablation front decends vertically at a rate given by

$$\frac{\partial}{\partial t}\left(s(x,y) \right) = V\frac{\partial s}{\partial \xi} \approx V\frac{\Delta D}{d}.$$

The temperature distribution is found by substituting $V\frac{\Delta D}{d}$ for V and $z-s(x,y)$ for x in Masters' solution, equation [15]:

$$T(z) = T_r \exp\left(-\frac{V}{\alpha}\frac{\Delta D}{d}\left(z - s(x,y) - Vt\frac{\Delta D}{d} \right) \right).$$

The quantity of heat contained in this heat wave is constant and equal to

$$Q' = \rho C_p \int_{s(x,y)}^{\infty} T(z)\, \partial z$$

$$= \rho C_p T_s \int_{s(x,y)}^{\infty} \exp\left(-\frac{V}{\alpha}\frac{\Delta D}{d} z\right) \partial z$$

$$= \rho C_p T_s\, \frac{\alpha d}{V \Delta D}$$

$$= \frac{k T_s}{v\left(\frac{\Delta D}{d}\right)} \quad \text{per unit area, or}$$

$$Q' = \frac{d k T_s}{\left(\frac{\Delta D}{d}\right)} \quad \text{over the entire spot per unit time.}$$

This result can be used in the following heat balance:

$$P = \frac{d k T_s}{\left(\frac{\Delta D}{d}\right)} + V H d^2 \left(\frac{\Delta D}{d}\right)$$

where:

$$H = \rho C_p \left(T_s - T_0\right) + L = \text{Enthalpy of removal}$$

The first term on the right side ofg equation [104] is the rate of heat loss by vertical conduction and the second term is the rate of heat delivered to material removal.

Nondimensionalizing,

$$\frac{P}{d^2 V H} = \frac{J}{V H} = \frac{k T_s}{d V H \left(\frac{\Delta D}{d}\right)} + \frac{\Delta D}{d}$$

which is a quadratic in $\frac{\Delta D}{d}$.

$$\left(\frac{\Delta D}{d}\right)^2 - \frac{J}{V H}\left(\frac{\Delta D}{d}\right) + \frac{k T_s}{d V H} = 0 \quad ;$$

$$\frac{\Delta D}{d} = \frac{J}{VH} \pm \sqrt{\left(\frac{J}{VH}\right)^2 - 4\frac{kT_s}{dVH}}$$

107

Since we know that $\frac{\Delta D}{d} \leq \frac{J}{VH}$,

$$\frac{\Delta D}{d} = \frac{J}{VH} - \sqrt{\left(\frac{J}{VH}\right)^2 - 4\frac{kT_s}{dVH}}$$

108

Eliminating $\frac{J}{VH}$ from the expression,

$$\frac{\Delta D}{d} = \frac{J}{VH}\left(1 - \sqrt{1 - 4\left(\frac{dkT_s}{P}\right)}\right).$$

109

This necessarily implies that

$$\frac{dkT_s}{P} < \frac{1}{4}\frac{J}{VH}$$

110

for this solution to be valid. This also implies that

$$\frac{\alpha}{Vd} < \frac{1}{4}\left(\frac{J}{VH}\right)^2$$

111

since

$$\frac{\alpha}{Vd} = \frac{dkT_s}{P} \times \frac{J}{VH}.$$

112

and therefore, if $\frac{J}{VH} \ll 1$, then $\frac{Vd}{\alpha} \gg 1$.

That is a necessary condition for this approximate solution to be valid. It is the same assumption that led to the "adiabatic" solution, but this answer can be considered more accurate when $\frac{J}{VH} \ll 1$ at high translation speeds.

3.5 Two-Dimensional solution

When the quantity $\frac{J}{VH}$ is large compared to unity, the heat source translating through the medium will be very steep and the temperature distribution in the vicinity of the kerf will correspond approximately to that developed by Swift-Hook and Gick [1973] for laser welding. It is a two-dimensional solution for the quasi-stationary temperature distribution around a moving vertical line source in an infinite medium:

$$ T(r,\phi,z) \;=\; \frac{P}{2\pi kz} K_0\!\left(\frac{Vr}{2\alpha} \right) exp\!\left(-\frac{Vr}{2\alpha}cos\phi \right) $$

113

Where:

$\frac{P}{z}$ = Power expended per unit depth

K_0 = Modified Bessel function of second kind of order zero

$r = \sqrt{\xi^2+y^2+z^2}$

and the assumption is made:

$$ \frac{\partial T}{\partial z} \;=\; 0. $$

114

With the temperature distribution defined *a priori* in this way, the heat transferred through the control volume (figure [11]) can be found by evaluating the integral

$$ \int_0^\infty \frac{\partial T}{\partial y} \; \partial\xi $$

115

along the vertical boundaries of the control volume.

$$\int_0^{\infty} \left(\frac{\partial T}{\partial y} \right)_{y=d/2} d\xi$$
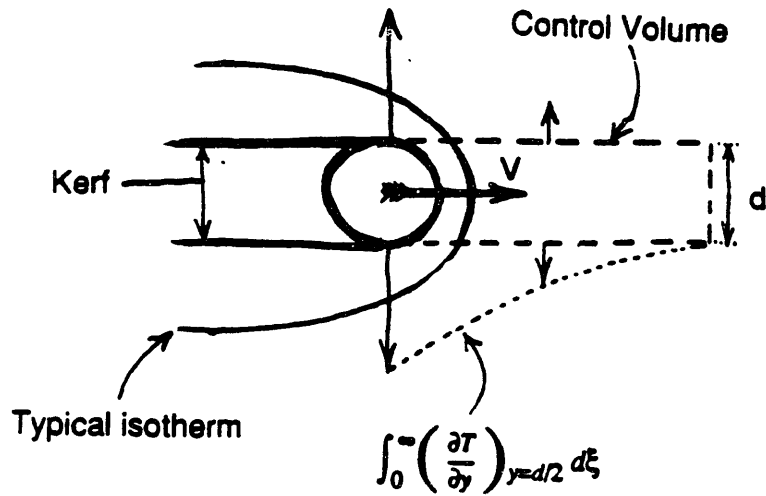
Figure 11. Heat conduction approximation for a vertical cylindrical heat source.

Swift-Hook and Gick supply approximations of the Bessel function for small and large arguments. They are:

for small arguments,

$$K_0 \left(\frac{Vr}{2\alpha} \right) = \ln \left(\frac{2e^{-.577}}{Vr/2\alpha} \right)$$

116

and for large arguments

$$K_0 \left(\frac{Vr}{2\alpha} \right) = \left(\frac{\pi \alpha}{Vr} \right)^{1/2} exp \left(-\frac{Vr}{2\alpha} \right)$$

117

These approximations allow one to evaluate the heat conduction conditions in an

approximate analytic fashion.

The laser is assumed to be a vertical line heat source, and the temperature field is given approximately by one of the above approximations. The quantity $\left(\frac{V_r}{2\alpha}\right)$ is small in regions closer than a distance $\frac{\alpha}{V}$ to the heat source, provided the spot diameter, d, is much smaller than the distance $\frac{\alpha}{V}$. Mathematically,

$$\left(\frac{Vd}{\alpha}\right) << 1.$$

<div align="right">118</div>

This is simply stating that the spot diameter is small comapared with the volume which is affected by heat conduction from the ablation surface.

Since d and α are constant, this condition presumes a slow translation speed which is consistent with the assumption

$$\left(\frac{J}{VH}\right) >> 1$$

<div align="right">119</div>

which is obtained in practice by reducing V and maintaining a high power density.

This condition is necessary to have a vertical line source as the absorbing surface under the laser spot, the conditions modelled by Swift-Hook and Gick. Although it is not strictly necessary for $\frac{Vd}{\alpha} << 1$, the case of $\frac{Vd}{\alpha} >> 1$ and $\frac{J}{VH} >> 1$ corresponds to conditions that may be unobtainable at moderate laser powers, and have alrady been modelled by equation [92]

It is assumed that the material moves under the beam in the feed direction with a velocity V. The material under the laser spot is vaporized to a depth z, forming a cylinder of diameter d equal to the spot diameter of the laser beam. A control volume is defined by the projection of this cylinder in the x-direction in advance of the laser beam,

as shown in figure 9. This control volume corresponds to the future contour of the kerf. Heat is conducted into the control volume through the surface of the vaporized cylinder, and out of the control volume through the lateral walls of the future kerf. These walls extend an arbitrary distance in advance of the laser spot, far enough such that all temperature gradients are negligible. The temperature field in the workpiece is assumed to be quasi-stationary, and is approximated by the following expression:

$$T(\xi,y,z) = \frac{P}{2\pi k \Delta D} exp\left(-\frac{Vr}{2\alpha} cos\phi \right) ln\left(\frac{2e^{-.577}}{Vr/2\alpha} \right).$$

120

When the temperature field is defined using the analytic approximation given above, the temperature gradient in the y-direction can be obtained as

$$\frac{\partial T}{\partial y}(\xi,y,z) = -\frac{P}{2\pi k \Delta D} exp\left(-\frac{V\xi}{2\alpha} \right) \frac{y}{r^2}$$

121

where:

$$\xi = rcos(\phi).$$

This temperature gradient may be integrated along the side walls of the control volume, that is, the future walls of the kerf:

$$\int_0^\infty \left(\frac{\partial T}{\partial y} \right)_{y=d/2} \partial\xi = -\frac{Pd}{4\pi k \Delta D} \int_0^\infty \frac{exp(-V\xi/2\alpha)}{\xi^2+d^2/4} \partial\xi$$

122

This integral has been evaluated by Ryzhik [1965]:

$$\int_0^\infty \frac{e^{-\mu x}}{\beta^2+x^2} \partial x = \frac{1}{\beta}\left(ci(\beta\mu)sin(\beta\mu)-si(\beta\mu)cos(\beta\mu) \right)$$

123

where:

$$\mu = \frac{V}{2\alpha}$$

$$\beta = \frac{d}{2}$$

$ci(x)$ = cosine integral function $= -\int_x^\infty \frac{cos(t)}{t} \, \partial t$

$si(x)$ = sine integral function $= -\int_x^\infty \frac{sin(t)}{t} \, \partial t$

These functions are approximated by the algebraic series:

$$ci(x) \approx C - ln(x) - \frac{x^2}{4} + \frac{x^4}{96} - \ldots$$

124

$$si(x) \approx -\frac{\pi}{2} + x - \frac{x^3}{18} + \ldots$$

125

and a graph of the function

$$\left(ci(\beta\mu) sin(\beta\mu) - si(\beta\mu) cos(\beta\mu) \right)$$

126

is shown in figure [12]

Substituting this into the heat balance (equation [95]) for a single pass we obtain

$$P = Vd \Delta D \rho C_p (T_s - T_0) + \frac{P}{\pi}\left(ci\left(\frac{Vd}{4\alpha}\right) sin\left(\frac{Vd}{4\alpha}\right) - si\left(\frac{Vd}{4\alpha}\right) cos\left(\frac{Vd}{4\alpha}\right) \right)$$

127

and

$$\frac{\Delta D}{d} = \frac{J}{VH}\left[1 - \frac{1}{\pi}\left(ci\left(\frac{Vd}{4\alpha}\right) sin\left(\frac{Vd}{4\alpha}\right) - si\left(\frac{Vd}{4\alpha}\right) cos\left(\frac{Vd}{4\alpha}\right) \right) \right] \, .$$

128

Figure 12. [ci(x)sin(x)-si(x)cos(x)] vs. x for 0<x<1.

If we apply the assumption that $\frac{Vd}{\alpha} \ll 1$ the term contained in the square brackets above is approximately equal to @$quad 1 - \frac{1.7}{\pi} \approx 0.46$. This is almost exactly the solution obtained by Swift-Hook and Gick for the same conditions (equation[56]).

In summary, the following approximate analytical solutions have been obtained which apply to a single pass cut:

For $\frac{Vd}{\alpha} \gg 1$; $\frac{J}{VH} \gg 1$:

$$\frac{\Delta D}{d} = \frac{J}{VH} \quad .$$

$$129$$

For $\frac{Vd}{\alpha} \gg 1$; $\frac{J}{VH} \ll 1$; $\frac{\Delta D}{d} \ll 1$:

$$\frac{\Delta D}{d} = \frac{J}{VH}\left(1 - \sqrt{1 - 4\left(\frac{dkT_r}{P}\right)} \right) \quad .$$

$$130$$

For $\frac{Vd}{\alpha} \ll 1$; $\frac{J}{VH} \gg 1$:

$$\frac{\Delta D}{d} = \frac{J}{VH}\left[1 - \frac{1}{\pi}\left(ci\left(\frac{Vd}{4\alpha}\right) \sin\left(\frac{Vd}{4\alpha}\right) - si\left(\frac{Vd}{4\alpha}\right) \cos\left(\frac{Vd}{4\alpha}\right) \right) \right] \approx 0.46\frac{J}{VH} \quad .$$

$$131$$

3.6 Two-Dimensional Solution for Multiple Passes

In formulating a model for multiple pass cutting, one must consider the limit as the depth of cut becomes very large with respect to the depth of focus of the objective. The laser beam diverges according to the ratio

$$d_{eff} = \frac{a_0 D}{f}$$

$$132$$

where:

d_{eff} = Effective spot diameter a depth D below focal point

a_0 = Diameter of the unfocused laser output beam

f = Focal length of the objective lens.

Reflections will tend to refocus the beam in the y direction, so to first approximation to the power resolved on the bottom of the kerf will be the same, but the spot will be spread along the bottom of the kerf to a length $\frac{a_0 D}{f}$ and the power density will be accordingly

$$J_{eff} = \frac{P}{d \times d(D)} = \frac{Pf}{d a_0 D}$$

133

where:

J_{eff} = Power density resolved on the kerf bottom.

This means that for deep cuts, $\frac{J}{VH}$ tends necessarily to a low value regardless of the translation speed, and the heat source becomes similar to a horizontal line moving lengthwise through an infinite medium.

This condition may be evaluated similarly to the previous condition where $\frac{J}{VH} \ll 1$, except by evaluating in two dimensions instead of one.

The temperature field will be radially symmetric about the heat source. Consider a control volume which extends arbitrarily in front of, to the sides of and below the heat source, and terminates immediately behind the source. Material flowing into the control volume is assumed to be at ambient temperature, and material leaving the control volume is either material removed from the bottom of the kerf at a temperature of T_r or as heated material in the vicinity of the kerf. This is illustrated in figure [13].

The heat balance for this control volume becomes

$$P = \Delta D \, d \, V \, H + V \rho \, C_p \int_{-\infty}^{+\infty} \int_{-\infty}^{+\infty} T \left(-\frac{a_0 D}{2f}, y, z \right) \partial y \, \partial z \,.$$

134

The moving horizontal line source creates a temperature field which is radially symmetric in the y-z plane and nearly corresponds to the field in two dimensions from

$$T(y,z) = T_r \exp\left(-\frac{y^2+z^2}{4\alpha \bar{t}}\right)$$
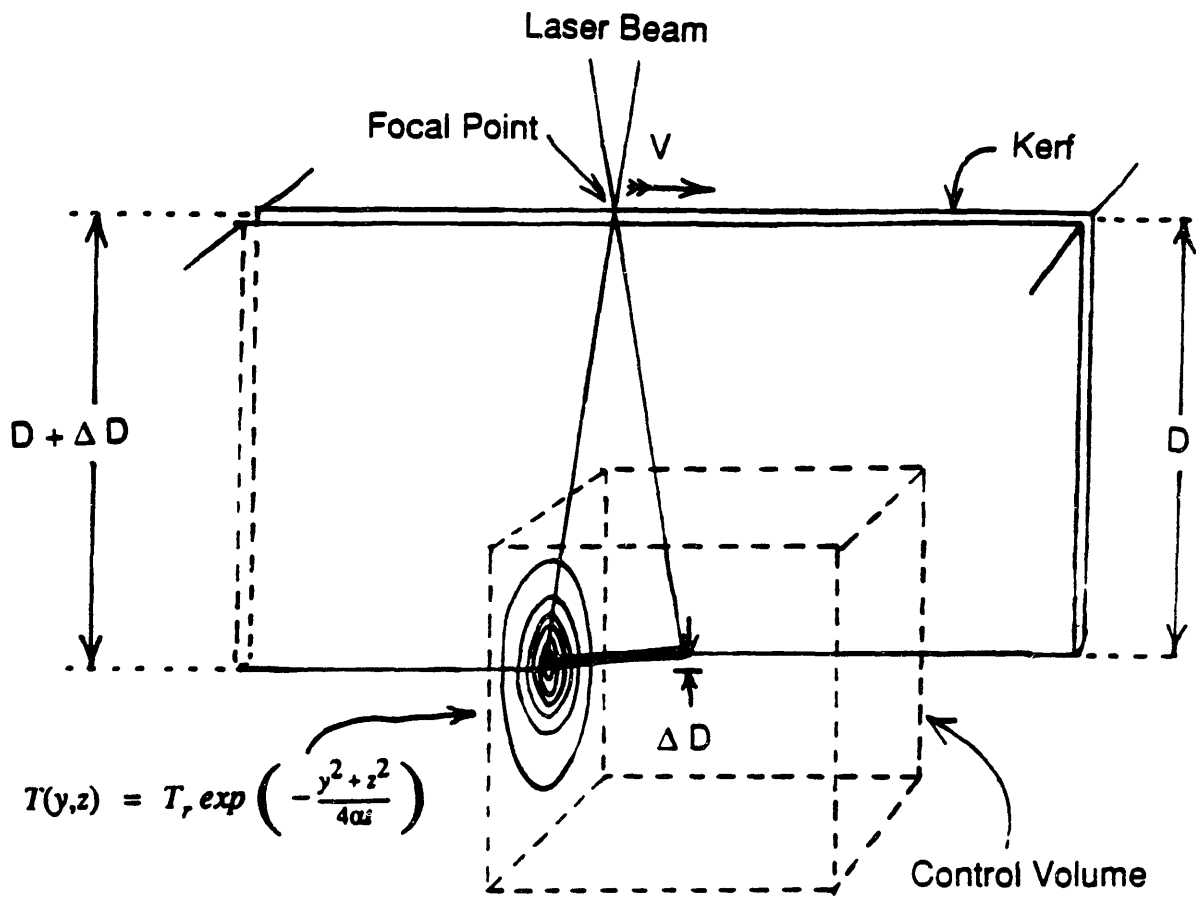
Figure 13. Heat conduction approximation for deep kerf formation.

the transient heating by a point source which appears at t=0 and is terminates at time t= $\frac{a_0 D}{Vf}$.

This temperature field is given analytically by

$$T(y,z) = T_s \exp \left(-\frac{y^2+z^2}{4\alpha t} \right)$$

135

where $t = \frac{a_0 D}{Vf}$.

Therefore, the integral

$$\int_{-\infty}^{+\infty} \int_{-\infty}^{+\infty} T \, \partial y \, \partial z = 4\pi\alpha t T_s = 4\pi T_s \frac{\alpha}{V} \frac{a_0 D}{f}$$

136

and the heat balance becomes

$$P = \Delta D \, dV H + V H 4\pi \frac{\alpha}{V} \frac{a_0 D}{f}$$

137

$$\frac{\Delta D}{d} = \frac{P}{d^2 V H} - \frac{4\pi a_0}{f} \frac{\alpha}{Vd} \frac{D}{d}$$
$$= \frac{J}{VH} - \frac{4\pi a_0}{f} \frac{\alpha}{Vd} \frac{D}{d}$$

138

where:

J = Power density at the focal point

$$\frac{J}{VH} = \frac{\Delta ED}{Hd} .$$

This predicts that a kerf using multiple passes must asymptotically approach a depth given by

$$\frac{J}{VH} = \frac{4\pi a_0}{f} \frac{\alpha}{Vd} \frac{D}{d}$$

139

$$\frac{D}{d} = \frac{f}{4\pi a_0} \frac{J}{VH} \frac{Vd}{\alpha}$$

$$= \frac{f}{4\pi a_0} \frac{P}{dkT_r} \ .$$

$$\text{140}$$

If this is regarded as a nearly continuous function,

$$\frac{\Delta D}{d} \quad = \frac{\partial}{\partial n}\left(\frac{D}{d}\right) = \frac{J}{VH} - \frac{4\pi a_0}{f} \frac{\alpha}{Vd} \frac{D}{d} \ ,$$

$$\text{141}$$

Then the solution is

$$\frac{D}{d} = \frac{f}{4\pi a_0} \frac{Vd}{\alpha} \frac{J}{VH} \left(1 - exp\left(-\frac{4\pi a_0}{f} \frac{\alpha}{Vd} n\right)\right) \ .$$

$$\text{142}$$

With an approximate analytic expression for depth of kerf as a function of laser power, surface speed, number of passes, and so on, it is now possible to estimate the variation of the cutting rate under different conditions. The most important question is: using a given power and spot size, how can one adjust the surface speed to give one the fastest approach to the maximum depth?

From the previous analysis, the greatest depth increment was obtained at high translation speeds such that heat did not diffuse far from the laser spot.

The cutting time in a multiple pass cut is proportional to $\frac{n}{V}$. Looking to the solution for depth increment for large $\frac{Vd}{\alpha}$ and small $\frac{J}{VH}$,

$$\frac{\Delta D}{d} = \frac{J}{VH}\left(1 - \sqrt{1 - 4\left(\frac{kT_r}{dVH} \frac{VH}{J}\right)}\right) \ .$$

$$\text{143}$$

For small n,

$$\frac{D}{d} = \frac{n\Delta D}{d} = \frac{nJ}{VH}\left(1 - \sqrt{1 - 4\left(\frac{kT_r}{dVH} \frac{VH}{J}\right)}\right) \ .$$

$$\text{144}$$

As the aspect ratio of the cut becomes large, the laser spot diverges and the cutting

rate will approach that predicted by the equation

$$\frac{D}{d} = \frac{f}{4\pi a_0} \frac{Vd}{\alpha} \frac{J}{VH} \left(1 - exp\left(-\frac{4\pi a_0}{f} \frac{\alpha}{Vd} n \right) \right) .$$

145

If V is varied while holding $\frac{n}{V}$ constant, the argument of the exponential is not changed. This suggests that the depth of cut will approach its asymptotic value of

$$\frac{D}{d} = \frac{P}{d k T_s} \frac{f}{4\pi a_0}$$

146

at the same rate independent of the surface speed.

If the spot diameter is increased, the asymptotic depth increases proportionally. Since the laser power is distributed over a larger spot, the power density decreases, and the cutting rate decreases in the same proportion.

If the laser power is increased, the asymptotic depth increases, and since the power density increases, the cutting rate increases.

This concludes the analytical modelling effort of this thesis. This effort was undertaken to gain qualitative insight into the variation of cutting rate with the several major process parameters. The method used was to evaluate the geometry of heat conduction in the workpiece for different extremes of cutting parameters. Approximate analytical solutions were introduced which for the most part were gleaned from previous modelling efforts in the literature dealing with laser materials processing.

Because of the approximate approach, numerical accuracy of model predictions with experimental results is not expected. Numerous well-documented phenomena which substantially affect laser cutting have been deleted from consideration for the sake of simplicity. Several of these include: vaporization of workpiece material, reflection of laser light, exothermic reactions between the workpiece and gas jet, convective heat transfer from the gas jet, refraction of the laser beam by shock waves in the gas jet. All of these phenomena contribute to the cutting process, however they are beyond the scope of this modelling effort.

These models can be used to illustrate the geometry of heat conduction in laser machining. Qualitative conclusions based on these models are the following.

The most advantageous coditions for blind cutting are those in which the laser radiation is absorbed on a nearly vertical surface, corresponding to the model derived in section 3.5. This is obtained at relatively low translation speeds. The model indicates a weak dependence on surface speed, as long as the speed is sufficiently low to allow a deep laser penetration.

The conclusion from section 3.2 is that higher speeds improve the cutting rate. It would be desirable to increase the cutting speed while maintaining a deep laser penetration, however without increasing the laser power the deep penetration is lost. If increased laser power density is available, i.e. through pulsing, then a higher surface speed may be used, thereby incerasing the energy efficiency.

A final conclusion is that there is a strong tendency for a very deep kerf to asymptotically approach a maximum depth, and it is necessary to define a criterion for determining the proper depth of cut for the laser lathe which optimizes the manufacturing rate.

This criterion has been derived in a rigorous and exact way based on the unique geometry of the converging beam cutting tool.

3.7 Numerical Simulation of Laser Cutting

In order to determine the dominant effects in laser machining, a numerical simulation of the process was attempted. Using a finite-difference method the heat conduction in the vicinity of a moving vaporization cavity was modelled in alumina. A two-dimensional model was used to simulate the conditions modelled analytically by Swift-Hook and Gick and others. In the previous section, an analytical approximation was developed assuming a slow translation speed and a point source. Since the heat source has a finite diameter, the numerical approach was used to calculate heat conduction near to a moving laser-supported vaporization cavity. This program is included in Appendix IV.

The program operates in three stages. First, the temperature field is calculated using a coarse array of 5 x 10 entries for a chosen number of iterations. The temperatures are then interpolated onto the fine grid, and the iterations continue a chosen number of times. Finally, the temperature gradient is integrated along a line to evaluate the heat conduction away from the future kerf.

Beginning with the two-dimensional form of the quasi-stationary heat equation,

$$\alpha \left(\frac{\partial^2 T}{\partial \xi^2} + \frac{\partial^2 T}{\partial y^2} \right) = -V \frac{\partial T}{\partial \xi},$$

$$147$$

the temeperature derivatives are approximated using the following differences:

$$\frac{\partial^2 T}{\partial \xi^2} + \frac{\partial^2 T}{\partial y^2} \approx \frac{1}{h^2} \left[-T_{i,j} + \frac{1}{5} \left(T_{i-1,j} + T_{i+1,j} + T_{i,j-1} + T_{i,j+1} \right) + \right.$$
$$\left. + \frac{1}{20} \left(T_{i-1,j-1} + T_{i+1,j-1} + T_{i-1,j+1} + T_{i+1,j+1} \right) \right]$$

$$148$$

and

$$\frac{\partial T}{\partial \xi} \approx \frac{1}{h} T_{i-1,j} - T_{i,j}$$

$$149$$

where:

h = Grid spacing

$T_{i,j}$ = Temperature of element i,j

$\alpha = \frac{k}{\rho c_p}$ = Thermal diffusivity.

The quasi stationary difference equation is

$$-T_{i,j} + \tfrac{1}{5}\left(T_{i-1,j} + T_{i+1,j} + T_{i,j-1} + T_{i,j+1}\right) + \tfrac{1}{20}\left(T_{i-1,j-1} + T_{i+1,j-1} + T_{i-1,j+1} + T_{i+1,j+1}\right) =$$
$$= -V h\left(T_{i-1,j} - T_{i,j}\right)$$

150

The temperature at a given location for a given iteration is found in the following way:

$$T_{i,j}^{new} = \tfrac{1}{5}\left(T_{i-1,j}^{old} + T_{i+1,j}^{old} + T_{i,j-1}^{old} + T_{i,j+1}^{old}\right) + \tfrac{1}{20}\left(T_{i-1,j-1}^{old} + T_{i+1,j-1}^{old} + T_{i-1,j+1}^{old} + T_{i+1,j+1}^{old}\right) -$$
$$- V h\left(T_{i-1,j}^{old} - T_{i,j}^{old}\right)$$

151

The heat source is supplied by the boundary conditions. The boundary conditions also provide for reflection on the axis of symmetry and continuity at the boundaries. These are obtained in the following ways:

$$T_{i,j} = T_s \quad \text{for} \quad \sqrt{(i-i_{spot})^2 + j^2} \le \tfrac{d}{2h} \; ;$$

152

$$T_{i,j-1} = T_{i,j} \quad \text{for} \quad j = 1;$$

153

$$h\frac{\partial T}{\partial \xi} \approx T_{i,j} - T_{i+1,j} \quad \text{for} \quad i = 1;$$

154

$$h^2 \left(\frac{\partial^2 T}{\partial \xi^2} + \frac{\partial^2 T}{\partial y^2} \right)_{i,j} = -T_{i,j}^{new} + \frac{1}{5} \left(T_{i,j}^{old} + T_{i+1,j}^{old} + T_{i,j-1}^{old} + T_{i,j+1}^{old} \right) +$$
$$+ \frac{1}{20} \left(2\,T_{i,j}^{old} + T_{i+1,j-1}^{old} + T_{i+1,j+1}^{old} \right) \quad for \quad i = 1 \quad ;$$

155

$$h^2 \left(\frac{\partial^2 T}{\partial \xi^2} + \frac{\partial^2 T}{\partial y^2} \right)_{i,j} = -T_{i,j}^{new} + \frac{1}{5} \left(T_{i-1,j}^{old} + T_{i,j}^{old} + T_{i,j-1}^{old} + T_{i,j+1}^{old} \right) +$$
$$+ \frac{1}{20} \left(T_{i-1,j-1}^{old} + 2\,T_{i,j}^{old} + T_{i-1,j+1}^{old} \right) \quad for \quad i = 50 \quad ;$$

156

$$H^2 \left(\frac{\partial^2 T}{\partial \xi^2} + \frac{\partial^2 T}{\partial y^2} \right)_{i,j} = -T_{i,j}^{new} + \frac{1}{5} \left(T_{i-1,j}^{old} + T_{i+1,j}^{old} + T_{i,j-1}^{old} + T_{i,j}^{old} \right) +$$
$$+ \frac{1}{20} \left(T_{i-1,j-1}^{old} + T_{i+1,j-1}^{old} + 2\,T_{i,j}^{old} \right) \quad for \quad j = 25 \quad ;$$

157

and

$$\left(\frac{\partial^2 T}{\partial \xi^2} + \frac{\partial^2 T}{\partial y^2} \right)_{i,j} = 0 \quad \text{at the corners.}$$

158

After calculating the temperature field using this algorithm, which must be repeated through several hundred iterations to converge, the program calculates the integral

$$\int_0^\infty \left(\frac{\partial T}{\partial y} \right)_{y=d/2} \partial \xi$$

159

by approximating the derivative

$$-\frac{\partial T}{\partial y} \approx \frac{1}{h}\left(T_{i,j} - T_{i,j+1}\right)$$

160

and adding the contributions for $j = \frac{d}{2h}$ and every $i > i_{spot}$.

Using the heat balance derived previously,

$$P = Vd\Delta D\rho C_p(T_{s(\xi,y)} - T_0) + \int_0^\infty 2k\Delta D\left(\frac{\partial T}{\partial y}\right)_{y=d/2} \partial\xi ,$$

161

the depth of a single pass cut can be predicted for relatively low translation speeds. Recall that for this two-dimensional approximation to be valid, the condition

$$\frac{J}{VH} = \frac{ED}{Hd} \gg 1$$

162

must apply. For alumina with a laser power of 1000 W and a spot diameter of 0.016 cm, this requires V ≪ 30 cm/sec for this approximation to be valid. Since alumina was cut at translation speeds as low as 0.5 cm/sec, predictions may be compared to experimental data.

Figure [14] shows predictions of depths of single-pass kerfs obtained from this numerical simulation compared to experimental data for alumina. Figure [15] shows a similar comparison made for mild steel.

These numerical simulations predict cuts which are approximately five to ten times deeeper than those which are obtained in practice. Therefore, heat conduction is not the only significant heat loss in laser cutting. In steel, one can assume that there is some reflection of laser radiation from the kerf. In section 5.6.4, the reflectivity of steel was found to be approximately 1/2 from a blind kerf. If significant amounts of material were evaporated from the kerf, this discrepancy could perhaps be explained.
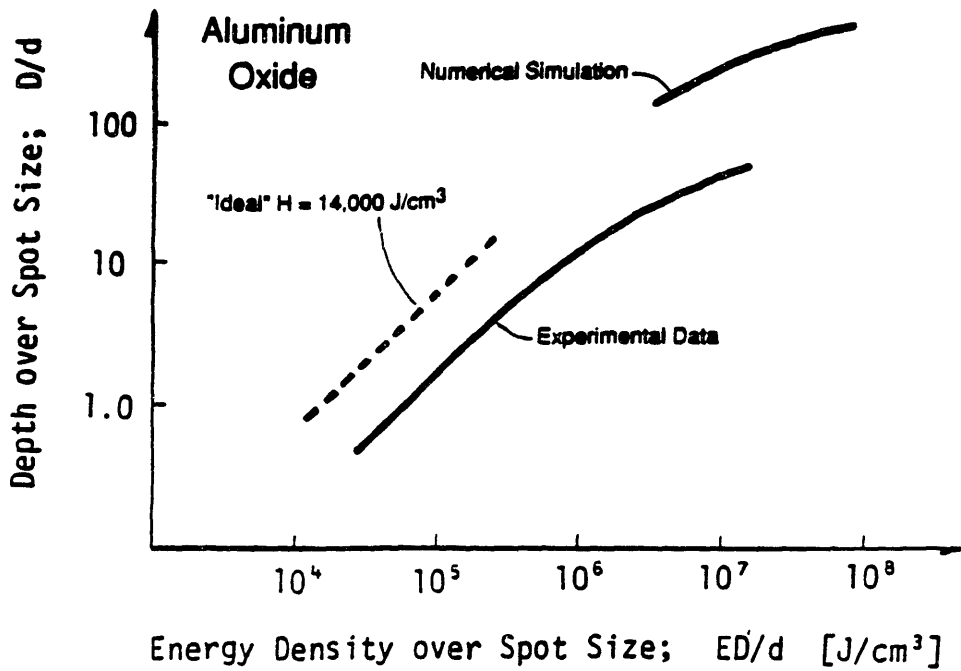
Figure 14. Comparison between experimental data and a numerical simulation of laser blind cutting of Al_2O_3.
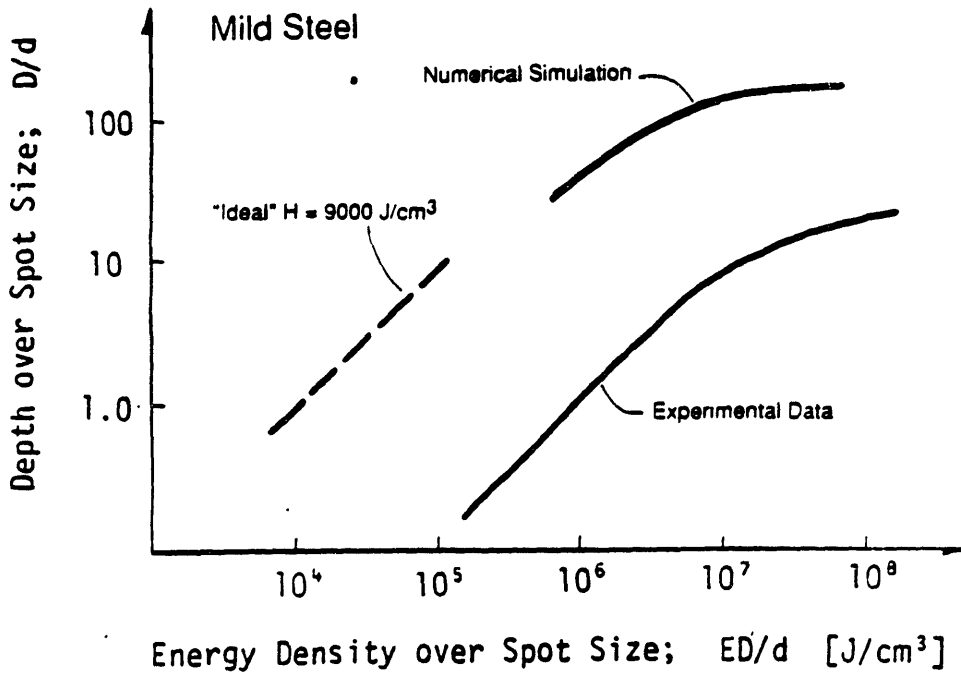
Figure 15. Comparison between experimental data and a numerical simulation of laser blind cutting of mild steel.

It should be noted that this numerical approximation is applied to a certain special case in which the laser penetrates to a depth of several times its focused diameter in a kerf formed in a single pass. The other significant conditions are those in which the laser penetrates to a depth approximately equal to its diameter, and in which the laser forms a kerf in multiple passes.

4. OPTIMIZATION OF THE LASER LATHE

4.1 Material Removal Rate

The laser lathe promises to overcome the limitations of laser macromachining in terms of energy efficiency and contouring capability. The improvement in energy efficiency is based on the fact that material is sectioned from the workpiece without having been melted by the laser. Heat from the laser is directed to making deep, intersecting kerfs in the most efficient way possible. Although it greatly enhances the contouring capability of lasers, the importance of this process would be greatly limited if the material removal rate (MRR) were not sufficiently high for industrial applications.

In conventional laser machining, the material removal rate is defined as the rate at which volumes of material are removed from the workpiece by melting and vaporization. This definition equates the material removal rate with the volume of a single kerf divided by the time it takes to form it. This quantity is hereafter referred to as the "kerf MRR":

$$MRR_k = \frac{Kerf\ Volume}{time} = wD\frac{V}{n}$$

163

where:

MRR_k = Kerf material removal rate

w = Width of kerf

D = Depth of kerf

V = Surface speed

n = Number of laser scans to form kerf

In the case of the converging beam cutting tool, the total quantity of material removed exceeds the volumes of the kerfs by a few orders of magnitude. A single cutting operation of the laser lathe can be thought of as the sectioning of a single ring from the

workpiece. During the operation, two kerfs are made in the workpiece along different planes. Since the two kerfs must intersect along a line, the depths of the two kerfs must be known in advance, so the two beams can be placed the right distance apart on the workpiece. This is illustrated in figure [16]. The two laser beams are hereafter named according to their orientation to the workpiece during orthogonal-beam turning. The "axial beam" is oriented parallel to the axis of a cylindrical workpiece, and the "radial beam" is oriented perpendicular to the axis, such that the beam would intersect the axis if the workpiece were entirely cut off.

$$P_a = f\ P_T$$

$$P_r = (1-f)\ P_T$$

```
ω  = Workpiece angular speed
R_k = Initial radius of workpiece
LB_a = Axial laser beam          P_a = Power carried by LB_a
LB_r = Radial laser beam         P_r = Power carried by LB_r
P_T = Total Power                D_a = Axial depth of cut
f  = Fraction of P_T in LB_a     D_r = Radial depth of cut
```
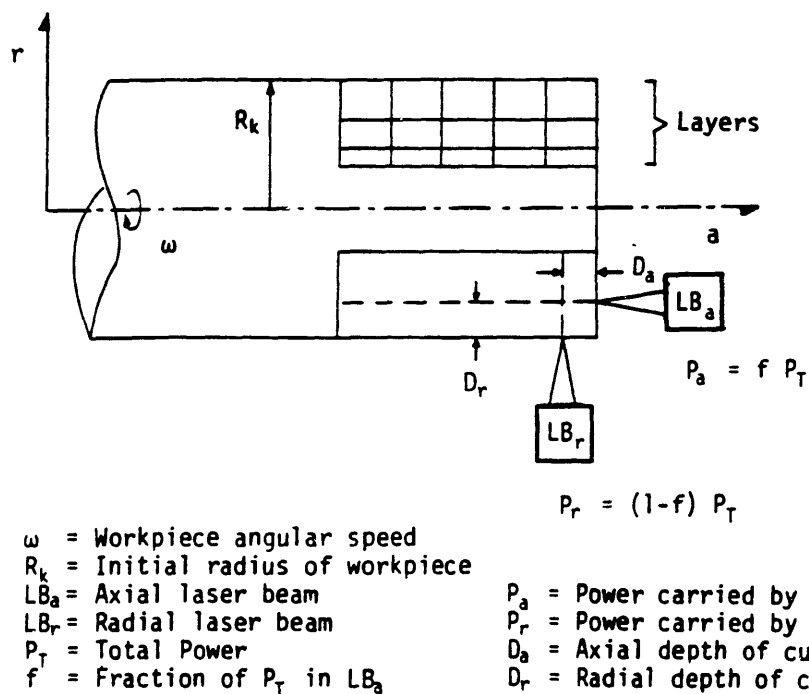
Figure 16. Machining parameters of the laser lathe.

The two beams, axial and radial, make axial and radial kerfs in the workpiece with depths D_a and D_r, respectively. The requirement that the two kerfs intersect means that the axial beam must strike a workpiece of radius R_0 at a distance R_0-D_r from the central axis. Similarly, the radial beam must be aimed to cut off a length D_a from the workpiece. A material removal rate for a single ring, the "ring MRR", can be defined:

$$MRR_r = \frac{Ring\ Volume}{time} = \frac{V}{nR_0}D_a D_r \left(R_0 - \frac{D_r}{2} \right) .$$

<div align="right">164</div>

It should be noted that in this expression, the width of the kerfs does not appear. The assumption has been made that the kerfs are substantially deeper than they are wide, which is the case in laser turning. Therefore, the depth of cut and the time to make the cuts are the only parameters which are considered when optimizing the material removal rate. The width of a cut figures indirectly into the opimization because it affects the energy efficiency, and therefore the cutting rate.

When the radius of the workpiece is allowed to approach infinity, this expression becomes applicable to rectangular milling:

$$MRR_m = \frac{V}{n}D_1 D_2$$

<div align="right">165</div>

where:

MRR_m = Material removal rate for milling

D_1, D_2 = Depths of intersecting kerfs

During a machining job, several rings will be removed sequentially from the workpiece. The diameter of the workpiece will change, and consequently the volume of a given ring, as well as the time to remove it, will not remain constant. Therefore, the "total MRR" is defined as the total volume removed in the job, divided by the total cutting time:

$$MRR_{total} = \frac{\sum_{i=1}^{q} v_i}{\sum_{i=1}^{q} t_i}$$

<div align="right">166</div>

where:

$$V_i = \text{Volume of a given ring} = 2\pi D_a D_r \left(R_i - \frac{D_r}{2} \right)$$

R_i = Outer radius of ring being cut

t_i = Time to form the axial and radial cuts

q = Number of rings cut during operation

4.2 The Cutting Efficiency Factor

While the volume of material to be removed in a laser turning or milling operation is very easily evaluated, the time necessary to perform the operation is by no means clear. Since a comprehensive theoretical model to predict the cutting rate in laser blind cutting does not accurately predict actual behavior, it is necessary to use information gathered from experimentation to predict the optimum machining parameters and maximize the total MRR.

It is possible to predict the material removal rate for the converging beam cutting tool using experimental data from single beam blind cuts. To do this, a simplified model of laser cutting is introduced.

It has been predicted analytically in the preceeding chapter of this thesis that under certain conditions, the heat delivered by the laser to the workpiece does not escape from the vicinity of the cutting front. When this phenomenon occurs (at least theoretically) the depth of cut increases according to the rate of heat input:

$$\Delta D = \frac{\Delta ED}{H}$$

167

where:

ΔD = Increase in depth of cut on a given laser scan

ΔED = Increment of energy applied per unit area of laser trace

H = Enthalpy of removal

This condition must be regarded as an idealized behavior which may never in practice be obtained. Nevertheless, it can be used to predict an "ideal" kerf MRR:

$$MRR_{k, ideal} = w \, V \, \Delta D$$
$$= w \, V \frac{\Delta ED}{H} \, .$$

168

Substituting

$$\Delta ED = \frac{2}{\sqrt{\pi}} \frac{P}{dV}$$

169

into the expression for the 'ideal' kerf MRR,

$$MRR_{k, ideal} = \frac{2}{\sqrt{\pi}} \frac{P}{H} \frac{w}{d} \, .$$

170

This is compared to the actual kerf MRR which has been defined as

$$MRR_{k, actual} = w \, D \frac{V}{n}.$$

171

To express the actual behavior in terms of the ideal behavior, a function is introduced called the "cutting efficiency factor", η.

$$\eta = \frac{MRR_{k, actual}}{MRR_{k, ideal}} = \frac{\sqrt{\pi}}{2} H D \frac{dV}{nP}$$
$$= \frac{HD}{ED}$$
$$= \frac{D}{d} \frac{VH}{nJ}$$

This expression can be solved for the depth of cut in terms of energy density,

$$D = \eta \frac{ED}{H}.$$

The cutting efficiency factor, η, is a dimensionless quantity which must always be greater than or equal to zero. When the laser beam is the only source of energy to the material, η must be less than or equal to one.

In the section dealing with the analytical modelling of the process, several dimensionless groups have appeared. The dimensionless efficiency factor η can be determined experimentally or derived theoretically as a function of these dimensionless groups.

The dimensionless groups are:

$$\frac{P}{HVd^2} = \frac{\Delta ED}{Hd} = \text{Dimensionless ED increment}$$

$$= \frac{J}{VH} = \text{Steepness of ablation surface}$$

$$\frac{D}{d} = \text{Dimensionless depth} = \text{Aspect ratio}$$

$$n = \text{Number of laser scans} = \frac{ED}{\Delta ED}$$

$$\frac{Vd}{\alpha} = \text{Dimensionless heat diffusion distance}$$

$$\frac{P}{dkTr} = \frac{J}{VH} \frac{Vd}{\alpha} \quad \text{Ratio of power density to thermal conductance of the workpiece}$$

$$\frac{f}{a_0} = \text{Divergence ratio of the objective lens}$$

where:

P = Laser power (CW mode)

$H = \rho C_p T_s + L$ = Enthalpy of removal

V = Translation speed

d = Diameter of focused laser spot

D = Depth of cut

n = Number of laser scans

k = Thermal conductivity

$\alpha = \frac{k}{\rho C_p}$ = Thermal diffusivity

T_s = Temperature at which material is removed from the workpiece

f = Focal length of objective lens

a_0 = Diameter of unfocused laser beam.

Of these dimensionless groups, the following four are of particular interest because of their importance to the modelling.

1. $\frac{J}{VH}$ has been seen before. In the analytical model presented earlier, it was found to be equal to $\frac{\partial v}{\partial \xi}$ under conditions where heat is contained in the vicinity of the kerf. In qualitative terms, it determines the "steepness" of the cutting front, and therefore the geometry of the heat source resolved on the absorbing surface. A small value of this parameter means that the depth increment per pass is small, and the heat source is nearly horizontal. A large value means that the heat source is nearly vertical.

2. $\frac{Vd}{\alpha}$ has also been seen before. It corresponds to a distance scale in the material which balances the spot size against a characteristic heat conduction distance for the translation speed used. If the quantity is large, the temperature field for a quasi-stationary heat source is compressed close to the absorbing surface. If the quantity is

small, the heat diffuses further from the heat source, and therefore conduction losses are greater.

3. $\frac{P}{dkT_s}$ is essentially identical with one of the dimensionless groups formulated by Hablanian in 1962. Although it is not dimensionally independent from the previous two groups, it is significant because it is proportional to the asymptotic limit depth for a multiple pass kerf derived previously (equation[140]).

4. $\frac{D}{d}$ is roughly equivalent to the aspect ratio of the kerf. During a single cutting operation, the only parameters which change as the cut progresses are n and D. Any variation in η during the operation must therefore be due to the variation of η with depth. As the cut becomes deeper, the bottom of the cut moves further from the focal point, and the area of the side walls of the kerf increase leading to greater heat dissipation.

In the definition of energy density using the variables P, d, V, and n, the constant factor of $\frac{2}{\sqrt{\pi}} = 1.12$ will be ignored. Furthermore, the width of cut will be assumed to be equal to the spot size. This has been found experimentally to be a good approximation.

By introducing these assumptions into the definition of the kerf MRR one obtains

$$MRR_{k\ actual} = \eta \frac{P}{H}.$$

<div align="right">174</div>

Using the approximate model derived theoretically in section 3.4,

$$\eta = \frac{1}{4\pi n} \frac{f}{a_0} \frac{V_d}{\alpha} \left(1 - exp \left(-4\pi n \frac{a_0}{f} \frac{\alpha}{V_d} \right) \right).$$

<div align="right">175</div>

If η is to be determined experimentally, it is calculated from the formula

$$\eta = \frac{HD}{ED}.$$

A cut is made in the material in question and its depth is measured. The depth is multiplied by the quantity H, the "enthalpy of removal" which includes the sensible and latent heat, and is a property of the material and the nature of the laser/material interaction. This is divided by the energy density used to form the cut, and the result is the value of η which corresponds to the various machining parameters. H can be estimated theoretically by estimating a temperature at which the material is removed from the workpiece:

$$H_{theo.} = \frac{\int_{T_0}^{T_s} \rho C_p(T) \partial T + \sum L}{1 - R_\lambda}$$

where:

T_0 = Ambient temperature

T_s = Assumed removal temperature

$\rho C_p(T)$ = Specific heat/unit volume as a function of temperature

$\sum L$ = Sum of latent heats of phase changes between T_0 and T_r at atmospheric pressure.

R_λ = Surface reflectivity of the workpiece at 10.6 μm.

The two quantities which give the most uncertainty to this definition are the temperature of material removal and the surface reflectivity. The temperature may be the melting point, the vaporization point, or some other temperature; and may not be constant over time. The reflectivity varies with temperature, as well as surface orientation. Therefore, the theoretical value of H can only be approximate, and it may be desirable to obtain H experimentally from cutting data.

To estimate the value of H from experimental data, the following definition is used:

$$H = \lim_{D \to 0} \frac{P}{MRR_{k,\,actual}}$$

$$= \lim_{D \to 0} \frac{nF}{D\,w\,V}$$

$$= \lim_{D \to 0} \frac{ED\,w}{D\,d}$$

<div align="right">178</div>

The quantity w/d is assumed to be unity, and so

$$H = \lim_{D \to 0} \frac{ED}{D}.$$

<div align="right">179</div>

Therefore, H can be found experimentally by performing a series of cuts with different energy densities and extrapolating the ratio of depth and energy density to zero depth. This is equivalent to assuming that η is equal to unity at zero depth and using H as a constant which incorporates the unknown effects of reflectivity and the temperature at the absorbing surface under the laser spot. In principle, H need not be invariant with different machining parameters, but it can be assumed to be nearly constant over a finite range of power, surface speed and spot size.

Although it may seem at this point that many approximations have been introduced to the model, it will be shown at the end of this chapter that the optimum material removal rate is determined by the geometry of the cutting tool, and is wholly independant of any arbitrarily defined constants.

4.3 Optimization of the Cutting Tool

By defining the depth of cut in terms of the energy density and the cutting efficiency factor, it is possible to obtain an expression for the optimum depth of cut which gives the maximum total MRR for the dual beam cutting tool. To reiterate, the total MRR has been defined thus:

$$MRR_{total} = \frac{\sum_{i=1}^{q} V_i}{\sum_{i=1}^{q} t_i}$$

180

where:

V_i = Volume of a given ring = $2\pi D_a D_r \left(R_i - \frac{D_r}{2} \right)$

R_i = Outside radius of the ring being cut

t_i = Time to form the ring

$q = l \times m$ Number of rings cut during operation.

$\sum_{i=1}^{q} V_i$ can be evaluated if one assumes that the rings are cut in the manner illustrated in figure [17]. The two depths D_a and D_r are assumed to be invariant throughout the operation, and the entire volume to be removed is sectioned in m layers and l rows such that $l \times m = q$. The volume of the hollow cylinder to be removed is

$$\sum_{i=1}^{q} V_i = l D_a \left(\pi R_0^2 - \pi (R_o - m D_r)^2 \right)$$
$$= q D_a D_r \pi (2R_o - m D_r)$$

181
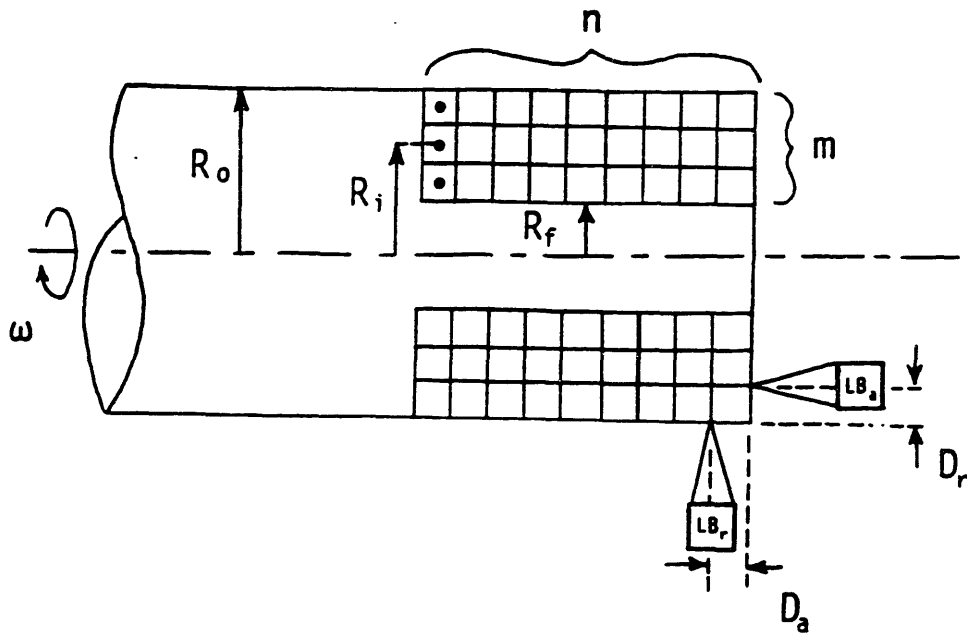
Figure 17. Nomenclature for the optimization of the laser lathe.

where:

R_o = Initial radius of the workpiece

The optimization will be carried out for laser turning, and the optimum conditions for rectangular milling are found by letting the radius of the workpiece tend to infinity.

With the volume of the material removed in the operation so defined, the time necessary to perform the operation is evaluated.

The depth of a cut obtained with a given energy density has been defined:

$$D = \eta \frac{ED}{H}$$

and

$$ED = \frac{nP}{dV} = \frac{P}{2\pi R_x d} t_i$$

182

where:

R_x = Average radius of the kerf.

For the axial kerf, $R_x = (R_i - D_r)$.

For the radial kerf, $R_x = (R_i - \frac{1}{2}D_r)$.

It is assumed that two beams of equal power P are operating simultaneously to form the axial and radial kerfs. The efficiency factor η is assumed to be equal for the two cuts. The time to form the radial cut is taken to be the time to form the entire ring, the axial cut having been completed in the same or less time. Therefore, the time to cut a given ring is

$$t_i = \frac{2\pi D_r dH}{P}(R_i - \frac{1}{2}D_r)$$

183

and the time to cut a series of rings $l \times m$ is

$$\sum_{i=1}^{q} t_i = \frac{2\pi D_r dH l}{\eta P}\sum_{i=1}^{m}(R_i - \frac{1}{2}D_r) .$$

184

R_i is given by

$$R_i = R_0 - (i-1)D_r$$

185

so

$$\sum_{i=1}^{q} t_i = \frac{2\pi D_r dH\, l}{\eta\, P} \sum_{i=1}^{m} \left(R_i - \tfrac{1}{2} D_r \right)$$

$$= \frac{2\pi D_r dH\, l}{\eta\, P} \left(mR_0 - D_r \sum_{i=1}^{m} \left(i - \tfrac{1}{2} \right) \right)$$

$$= \frac{2\pi D_r dH\, l}{\eta\, P} \left(R_0 - \tfrac{m^2}{2} D_r \right)$$

$$= \frac{\pi D_r dH}{\eta\, P}\, q\, (2R_0 - mD_r)$$

186

By combining this expression with the one giving the total volume to be removed, a very simple expression for the total MRR is obtained:

$$MRR_{total} = \frac{\sum_{i=1}^{q} v_i}{\sum_{i=1}^{q} t_i}$$

$$= \frac{q\,\pi D_d D_r \left(2R_o - mD_r \right)}{\frac{\pi D_r dH}{\eta\, P}\, q \left(2R_0 - mD_r \right)}$$

$$= \frac{D_a}{d} \eta \frac{P}{H}.$$

187

Assuming that rings with equal axial and radial kerfs are produced, $D_a = D_r = D$, it can be concluded that

$$MRR_{total} = \frac{D}{d} \eta \frac{P}{H}.$$

188

If this is compared with the expression obtained previously for the kerf MRR

$$MRR_{k, actual} = \eta \frac{P}{H},$$

189

the difference between dual beam and single beam laser cutting becomes clear. The dual beam cutting tool relies on the production of deep, narrow kerfs to maximize the material removal rate, while in single beam cutting, the greatest material removal rate is obtained with shallow cuts. Since η decreases with increasing depth of cut, it is important to find the variation of η with depth in order to predict the optimum conditions.

To maximize this material removal rate, the material removal rate is differentiated with respect to depth of cut:

$$\frac{\partial}{\partial D}(MRR_{total}) = \frac{\eta P}{dH} + \frac{DP}{dH}\left(\frac{\partial \eta}{\partial D}\right) = 0.$$

190

Solving for the optimum depth and nondimensionalizing,

$$\left(\frac{D}{d}\right)_{optimum} = \frac{-\eta}{d\frac{\partial \eta}{\partial D}}$$

191

Since the radius of the workpiece is not contained in this expression, it also applies to rectangular milling. If the radius of the workpiece is large enough compared with D_a and D_r, this expression will apply to laser turning.

4.4 Significance of the Optimum Depth of Cut

To optimize the dual-beam cutting process in the manner just described, it is necessary to determine the function η over a range of depth, because the derivative of η with respect to depth appears explicitly in the expression for the optimum depth of cut. The experimental data are used to construct a graph of depth of cut versus energy density. Since both depth and energy density can vary by several orders of magnitude, the data are plotted logarithmically. There are four independant ways of varying the energy density in a given cut, and experiments were performed holding three parameters constant, and varying the fourth one. A graph showing typical behavior is shown in figure [18]. The line labelled "theortical" is a graph of $D \times H$ for a particular

value of H over the domain of D. The line labelled "experimental" is a graph of D obtained experimentally by varying ED. When the data are plotted logarithmically, the horizontal distance between the two lines at a given depth of cut corresponds to the logarithm of the ratio

$$\frac{H \ D}{ED} = \eta \ .$$

<div align="right">192</div>

To find the optimum depth of cut it is not strictly necessary to calculate η for every depth and subsequently find the depth which satisfies equation [191]. Instead, it is useful to construct lines of constant MRR_{total} in the plane of depth vs. energy density. To do this we express the total MRR in terms of D and ED:

$$MRR_{total} = \frac{D^2 \ P}{ED \ d} \ .$$

<div align="right">193</div>

To make the graph more dimensionally compatible with equation [193], the variables D/d and ED/d are introduced. D/d is the aspect ratio of the cut, as seen previously, and ED/d is energy density normalized with respect to a cut with aspect ratio equal to unity. Using these variables, and making the assumption of constant laser power, lines of constant bulk material removal rate (the quantity to be maximized) can be plotted next to experimental data in figure [19].

A constant bulk material removal rate for the dual-beam cutting tool corresponds to a line of positive slope 1/2 on the logarithmic plot. The depth of cut which produces the maximum bulk material removal rate lies on the segment of the experimental curve which is tangent to this family of lines.

The previous statement defines the optimum machining conditions independently of any arbitrarily defined constants. The quantity

$$\frac{D^2}{ED \ d} = \frac{MRR_{total}}{P}$$
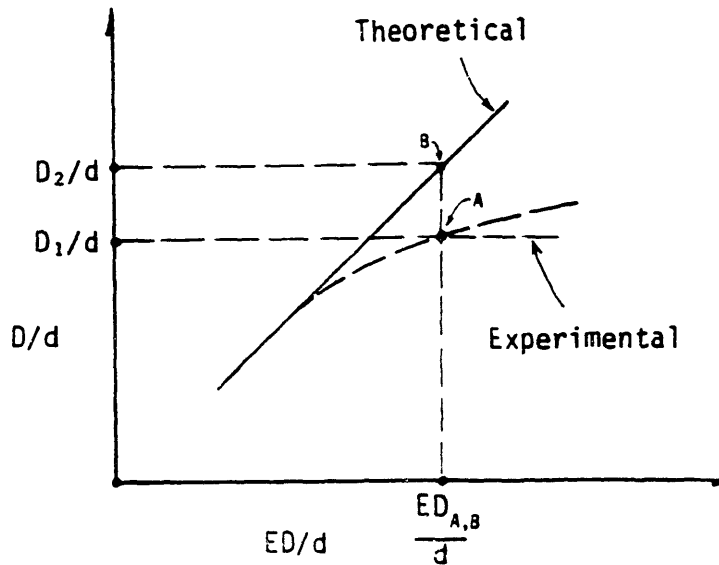
Figure 18. Comparison between "ideal" behavior and experimental data for determining the cutting efficiency factor, η.
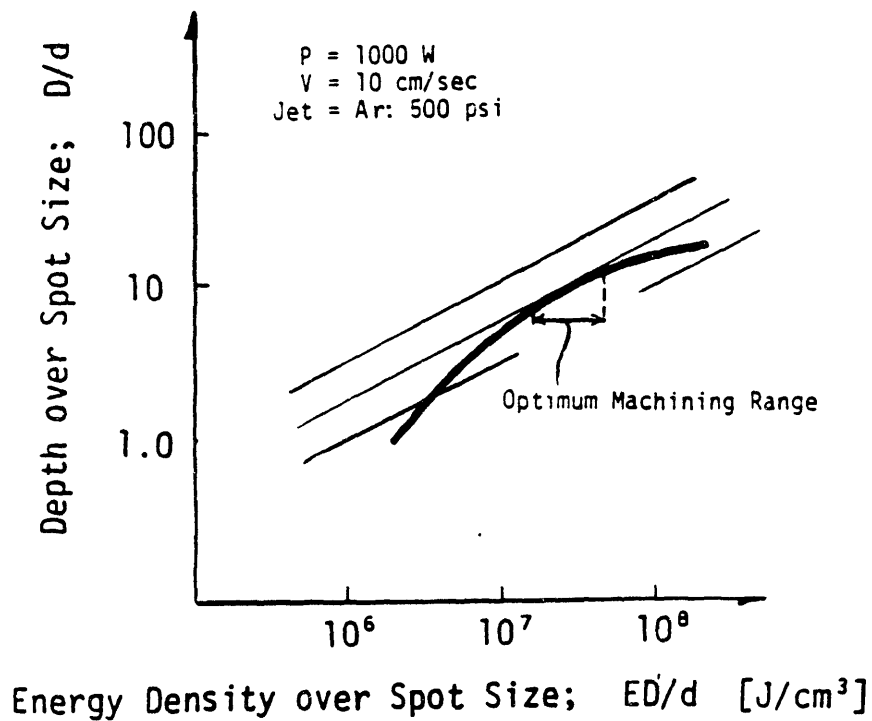
Figure 19. Family of lines of constant MRR for determining optimum machining conditions for the laser lathe.

corresponds to the energy efficiency of the dual beam cutting tool, expressed as total MRR per unit power.

Finally, it bears mentioning that the optimum cutting conditions for the dual beam cutting tool do not correspond to the maximum value of η. The variable η expresses the energy efficiency for material removal from a single kerf. In single-beam cutting, the maximum cutting efficiency is obtained with shallow cuts. Because of the geometry of dual beam laser machining, the maximum bulk material removal rate is obtained with cuts which are much deeper than those which have a high kerf material removal rate. Typically, material is removed from a single-beam kerf at a very high rate until the depth of the kerf exceeds the depth of focus of the laser. This corresponds to an aspect ratio of approximately 5:1 or 10:1. By contrast, the dual-beam cutting tool removes material at the highest rate when kerfs have an aspect ratio of approximately 20:1 or 50:1.

To obtain cuts which are 50 to 100 times as deep as they are wide, it is essential to provide an assist gas jet of some kind. In the experimental program, different jet configurations were tried. The typical configuration normally used in conventional laser "through" cutting of metals was found to be ineffective in continuous-wave blind cutting. In this configuration, the assist gas is applied through a nozzle which also delivers the focused laser beam. The gas jet and beam strike the same point in the same direction, and this is very effective for impelling the melted material entirely through the workpiece. Various shapes of gas nozzles have been tried by other researchers and the industry normally uses oxygen at pressures ranging from 1 to 3 bars.

In laser "blind" cutting, the material must be removed from the kerf in a direction 90 degrees away from the direction of the incoming laser beam. Because of this, a different nozzle configuration was developed to provide horizontal impulse to the molten material. Different assist gasses used were argon, oxygen, and compressed air. Pressures ranged from 7 to 70 bars for argon, 2 to 7 bars for oxygen, and 2 to 35 bars for compressed air.

5. EXPERIMENTAL PROGRAM

The experimental program in this thesis consisted of three distinct phases. In the first phase, the cutting process was studied experimentally using conventional laser machining configurations to evaluate their performance in forming blind cuts. In the second phase, different improvements to the cutting process were designed and tested. In the third phase, the concept which provided the greatest improvement to the process was further optimized and tested on a wide variety of materials. These materials were oxide and nonoxide ceramics, ferrous and nonferrous metals, and fiber-reinforced resin composites.

5.1 Phase I

Experiments perfomed in the observation phase took place before January, 1985. These consisted of data taken using stationary targets, and experiments using focused and unfocused laser beams on moving targets. Although all of the data which was taken before Sept, 1984 was collected by other students, this data has been unreported, so it has been included for completeness.

1. Experimental Configuration

Experiments prior to 1986 using laser powers of greater than 50 watts were performed at Laser Industries, Inc. in Lawrence, Ma. The configuration of the workpiece and laser is shown schematically in figure [20]. This configuration is most commonly used in conventional laser machining, in particular, "through" cutting of sheet steel. The workpieces were mounted on an X-Y table and translated under the laser beam using numerical control. The laser, a Photon 1200 CO_2 laser, had a collimated output beam in the gaussian mode of approximately one inch diameter. The beam was directed vertically to the workpiece and focused with an objective lens. A focal length of five inches was used throughout this phase to maintain consistency and the diameter of the focused spot was .005 in. (.013mm)

The focused beam was directed through a narrow nozzle such that the focal point of the objective lens was approximately 1/4 inch (6 mm) below the nozzle. An inert shield
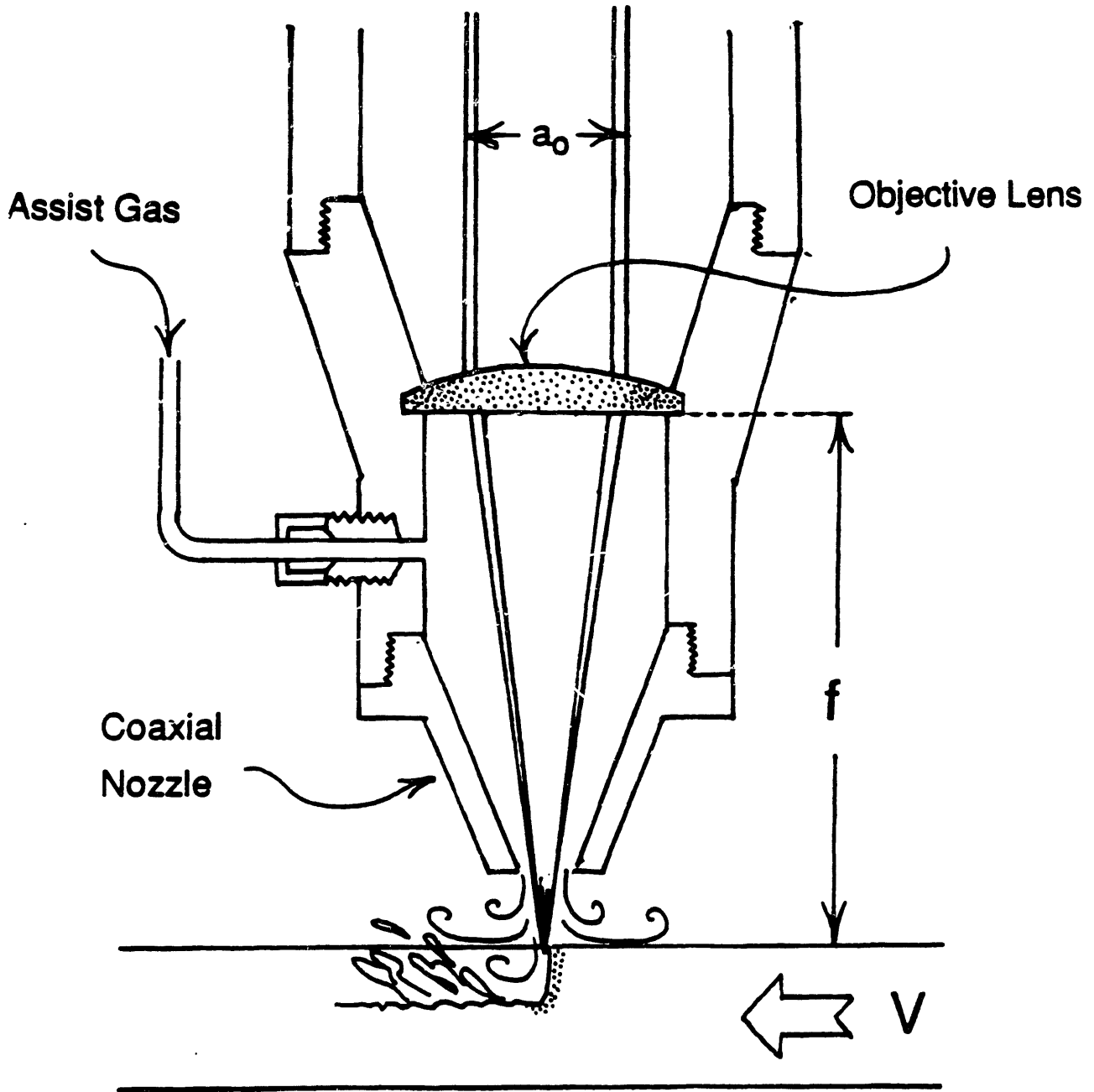
Figure 20. Coaxial nozzle configuration used in conventional laser machining.

gas was used to protect the lens from material sputtered from the workpiece during cutting. This shield gas was directed through the same nozzle which delivered the beam. Its pressure was typically between 5 and 20 psi, and did not exceed 50 psi because the objective lens could not support high pressures. This nozzle is hereafter referred to as the "coaxial nozzle" because of its orientation to the laser beam.

In coventional laser processing of materials, the coaxial nozzle is used in different ways. In laser welding, the shield gas is inert and serves only to protect the lens. In this case, it is not desirable to blow molten material away, so lower pressures are used. In "through" cutting, the coaxial jet serves to force molten and vaporized material along the axis of the laser beam, thus keeping it within the beam until it departs from the workpiece. Often in this case, the shield gas is chemically active. It must be inert to the objective lens at ambient temperatures and active to the workpiece at the extreme temperatures which exist under the focused laser beam. Oxygen is used for most metals. One of the questions addressed in this research was whether any chemicals exist which satisfy these requirements for ceramics. This topic will be addressed in greater detail in the discussion of Phase II.

2. Results

A typical cut obtained during this phase of the experimentation are shown in profile in figure [21]. Specimens of Al_2O_3 were cut using the conditions given in Appendix II and were analyzed in the following way.

After sectioning with a diamond saw, the cuts were stained with dye to enhance contrast between melted and unmelted material. They were examined under an optical microscope with a micrometer stage, and the depth of cut was defined as the greatest depth to which material was melted. Since resolidified ceramic has a different grain structure from sintered ceramic, this boundary is the easiest to locate. By measuring the greatest melted depth, a single-pass laser cut measurement will not be affected by the degree of material removal. Early multiple-pass cuts were interfered by resolidified material. With inadequate material removal, laser energy is dissipated by remelting of solidified ceramic left over from previous scans.

The depths of cuts obtained in this phase are plotted logarithmically with respect to energy density in figure [22].

3.Discussion

The central problem to laser blind cutting was found to be that of material removal. The cuts illustrated in figure [21] are actually little different from welds because of the volume of material which resolidified in the kerf after the laser passed over. Cuts which are partially welded do not separate, and in brittle materials the additional problem of cracking requires that heat be carried away from the kerf as quickly as possible after the laser has passed over a particular point.

Experiments were performed using various spot sizes ranging form a focused spot of approximately 0.005 in. (1/8 mm) diameter to an unfocused spot of.04 in. (1 mm) diameter. These were done for two reasons: to observe the variation of cutting rate with spot size in hopes of finding a functional relation, and to observe the formation of cuts on a large enough scale that the process could be observed directly.

The relationship between cutting rate and spot size proved to be illuminating. A large laser spot was found to be capable of cutting deeper than a focused spot, although at a necessarily slower rate because of the decreased power density. The cutting rate was found to be relatively independent of surface speed for the relatively narrow range tested: 10 to 100 in/min (.33 to 3.3 cm/sec). When the data are plotted using the dimensionless aspect ratio D/d and the normalized energy density ED/d, the data are found to fall along the same curve, shown in figure [23].

This curve has a lower asymptote which corresponds to a constant rate of heat input per unit volume of material illuminated by the laser beam. The material which is illuminated may or may not be removed. If it is removed, a straight, narrow kerf results. If the material is resolidified, the "kerf" (actually a weld) will be approximately the same depth, although wider.

As the depth of the kerf approaches approximately five times the spot size, the linear relationship breaks down and more energy is dissipated per unit depth. The beam

Figure 21. Scanning electron micrograph of a typical Phase I laser cut in Al₂O₃.
Conditions: P = 750 W, V = 1 cm/sec, d = .013 cm, n = 1 pass. M = 40 x.
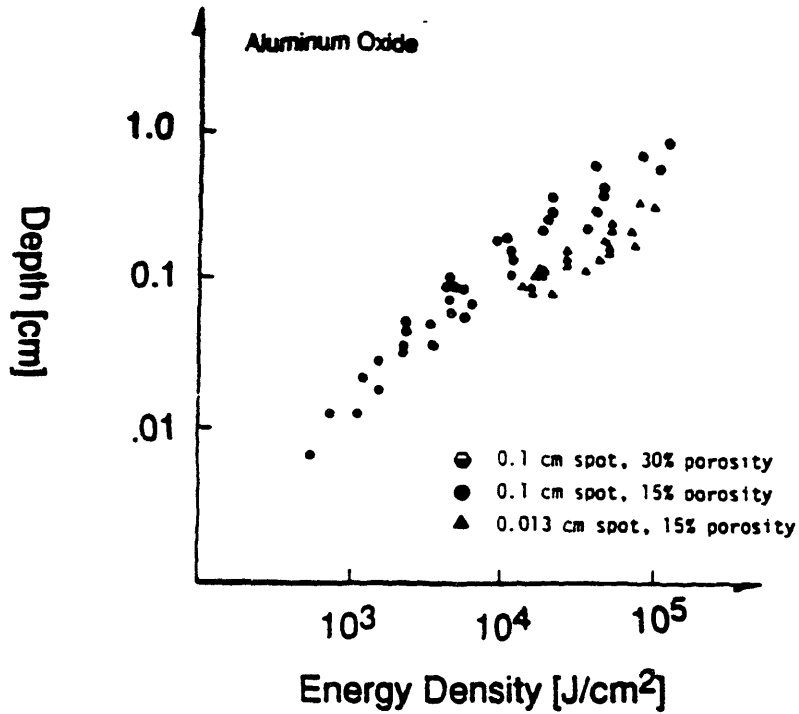
Figure 22. Depth of cut vs. Energy Density for Phase I experiments in laser blind cutting of Al_2O_3.
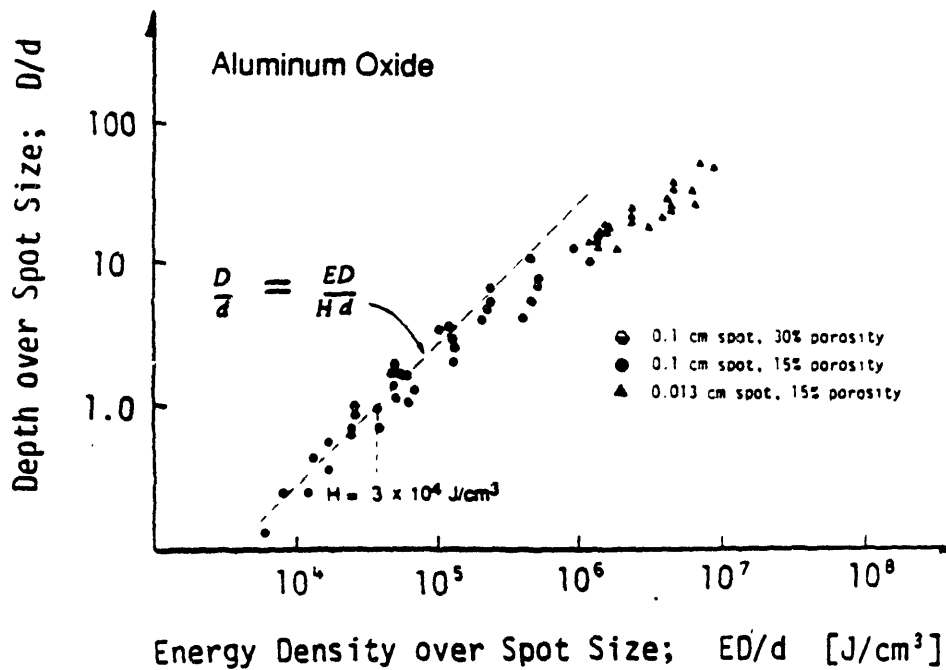
Figure 23. D/d vs. ED/d for Phase I experiments in laser blind cutting of Al_2O_3, showing experimentally determined enthalpy of removal, H.

divergence ratio $\frac{a_0}{f}$ for these experiments was 1/5, and the depth of focus at the focal point is 5 times the spot size. One hypothesis is that cuts made with objective lenses with different focal lengths will diverge from the lower (linear) asymptote at D/d equal to the depth of focus of the lens. This is supported in the theoretical model, which predicts that the limit depth is proportional to the reciprocal of the divergence ratio.

It should be noted that in this test, the dimensionless quantity J/VH was varied from approximately 2 to 2000. It is extremely significant that very little variation in the cutting efficiency, η, with speed and spot size was observed. The dimensionless group Vd/α varied between 1/3 and 3, which indicates that heat conduction would have played a varying role in dissipating laser energy from the kerf. It is possible that since alumina is partially translucent to CO_2 radiation (see Ready, also Wagner, also Dabby & Paek) the material could be illuminated to a depth which exceeds α/V, the characteristic heat diffusion distance. Wagner claims that the absorbance of alumina at 10.6μm is 30 cm^{-1} which means that 80% of the laser radiation is absorbed within 0.5 mm of the surface. Steel, which either absorbs or reflects all of the radiation within 0.01μm of the surface, was found to exhibit very complex behavior which was highly dependent on J/VH. No experiments were done to test this hypothesis.

The direct observation of the cutting process was dangerously illuminating. The laser beam itself is invisible, and is absorbed by ordinary glass or plastic goggles. To watch the transport of molten alumina at searing white heat, it was necessary to wear an arc-welder's helmet and press my head up next to the focusing lens. Head to head with the laser, these observations proved to be most useful to the research project. Although entirely qualitative, they directed the course of the research over the next year.

The laser power was 1000 watts, and the focal point of the 5 in objective was 0.2 inches above the workpiece. This gave a spot size of 1mm which was large enough to see, and moved the orifice of the coaxial nozzle out of the line of sight. Compressed air of 20 psi was directed into the kerf, and the translation speed was 25 in/min (1 cm/sec). The alumina was melted by the laser, and the liquid appeared to be roughly as viscous as molten wax. The molten alumina was accelerated by the assist gas away from the

laser spot down the kerf which had just been created. As soon as it left the laser spot, it cooled quickly and became more viscous. It finally froze about 1/2 inch down the kerf from the position of the spot, clogging the kerf. The overall appearance was like wax dripping off a candle.

The fact that the kerf was entirely clear up to 1/2 inch from the spot indicated that the mobility of the molten material was not a problem until it had cooled down greatly. Therefore the molten material needed a larger impulse to clear it from the kerf. Furthermore, the impulse from the coaxial jet was in the wrong direction, forcing the molten material against the bottom of the kerf. The primary thrust of Phase II was the development of an off-axis gas jet with a large impulse, oriented in the direction of the kerf.

5.2 Phase II

The second phase of the experimental program proceeded from November, 1984 through July, 1986. During this phase, three different variations to the cutting process were attempted, in order to determine which gave the best improvement over the process studied in the first phase. The three variations were: controlled cracking, chemically active assist gas for ceramics, and high-impulse gas jet. Of these three, the high-impulse gas jet proved the most successful, although the other two processes achieved moderate success, as will be discussed.

1. Controlled Cracking

Since ceramics are brittle, they are prone to cracking during laser machining. The cracking comes as a result of thermal stresses in the heated material adjacent to the kerf, and presents a great problem when there is substantial resolidification in the kerf. Two ways of dealing with this problem are to minimize the heating of the kerf by scouring molten material from the workpiece with a gas jet, or by directing the elastic energy created by the laser to the formation of cracks which propagate in the intended direction of cut. The latter of these approaches is called controlled cracking. Materials for which this process may be significant are nonporous ceramics such as glass, alumina, and silicon carbide.

The basic premise of controlled cracking is to induce stresses in the workpiece such that a crack can be formed which will propagate to a fixed depth into the workpiece and stop. The material is separated in the same way as a kerf, but with a vanishingly small width, and requires much less energy to form. The laser is perhaps the only tool in existence which offers the possibility of doing this because of the extreme precision that is possible in the delivery of heat. The heat can be pinpointed by focusing the beam, or distributed into complex shapes using various optical modes of the laser itself, and different types of lenses such as cylindrical lenses.

Cracks are nucleated on flaws in the material, and in controlled cracking one introduces flaws which prefer cracking in the desired direction. This is accomplished with the laser by passing over the line of the intended kerf before the crack is formed. There are two possibilities when this is done: to scribe a shallow groove on the surface, or to drill a row of holes into the workpiece. The second method showed more promise for the following reasons.

Since the process involves the formation of cracks which propagate to a certain preplanned depth and stop, a row of holes of the intended depth only requires the crack to grow laterally between the holes, terminating and renucleating as each hole is encountered. Any single crack does not propagate further than the distance between two holes, a variable which is commanded by the operator, and can be much less than the intended depth of cut. Also, the walls of laser-drilled holes have a very uniform structure which favors the nucleation of cracks laterally from the hole. They tend to be scored with microcracks oriented vertically along the walls of the hole, as shown in figure [24].
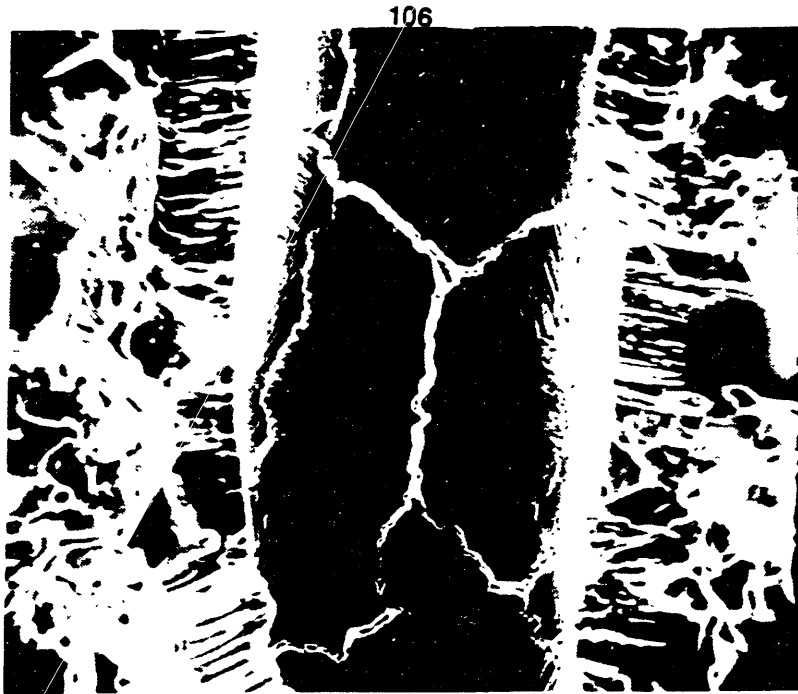
Figure 24. Scanning electron micrograph showing microcracks in resolidified material in a laser-drilled hole in Al_2O_3. M = 100 x

To create a crack which travels between two holes, it is necessary to create a tensile stress which is perpendicular to the plane of the intended kerf. Stability considerations require that this be a principal stress, and that there be a compressive stress along the direction of motion of the workpiece. When the laser is used to create this stress, there must be a stress couple present in the workpiece, since the laser cannot itself pull or push the material. A moving heat source tends to create a tensile stress wave in front of itself because of the asymmetry of the thermal strain. The heated material behind the heat source exists in hydrostatic compression as long as it remains hot and solid, and because the heated zone terminates abruptly at the laser spot, the stress couple creates a large tensile stress in front of the laser spot which is indeed a principal stress accompanied by a compressive stress perpendicular to it. Therefore, a scanning laser beam which heats the workpiece without melting it was attempted for the propagation of controlled cracks.

The experimentation in controlled cracking wasnot extensive. The principal problem encountered in the experimentation was that there was no practical way to observe the cracks which were formed in opaque materials. It was found that in glass controlled

cracks could be grown which entirely connected a row of holes 1 mm apart and 4 mm deep in two scans, one to drill the holes with a focused pulsed beam, and one to form the crack with a 1 mm diameter CW beam. Nonporous alumina was also cleaved in the same way, although no practical nondestructive method of measuring the cracks was found.

2. Chemically Active Assist Gas for Ceramics

In laser cutting of metals, particularly steels, oxygen is used to enhance the cutting rate because of the rapid exothermic reaction between the molten metal and the oxygen. A stream of oxygen gas has potentially more power in its chemical activity with steel than the laser has in its radiation. Ceramics are vastly different from metals in this respect, and they can be divided into two major classes: oxides and non-oxides. Oxides include alumina, quartz, glass and zirconia, and nonoxides include silicon carbide, silicon nitride, diamond, and boron nitride. For the non-oxides, oxygen is chemically active and can be regarded as the best choice if a chemically active gas is to be used. Since oxides are already fully oxidized, one must resort to less obvious chemicals to provide chemical enhancement to laser cutting.

All of the chemical bonds in an oxide ceramic are between positively ionized species, such as silicon or aluminum, and a strongly binding cation, specifically oxide. All of the valence electrons on the anions are closely associated with the cations. This condition also exists to some degree in non-oxides such as silicon carbide, but the cation (carbon) is not as strongly binding as oxygen and may itself be oxidized. There is only one cationic species which is more strongly binding than oxide: fluoride. Fluorine can replace oxygen in an oxide ceramic, and since fluoride ions only bind to one anion at a time, a fluoride-doped oxide ceramic is less viscous at a given temperature than the pure oxide. In this way, a fluoride-bearing assist gas will "flux" the ceramic so it will flow more easily from the kerf.

The general form of the reaction between fluorine and an oxide ceramic is

$$M_x O_y + z F_2 \rightarrow M_x O_{y-z} F_{2z} + \frac{z}{2} O_2$$

where:

M is the anion in the ceramic,

x & y are the stoichiometric quantities of M and O in the ceramic, and

z can be any number less than or equal to y and can have a very pronounced effect at small values.

The problem with this concept should be immediately apparent to anyone familiar with the toxicity of fluorine and fluorine-bearing chemicals. How does one deliver the fluorine to the cut without poisoning the operator or corroding the equipment? The elevated temperature of the molten ceramic can dissociate fluorine-bearing compounds, some of which are nontoxic, but one must be certain that the byproducts are themselves nontoxic as well. After extensive research into fluorine-bearing compounds, only one gaseous chemical was found which was itself totally nontoxic and all possible reaction products were relatively nontoxic. By "relatively nontoxic" what is meant is that the reaction products were acid anhydrides which were corrosive and irritating at low levels, but not carcinogenic or neurotoxic. This gas was sulfur hexafluoride, SF_6.

This segment of the experimental program was mercifully shortlived. During the first experiment using SF_6 it was discovered that the gas absorbs CO_2 radiation very strongly due to a vibration resonance in SF_6 and the ambient gas which accumulated in the lab entirely absorbed the laser beam inside the beam delivery tube, with absolutely no power delivered to the workpiece.

During the brief moments when the laser and gas were working together, a noticable clearing effect was seen in the cuts. The ejected material was in the form of a fine powder, and the cuts were very narrow and straight. They were virtually identical to cuts made using the high-impulse gas nozzle six months later using nitrogen as a assist gas.

To operate a laser cutting tool using these chemicals it would be absolutely essential

construct a sealed chamber around the workpiece, and to provide an adequate gas reclamation/purification system. The expense of the chemicals involved requires that they be recycled, and the serious hazards associated with fluorides require that the personnel, the hardware, and the environment be isolated from the cutting tool.

3. High-Impulse Gas Jet

To address the problem of material removal from a laser blind kerf, a series of prototype gas nozzles were constructed and tested on various materials. During most of the early development of the nozzle, an Apollo 50 watt CO_2 laser located at the MIT Laboratory for Manufacturing and Productivity was used. This laser could not cut aluminum oxide effectively, so the development work was performed on fiber-reinforced resin composites. These experiments are discussed in their complete form in the Master's thesis of Stefanos N. Kordas (MIT Mech. E. 1986), and will merely be summarized here.

Kordas describes the fabrication of a supersonic gas jet to deliver an inert shield gas to deep blind kerfs in glass reinforced epoxy composites. This nozzle had a converging-diverging orifice with a throat diameter of 0.025 in., a divergence angle of 10 degrees and an exit diameter of 0.060 in. This nozzle is illustrated in figure [25]. It was directed at an angle of 45 degrees off the axis of the laser beam. It was found to restrict charring of the resin matrix to a layer $20\mu m$ thick on the walls of the kerf. It also minimized the destructive effects of the higher thermal conductivity of the fibers with respect to the matrix. The kerfs were found to be very slightly wider than the diameter of the laser spot, and exceptionally straight. The nozzle was designed to operate with a 500 psi gas supply, and the jet stream could cut paper and puncture skin.

A cutting head was designed and constructed which incorporated a supersonic nozzle and a coaxial jet in a single part. This helped ensure exact alignment of the jet stream with the axis of the laser beam in a cutting head that was compatible with standard laser hardware. This head is illustrated in figure [26]. After testing it on the 50-watt laser at MIT, the nozzle was connected to the Photon 1200 to cut aluminum oxide, glass-reinforced epoxy and mild steel.

0.06 in.

3/8 in.

0.025 in.

1.5 in.
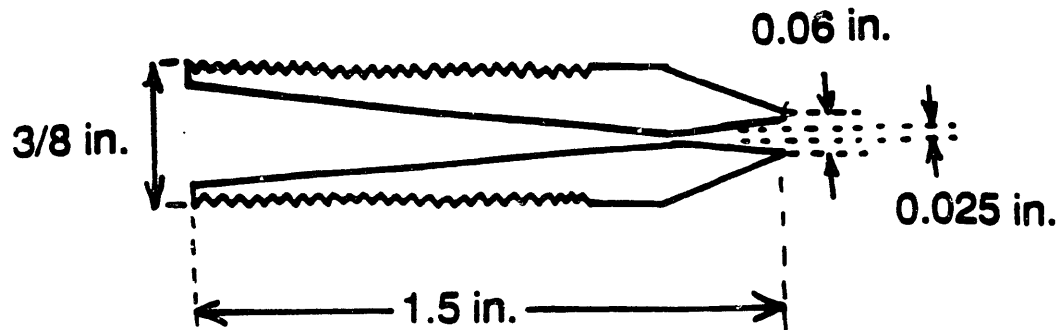
Figure 25. Diagram of supersonic nozzle developed during Phase II and modified in Phase III.

Focused Laser Beam

High Pressure N_2

Low Pressure He

Supersonic Nozzle

Focal Point
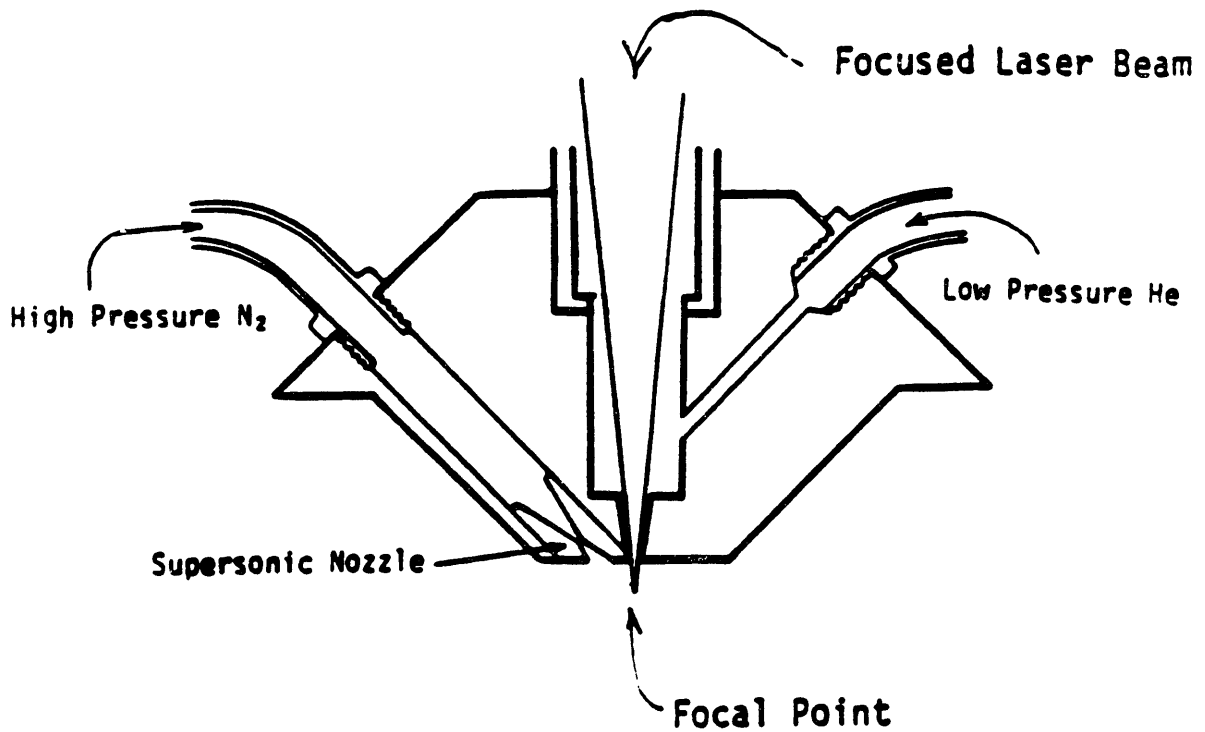
Figure 26. Diagram of first prototype laser cutting head for blind cutting.

These experiments were performed on November 12, 1985, and the numerical data is included in **Appendix II**. The experimental setup slightly different from that used in Phase I and is illustrated in figure [27]. The specimens were all cylindrical rods with a diameter of 1-1/2 in. They were rotated under the cutting head at various speeds using a variable-speed DC motor and a dead center. The laser was focused on the surface of the workpiece and compressed nitrogen gas was fed to the supersonic nozzle at 500 psi. The laser power was kept constant at 1000 watts CW for ten seconds in each cut. The only parameter which was varied was the surface speed, and the number of passes was adjusted to maintain a constant energy density. The surface speed was varied from .79 in./sec to 169 in./sec (2 cm/sec to 430 cm/sec). The energy density was chosen because it was in the optimum range deduced from experimental data for alumina.

The profiles of cuts made at the same speed with and without the supersonic gas assist are shown in figure [28]. The cuts made with the supersonic assist are narrower and deeper than those made without it. The best cuts in alumina and steel were obtained at a surface speed of between 5 and 10 cm/sec using the nozzle. Cuts made without the supersonic assist all contained resolidified material, while most cuts made with it were almost totally clear. At lower speeds, the nozzle did not clear the kerf effectively. Using this cutting head, the first ceramic rings were machined using sequential radial and axial cuts.

The variation of cutting rate with surface speed for alumina and mild steel at constant energy density at 1000 W are shown in figure [29]. In alumina, the depth of cut remains constant over a range of slower speeds, and begins to decline when the surface speed exceeds 4 in./sec (10 cm/sec). In steel, there is a clearly defined optimum surface speed at 1000 w; approximately 3 in./sec (7.5 cm/sec).
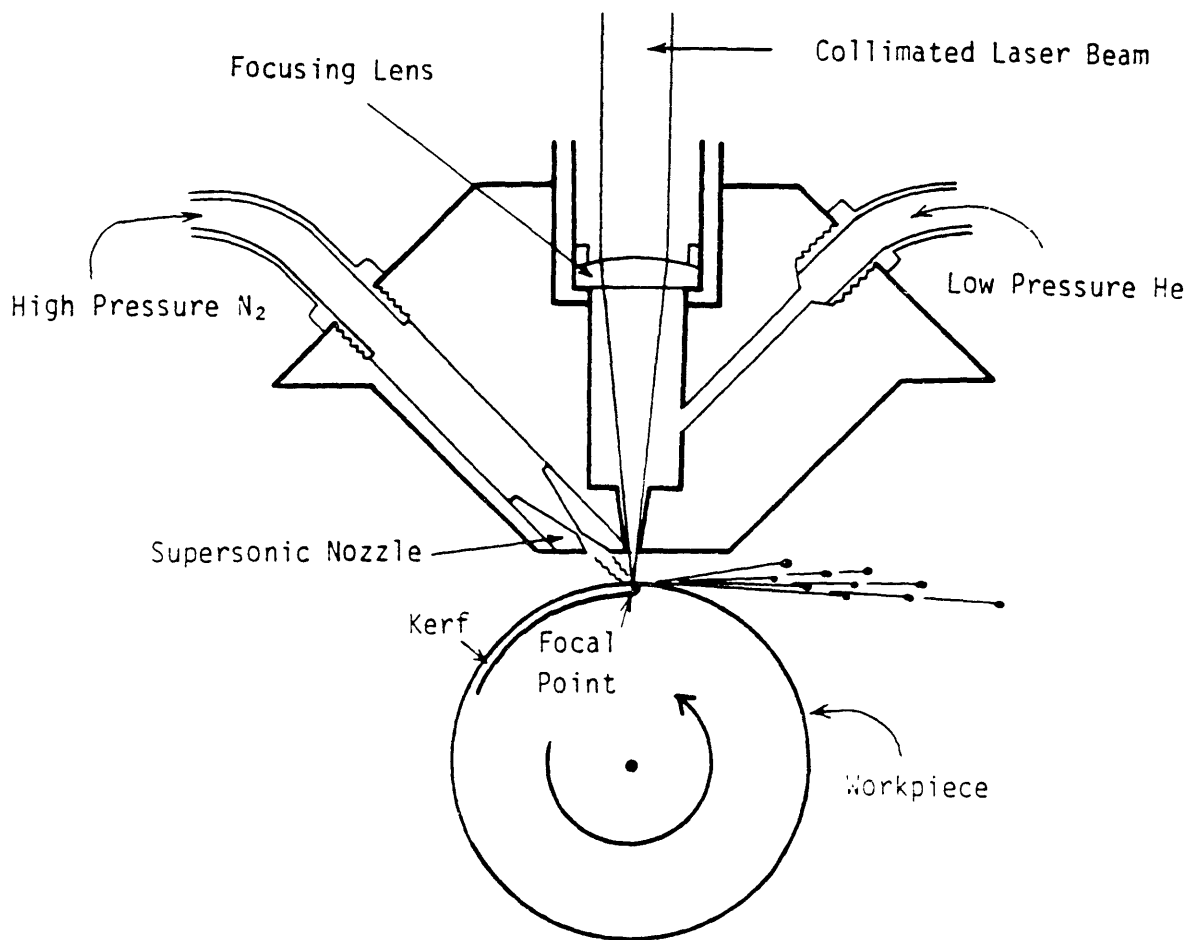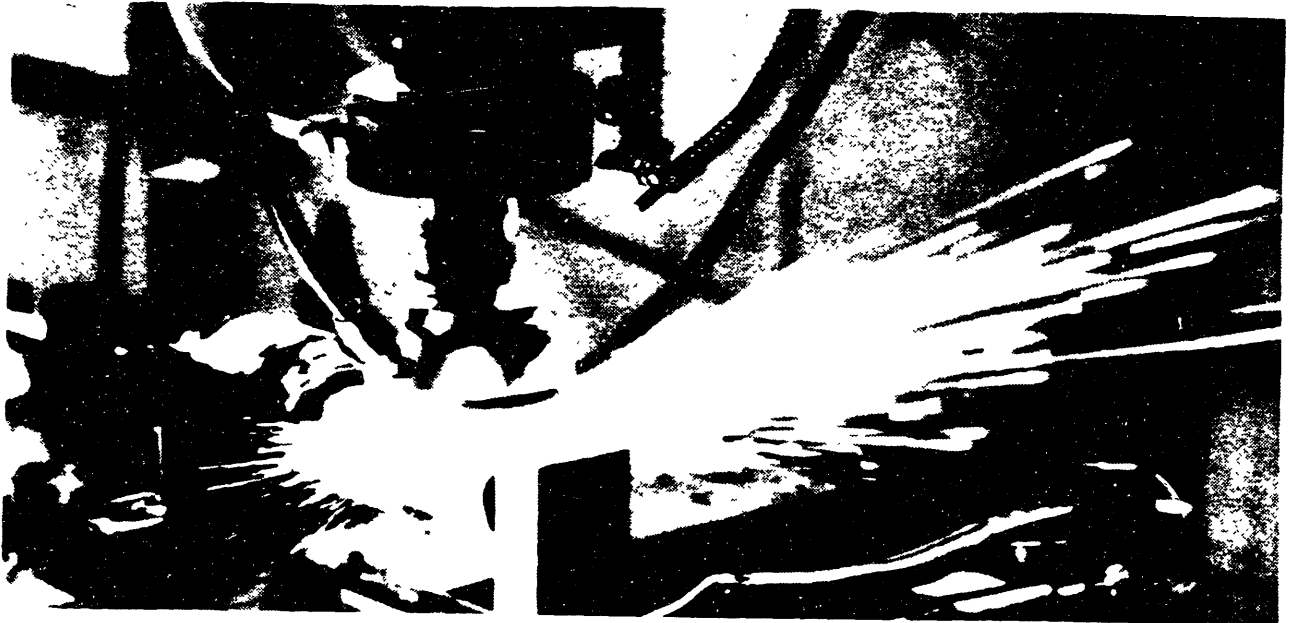
Figure 27. Experimental configuration for Phase III experimentation.

Without nozzle

a.

P = 1000 W

V = 20 cm/sec

d = .013 cm

17 Passes

Depth = .29 cm

D/d = 23

Without nozzle

b.

P = 1000 W

V = 10 cm/sec

d = .013 cm

8 Passes

Depth = .38 cm

D/d = 30

Without nozzle

With nozzle

c.

P = 1000 W

V = 20 cm/sec

d = .013 cm

17 Passes

Depth = .50 cm

D/d = 40

with nozzle

d.

P = 1000 W

V = 10 cm/sec

d = .013 cm

8 Passes

Depth = .52 cm

D/d = 42
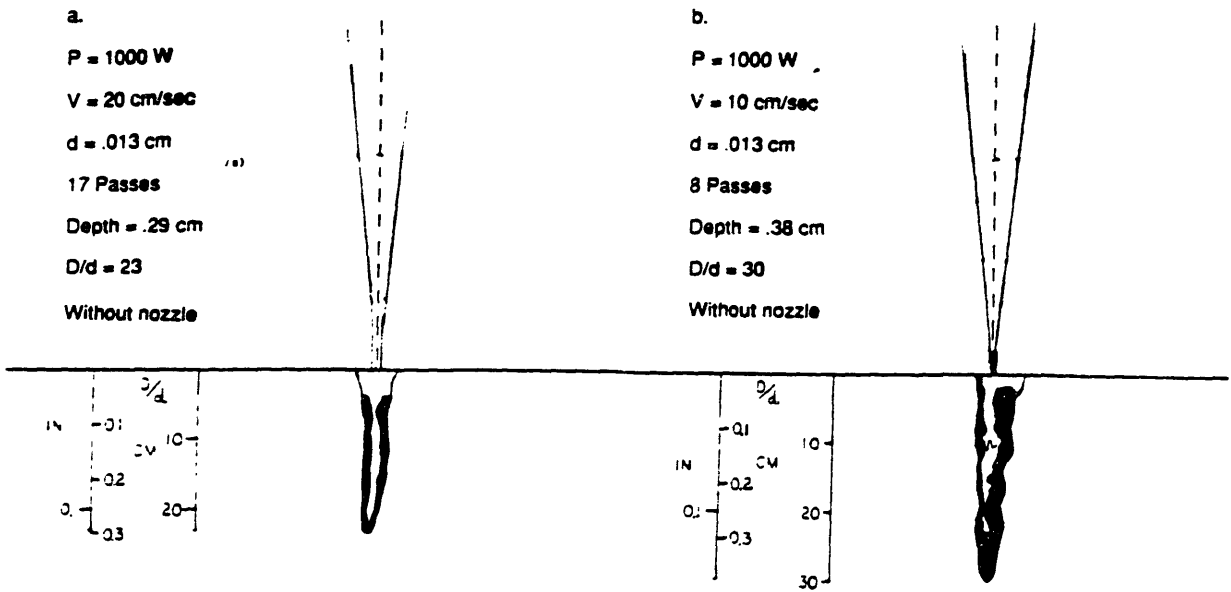
with nozzle
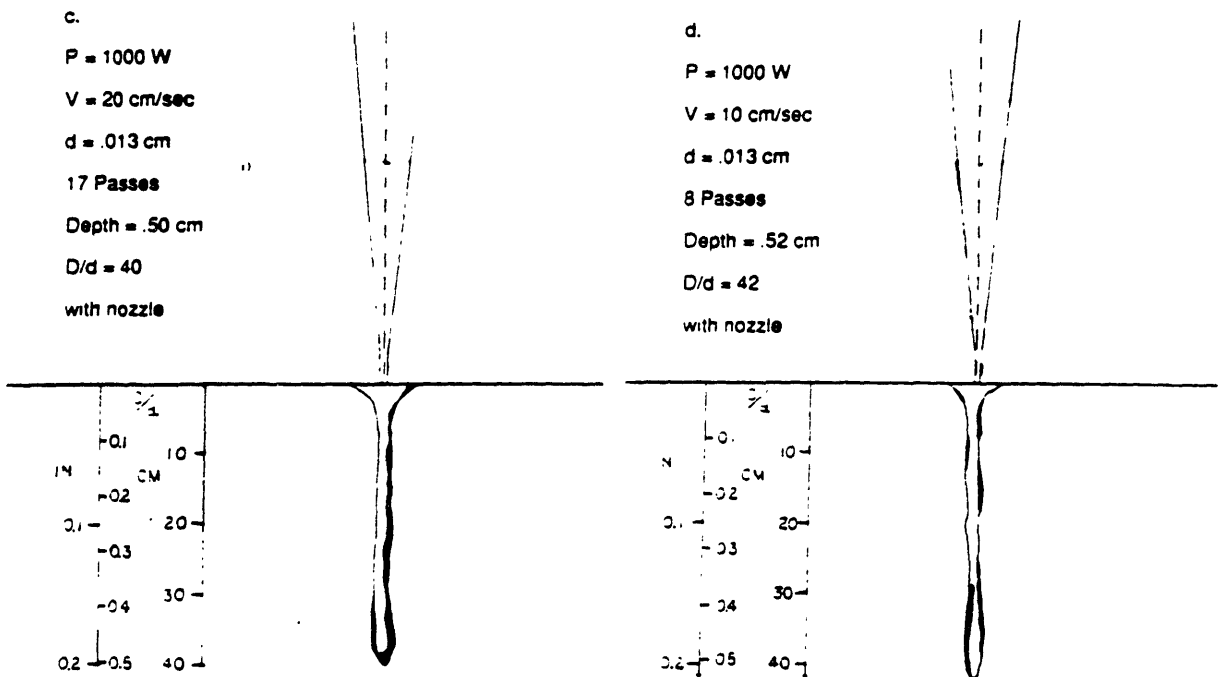
Figure 28. Examples of laser blind cuts in Al_2O_3 made with and without high-impulse gas assist.
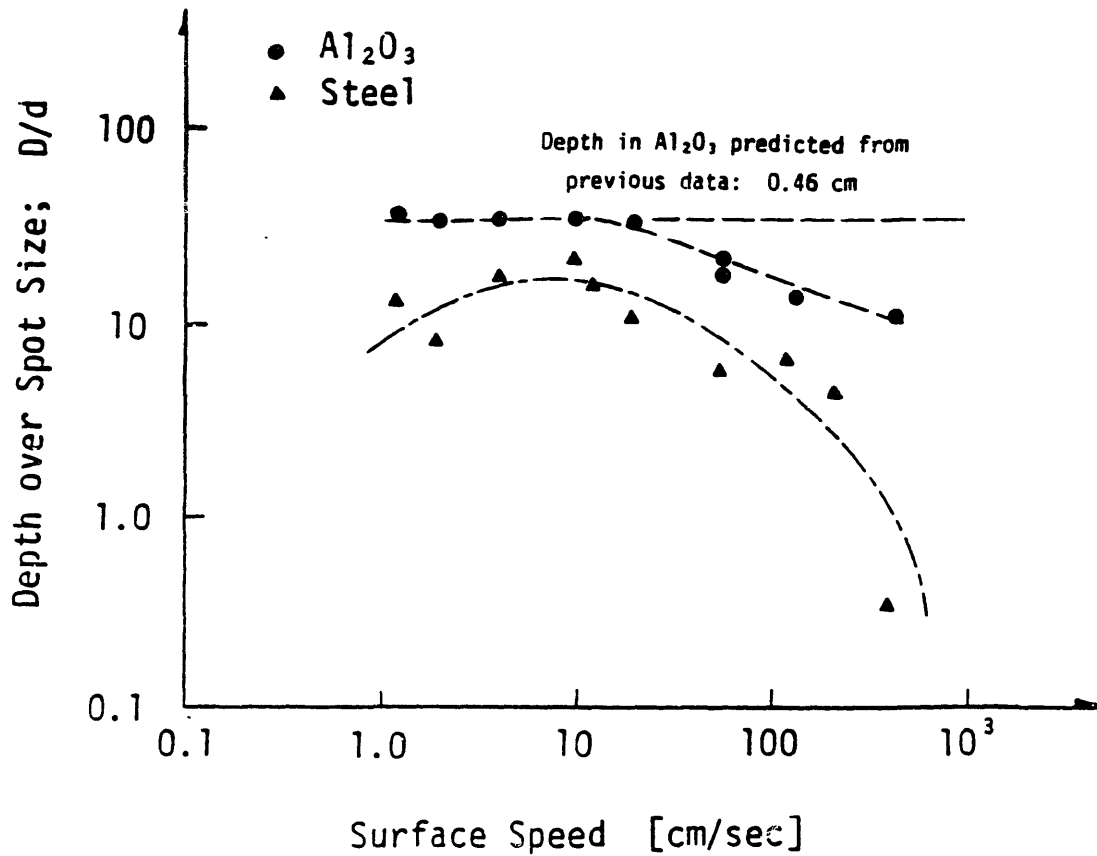
Figure 29. D/d vs. Surface speed at constant energy density ED/d = 8.4 x 10^7 [J/cm^3] for laser blind cutting of Al$_2$O$_3$ and mild steel.

With the high-impulse cutting head, it is possible to make multiple-pass blind cuts which are not interfered with by resolidified material.

5.3 Summary of Conclusions from Phases I and II

1. The depth of a single-pass cut is the same regardless of material removal.

2. Under CW conditions, the depths of cuts can vary by as much as 30% in the same cut. It was not clear whether this was due to fluctuations in the laser power, or in the surface speed of the workpiece.

3. In alumina, over the range of speeds from 10 to 240 in./min (.4 to 10 cm/sec) and spot sizes from 0.005 to 0.04 in. (.0125 to .1cm) the relationship between aspect ratio D/d and normalized energy density ED/d is uniform, provided there is adequate material removal from multiple-pass cuts.

4. An optimum surface speed exists for alumina and steel, above which the cutting rate for a given power decreases with increasing speed. Furthermore, cuts in steel are several times shallower than cuts in alumina made at the same energy density. This phenomenon was studied further in Phase III.

5. Based on this experimental data, the theoretical material removal rate for two laser beams operating simultaneously can be calculated. The maximum material removal rate is obtained for depths of cuts between 10 and 40 times the spot diameter. For the laser used, this corresponds to cuts 1 to 5 mm deep. The material removal rate for two intersecting cuts in this range is 0.6 in.^{3}/min (10 cm^3/min) for two 1000 W beams operating simultaneously. If the laser power is increased, the material removal rate increases in direct proportion.

6. The quantity H, the effective enthalpy of removal for alumina, can be calculated from this data. Its value is 3×10^4 J/cm^3. The quantity derived theoretically is

$$H = \rho C_p \left(\frac{T_m + T_v}{2} - T_0 \right) = 1.4 \times 10^4 \text{ J/cm}^3 .$$

This discrepancy is due to the rate of heat conduction away from the vicinity of the kerf.

7. To form the deep, narrow blind kerfs which make the dual-beam cutting tool

feasible, it is necessary to impel molten material from the kerf using an off-axis gas nozzle.

8. Controlled cracking could be a viable technique for machining very brittle materials, but much more development is needed.

9. Chemically active assist gases for oxide ceramics are impractical, expensive and hazardous. If they are useful at all, it is only for highly specialized operations.

5.4 Phase III Experimentation

In the third phase of the research project, which began in May, 1986, the design of the high-impulse cutting head was improved and further prototypes were constructed. These prototypes were tested in cutting a wide variety of materials:

Al_2O_3, SiC, Si_3N_4, cemented WC, mild steel, AMS 5613 stainless, 303 stainless, invar, inconel, monel, nickel, titanium and molybdenum.

Since the laser cutting process depends on the optical and thermal properties of the workpiece and not its hardness, it was anticipated that similar metals would cut at approximately the same rate regardless of their respective hardness. Mild steel was chosen as the control material, and the cutting rates in the other materials were compared to those in mild steel. Most of the experimentation was performed on mild steel, because this material is easy to section for measurement. Its behavior was found to be considerably more complex than that of alumina.

1. Experimental Conditions

In this phase of the research, a Coherent General model 51 CO_2 laser was used at the C.G. facility located in Sturbridge, Ma. The power ranged from 150 to 1500 watts, with a collimated beam diameter of approximately 3/4 in. (2 cm). The focused spot diameter for a 5 in. focal length objective was .007 in. (.016 cm). Workpieces were cylindrical rods rotated at various speeds with the laser beam oriented perpendicularly to the axis of rotation. The beam was focused on the surface of the workpiece and several different configurations of gas jets were tested to enhance material removal

from the blind kerfs. Different assist gases used were argon, oxygen, and compressed air.

The specimens were sectioned and polished across their diameter, and the cross-sections of the kerfs were examined microscopically. Besides depth of kerf, the kerf width and straightness was measured. The depth of kerf is the primary parameter for determining the manufacturing rate; while the width and degree of straightness determine the accuracy of the machining process.

Extensive tests were performed on mild steel to determine the effects of the machining parameters of laser power, surface speed, and nature and pressure of the assist gas on the cutting rate. Argon was chosen as an inert gas to provide simple mechanical clearing action on the cut. Various nozzles were used, and pressures were varied from 200 to 1000 psi. Oxygen was used as a reactive gas with little mechanical impulse; pressures were varied from 10 to 100 psi. Finally, compressed air was used which provided both mechanical and chemical action; pressures ranged from 100 to 1000 psi.

In most cases, experiments were performed by forming a series of cuts in a workpiece and measuring the variation of the dimensions of the kerf with machining parameters. In one experiment, performed August 1, 1986, the temperature rise and weight change were measured in small workpieces in order to measure the fraction of heat dissipated in the workpiece, and the cooling effect of the gas nozzle.

The cutting head which was developed in this phase is shown in figure [30]. It consists of three parts which thread together. The first part was a coaxial nozzle designed to screw into the lens mount on the laser and support the off-axis nozzle. The second part was a bracket with two threaded holes which align the two nozzles such that their two gas streams intersected at the focal point of the objective lens. The third piece was an interchangable gas nozzle, which threaded into the bracket and was held in place by a locknut. High-pressure gas was fed through a hose which threaded onto the off-axis nozzle. Various sizes and shapes of orifice were tested for the off-axis nozzle, and the one which accomplished material removal most effectively is shown in figure [30]. The

orifice was elliptical, 0.02 in. wide and 0.10 in. long. It was made by machining a circular orifice with a diameter of 0.08 in. and hammering the tip of the nozzle until the orifice flattened out. The nozzle was oriented such that the long axis of the orifice was coplanar with the kerf. This provided the high impulse from a large orifice in a flat stream which penetrated the kerf.

2. Results and Discussion

The depths of cuts obtained for the materials tested are plotted in figure [31] as the dimensionless aspect ratio D/d versus the normalized energy density ED/d. The cutting rate in mild steel was found to vary greatly with machining parameters, so the average values are plotted in this figure as a summary of the data, with greater detail to follow.

The most striking observation represented by this graph is that alumina cuts roughly twenty-five times faster than steel to a given depth at 1000 watts CW. SiC was machined roughly at 1/2 the rate of alumina, and Si_3N_4 at 1/4 the rate of alumina. Tungsten carbide cut at approximately the same rate as steel, and some of the alloys tested cut approximately twice as fast as steel. Two of the metals tested, monel and nickel, were more difficult to cut than mild steel, and molybdenum could not be machined at all. The experimentally determined values of H, which is directly proportional to the cutting rate at constant power, are given in table [1].

The curves in figure [31] are similar in the way they diverge from linearity (lower asymptote) at approximately the same value of D/d. Because of this, the following empirical relation can be fitted:

$$\frac{D}{d} \approx -5 + 10 \sqrt{\left(\frac{1}{10}\frac{ED}{Hd}\right) + \frac{1}{4}}$$

196

where H is the experimentally determined quantity given above.

For alumina, it is a constant over a moderate range of conditions, for steel, it is variable, dependent on power, speed, spot size, and cutting gas.

Front View

Side View

Focused Laser Beam

High Pressure Argon

Low Pressure Helium

Nozzle Orifice

0.10"

0.02"

Coaxial Nozzle

Cross Nozzle

Focal Point
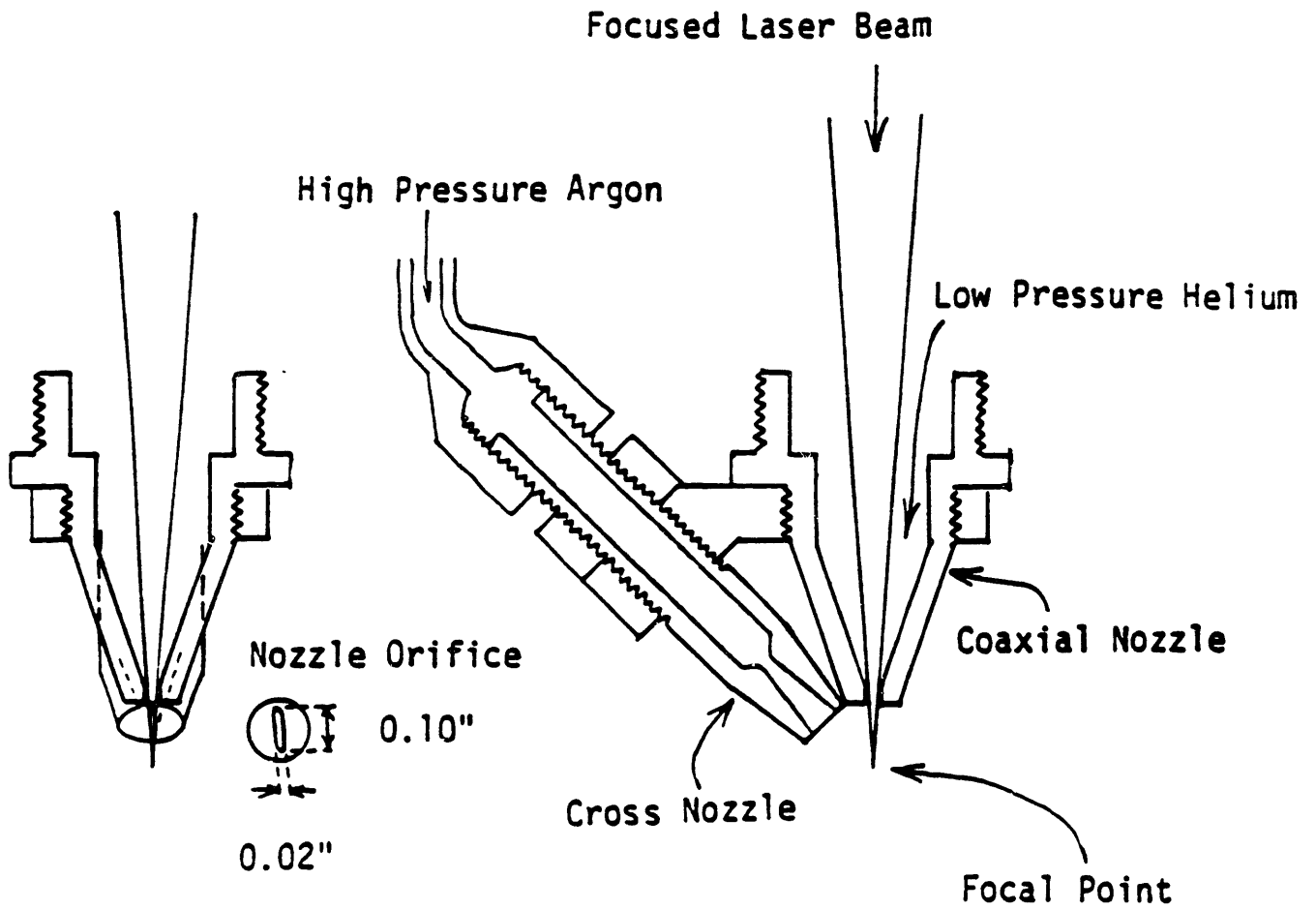
Figure 30. Diagram of second prototype laser cutting head for blind cutting.
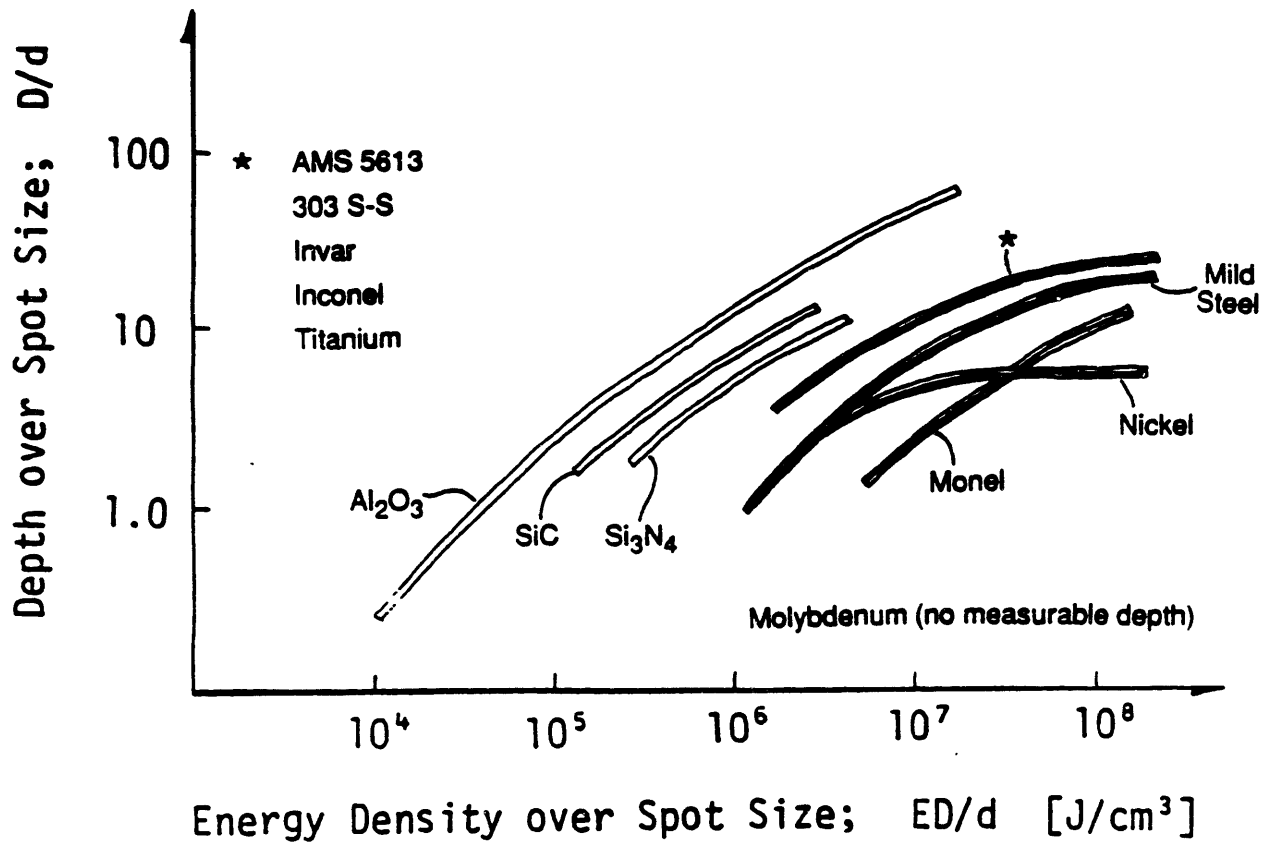
Figure 31. D/d vs. ED/d for laser blind cutting of Al_2O_3, SiC, Si_3N_4, Mild Steel, Nickel, Monel, Molybdenum, AMS 5613 S-S, 303 S-S, Invar, Inconel, and Titanium.

Material	Enthalpy of Removal (experimental) J/cm^3	Enthalpy of Removal $\rho C_p(T_s - T_0)$, J/cm^3	Total MRR / Unit power cm^3/J
Alumina	3×10^4	1.4×10^4	1.6×10^{-4}
Silicon Carbide	6×10^4	2×10^4	8×10^{-5}
Silicon Nitride	1×10^5	9×10^3	5×10^{-5}
Mild Steel	5×10^5 to 10^6	9×10^3	6.3×10^{-6}
AMS 5613 303 S-S Invar Inconel Titanium	5×10^5	9×10^3	1.5×10^{-5}
Nickel	1×10^6	9×10^3	2.5×10^{-6}
Monel	4×10^6	9×10^3	2.5×10^{-6}
Molybdenum	Could not be measured	1.1×10^4	nil

5.5 Discussion of Blind Cutting of Ceramics

Profiles of representative cuts made in Al_2O_3 are shown in figure [32]. Experimental conditions are marked on the figure. In general, cuts made using the high-impulse gas nozzle were straighter, narrower, and clearer than those made using an ordinary coaxial nozzle. Some damage due to cracking of the workpiece was observed in dense alumina, but little occured in ceramic of 10% or more porosity. Blind cuts could be made to depths of 3/8 in. (9 mm) in porous alumina with very little cracking. Dense alumina would crack if cut deeper than 1/8 in. (3 mm). Porous silicon carbide was machined to depths of 0.1 in. with no difficulty, however, dense silicon carbide (Hexoloy; Union Carbide) cracked so severely that cuts of any depth could not be formed without destroying the workpiece. Dense silicon nitride machined to depths of 0.1 in. with only slight cracking. Cemented tungsten carbide machined well with no cracking at the same rate as mild steel.

It was found in general that when molten ceramic is allowed to resolidify in the kerf, cracking was much more severe than if it were adequately removed. Dense silicon carbide proved difficult to cut because of the high viscosity of the ceramic in its molten state. Silicon nitride, on the other hand, machined very cleanly because it decomposes into elemental vapor components at atmospheric pressure without melting.

Resolidification of molten ceramic in the kerf is the primary cause of cracking. The silicon carbide specimens which cracked did so a short time after the laser passed over the kerf. Very slender kerfs were formed by the laser which were mechanically unstable because of the thermal stresses created by resolidifying material. This hypothesis is also borne by observations of cutting of alumina with and without a high-impulse gas assist.

Materials which are evaprated by the laser without melting can be expected to machine with little or no cracking. One material mentioned is silicon nitride, which is an artificial ceramic synthesized fron volatile components. Another ceramic which behaves in this way is quartz. Quartz (silicon dioxide) decomposes under the laser beam to silicon monoxide and oxygen. The silicon monoxide burns immediately in air to reform

quartz as a very fine-particle white smoke. Molten quartz is never observed under a CO_2 laser beam.

5.6 Discussion of Blind Cutting of Steel

The material which was studied most thoroughly during the third phase of the experimental program was mild steel. Besides comparing its machinability with the other materials tested, process parameters were varied in order to find the best combination for the machining of steel.

1. Optimum Assist Gas

One of the most important issues addressed in this segment of experimentation was what assist gas produced the best effect in machining steel. Three gases were tried.

• Argon was used to provide a mechanical clearing action with no chemical reactivity. The pressure used was usually 500 psi.

• Oxygen was used at a substantially lower pressure (25 - 100 psi) to determine the effect of chemical activity without high impulse.

• Compressed air was used at a range of pressures (100 - 500 psi) to produce a combination of chemical activity and high impulse.

The experimental results are presented graphically in figure [33]. Oxygen and air were found to machine steel at approximately the same rate, and argon was substantially slower. Magnified cut profiles for the three gases are shown in figure [34]. Cuts made with argon were the narrowest, very closely approaching the diameter of the focused spot. Cuts made with oxygen are substantially wider, and typically flare out along the top edge. Compressed air produces cuts which are slightly wider than those produced with argon, and have straight sides with no flaring.

It was decided that compressed air was the best assist gas to use for machining steel. The pressure was varied and it was found that air at 100 psi machined as effectively as air at 500 psi.

a.

P = 1000 W

V = 2 cm/sec

d = .013 cm

2 Passes

Depth = .43 cm

D/d = 35

b.

P = 1000 W

V = 3.8 cm/sec

d = .013 cm

3 Passes

Depth = .52 cm

D/d = 42

c.

P = 1000 W

V = 10 cm/sec

d = .013 cm

8 Passes

Depth = .52 cm

D/d = 42

d.

P = 1000 W

V = 20 cm/sec

d = .013 cm

17 Passes

Depth = .50 cm

D/d = 40
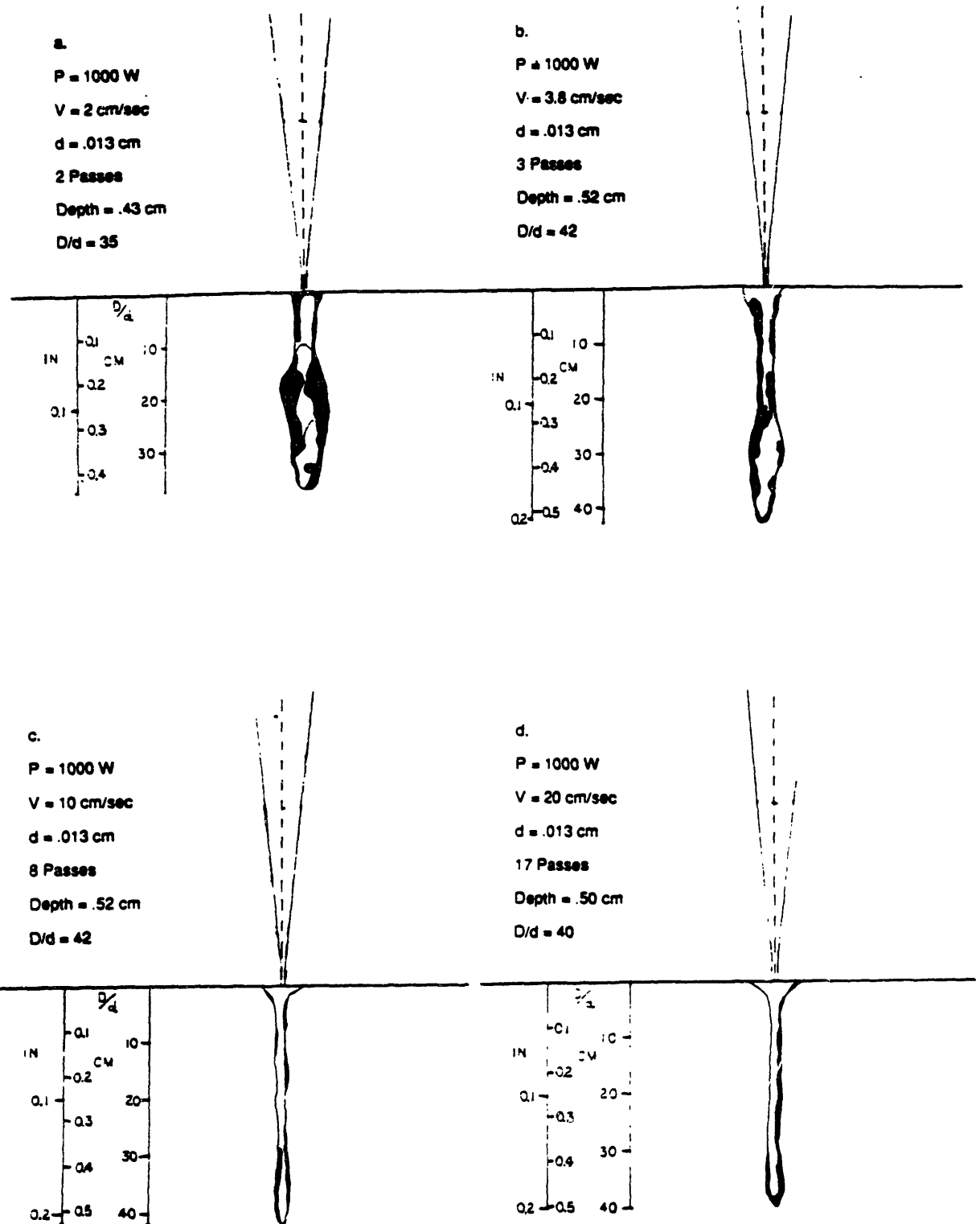
Figure 32.   Cut profiles in Al_2O_3 showing effects of varying surface speed in laser blind cutting.
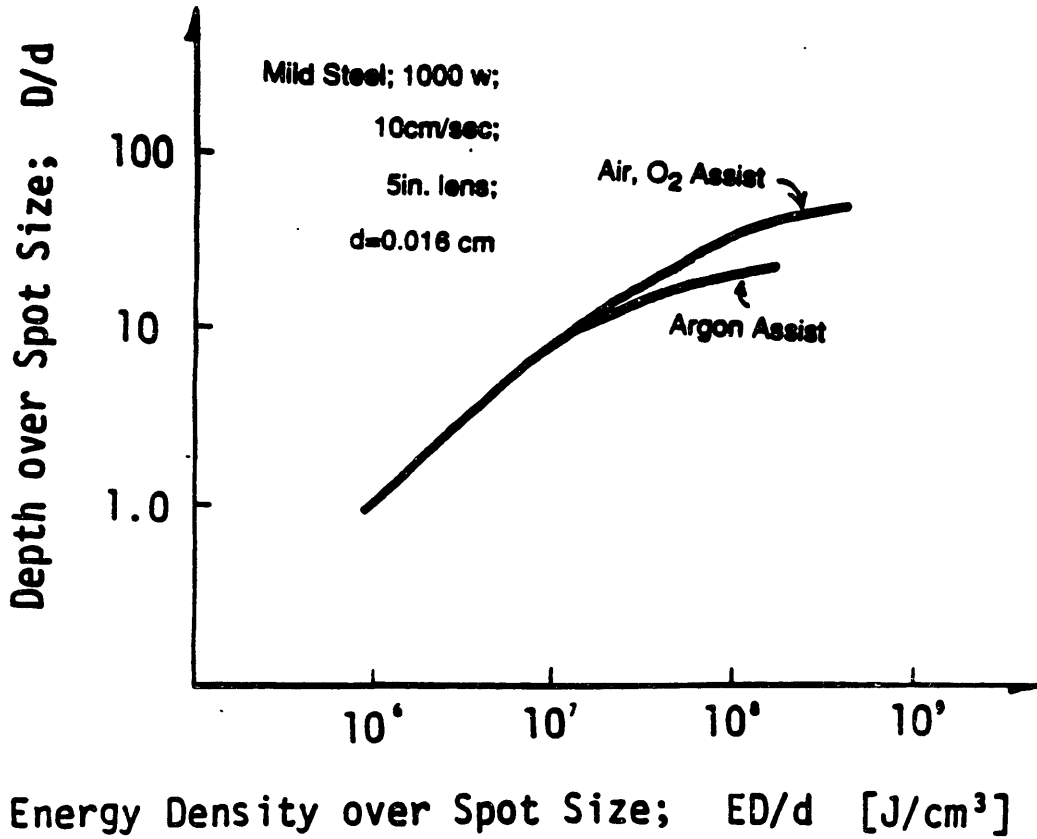
Figure 33. D/d vs. ED/d for mild steel, showing enhancement of cutting rate using an oxidizing asist gas.
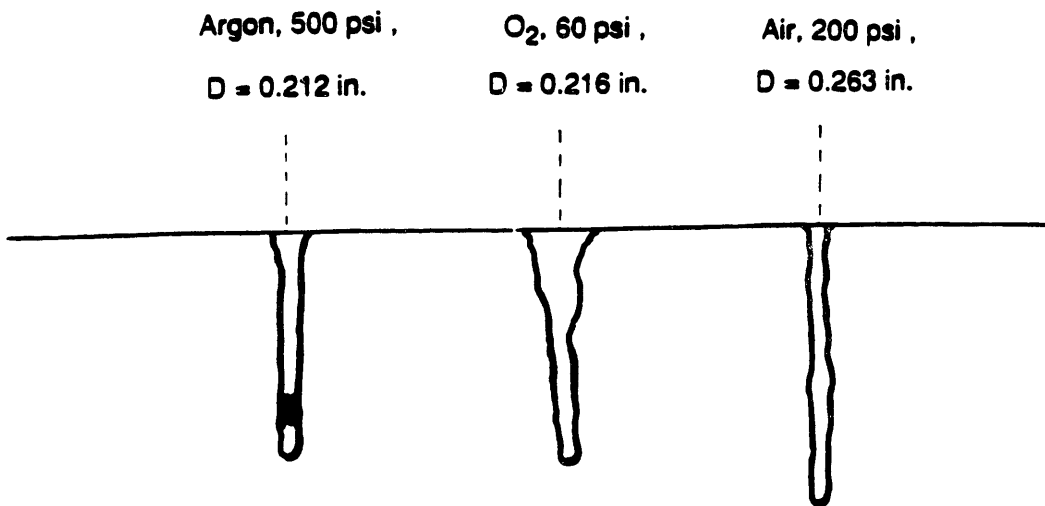
Figure 34. Cut profiles in mild steel comparing differences between argon, oxygen, and compressed air assist gases. Conditions for all three: P = 1000 W, V = 10 cm/sec, d = 0.016 cm, n = 50 passes.

2. Variation of Laser Power

The next series of tests determined the effect of varying the power and surface speed in machining of steel. The laser power was varied between 150 W and 1500 W in continuous-wave mode. Cuts were made at speeds of 10, 5, and 2 cm/sec for various amounts of time such that the energy densities overlapped. These data are plotted in figures [35], [36], and [37]. In figure [35], cuts made at 10 cm/sec show a very clear increase in cutting efficiency, η, as the power increases.

It is very important to note that when the data are plotted in this way, the quantity of time required to make a cut of a particular depth has been suppressed from the graph. A line which is higher or to the left of another line shows that less energy is required to produce a cut of a given depth, regardless of the cutting time. A laser beam with a higher power will necessarily cut faster than one at a lower power because the same energy is delivered in less time. The graph in figure [35] shows that as the laser power increases, the cutting rate increases in higher proportion. For example, a 1500 W laser beam will cut approximately three times as fast as a 1000 W laser beam to a depth of 0.1 inches in mild steel at 10 cm/sec.

Figure [36] shows data for 5 cm/sec surface speed in mild steel. Here, the cutting efficiency at 1500 W is the same as that for 1000 W, and the efficiency at 500 W and 700 W is only slightly less than that. In figure [37], data is shown for 2 cm/sec. At this speed, 500 W and 700 W have the same cutting efficiency η as 1500 W at 10 cm/sec. This is to say that a cut to a given depth is accomplished by a 500 W laser at 2 cm/sec in three times the time as a 1500 W laser at 10 cm/sec. The cuts which were attempted at 1500 W and 1000 W at the slowest speed were unsuccessful due to inadequate material removal.

For each of these conditions:

1500 W, 10 cm/sec;

1500 W, 5 cm/sec;
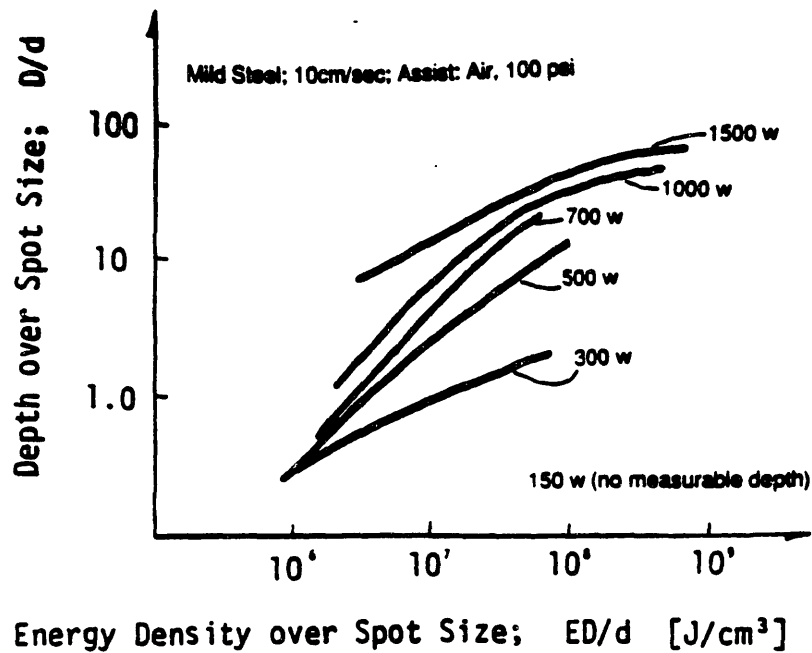
Figure 35. D/d vs. ED/d for mild steel at various powers. Conditions: V = 10 cm/sec, d = 0.016 cm, Assist = Air, 100 psi.
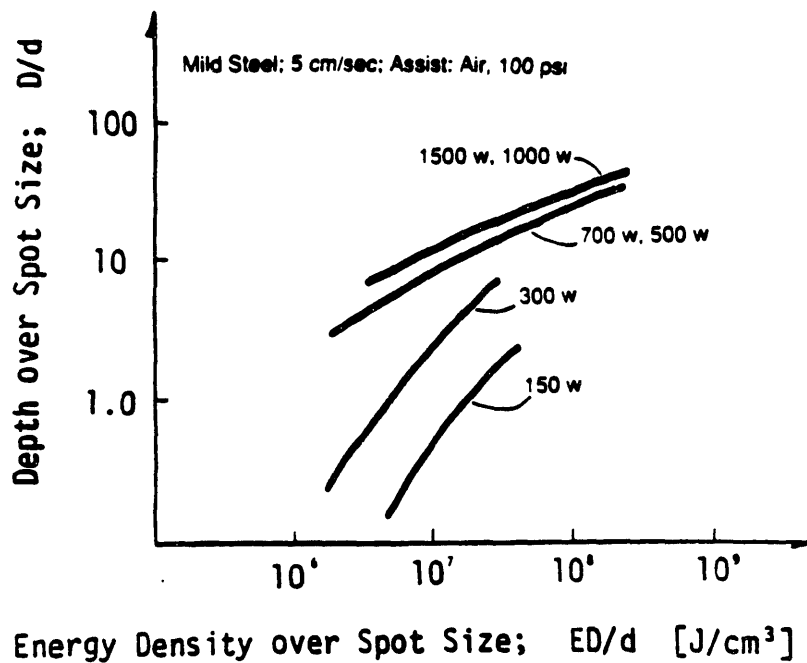
Figure 36. D/d vs. ED/d for mild steel at various powers. Conditions: V = 5 cm/sec, d = 0.016 cm, Assist = Air, 100 psi.
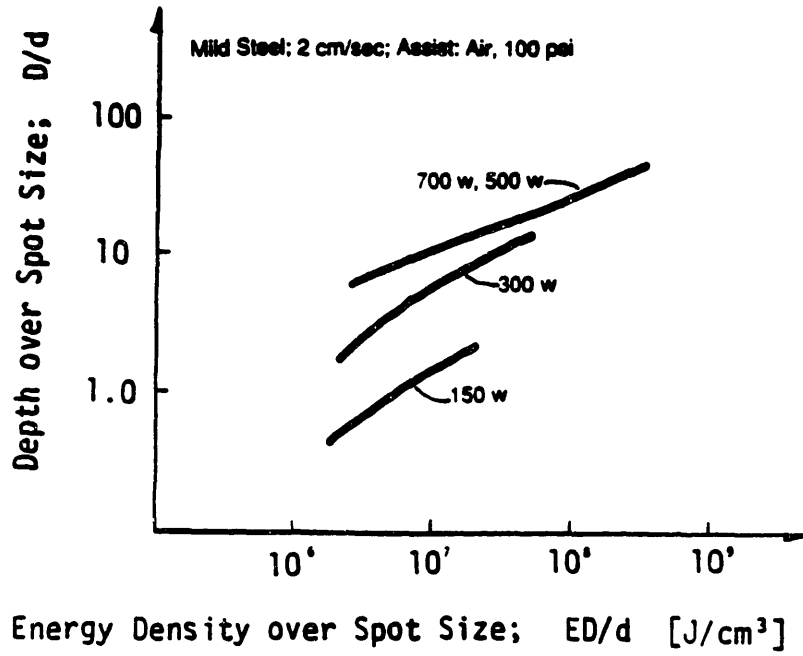
Figure 37. D/d vs. ED/d for mild steel at various powers. Conditions: V = 2 cm/sec, d = 0.016 cm, Assist = Air, 100 psi.

1000 W, 5 cm/sec;

700 W, 2 cm/sec; and

500 W, 2 cm/sec

(spot size, d = 0.016 cm),

the quantity J/VH is between 50 and 100. Cuts from which material removal was inadequate had J/VH equal to 200 or greater. Cuts with poor efficiency were made with J/VH between 10 and 50, and when J/VH was less than 10, the laser did not cut the steel at all.

The quantity Vd/α is independent of power, and for this test, d/α is approximately 1/10 [sec/cm] so at 10 cm/sec, Vd/α is roughly unity. This means that substantial amounts of heat are being lost in the kerf. If the surface speed were increased to roughly 100 cm/sec, and J/VH kept the same, it is likely that the energy efficiency of the laser would be nearly the maximum possible for the machining of steel.

Since the thermal diffusivity of alumina is roughly 1/10 times that of steel, we see at 10 cm/sec a condition where Vd/α is ≈ 10, and at 1000 W, J/VH is about 30. Although alumina melts 500°C hotter than steel, the lower thermal diffusivity allows it to be machined 25 times faster than steel.

It may not be true that a 15 kW laser focused to 0.016 cm at a surface speed of 100 cm/sec will machine steel 250 times faster than is currently possible with a 1500 W laser, but this hypothesis is supported by both the theory and the data.

These data were taken using the laser in the continuous wave mode. It was anticipated that continuous wave cutting would be easier to model, and the experimentation was restricted to continuous-wave so as not to complicate the results. Several experiments have been done since the completion of the experimental program presented here which suggest the following.

When a laser is operated in pulsed mode, the instantaneous power of the beam can

greatly exceed the average power. Because the power density, J, is very high during a pulse, the cutting efficiency is characteristic of the peak power. The quantity of time required to obtain a given energy density is inversely proportional to the average power, which is much smaller than the peak power. Therefore it is anticipated, and preliminary experiments have indicated, that a pulsed laser with a given average power will cut faster than a CW laser of the same average power.

3. Variation of Surface Speed

A further series of experiments were performed with a CW laser beam at 1000 W and the surface speed was varied between 2 cm/sec and 100 cm/sec. These data are presented in figures [38], and [39]. Figure [38] shows the data plotted as D/d vs. ED/d for each speed, and figure [39] shows the same data plotted as D/d vs. V for different energy densities. Figure [38] (D/d vs. ED/d) shows that the cutting efficiency is roughly constant at the low speeds, and diminishes for the higher speeds. Figure [39] (D/d vs. V) shows this much more clearly. The curves in this graph tend to a maximum at a speed of roughly 5 to 10 cm/sec (J/VH = 40-80) and drop off quickly. At 100 cm/sec, J/VH = 4 and the cutting efficiency is roughly 1/10 of its value at 10 cm/sec. At the maximum speed tested, using data from figure [29], V=420 cm/sec, J/VH is approximately one and the cutting efficiency is nil.

This indicates that laser cutting of metals is much more sensitive to J/VH than it is to Vd/α. according to the model, as Vd/α increases, the energy efficiency should increase. What has been found is that the efficiency decreases rapidly if J/VH is less than 30.

4. Calorimetry Tests

During the experimental phase of this project, severe heating of steel workpieces was observed. Also, the volume of material removed from the workpiece accounted for only 1% of the heat supplied by the laser. The two factors which were most uncertain were the quantity of laser radiation reflected from the blind kerfs and the cooling effect of the gas assist nozzle. In order to quantify these two effects, a series of experiments were perfomed in which the temperature rise and weight change of steel workpieces was
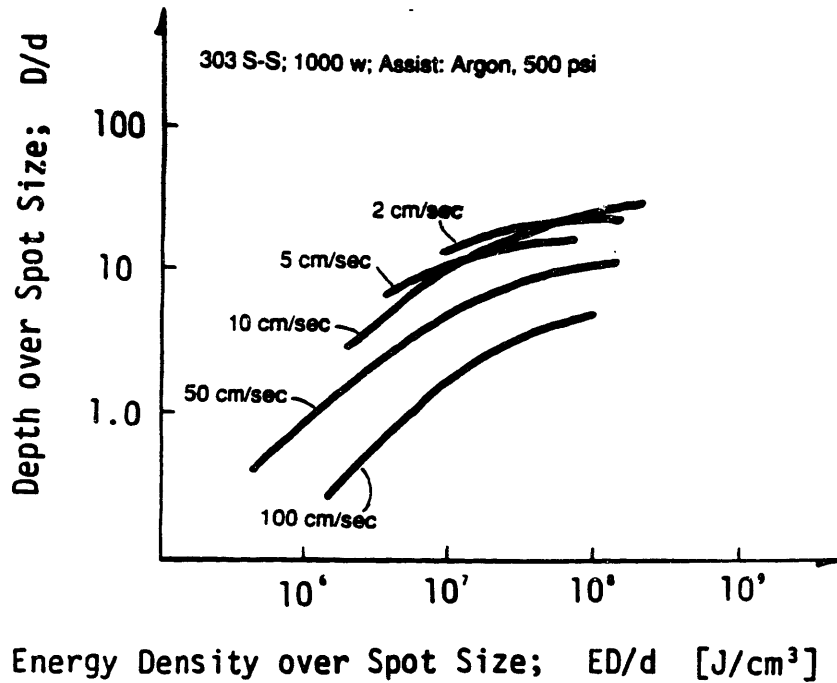
Figure 38. D/d vs. ED/d for 303 stainless steel at various surface speeds. Conditions: P = 1000 W, d = .016 cm, Assist = Argon, 500 psi.
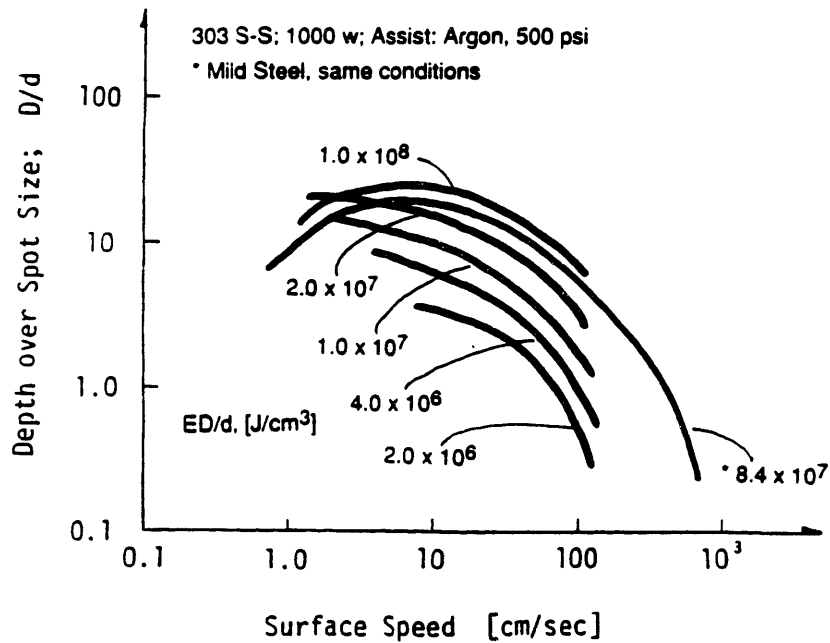
Figure 39. D/d vs. Surface speed for 303 stainless steel for various energy densities. Conditions: P = 1000 W, d = .016 cm, Assist = Argon, 500 psi.

measured for cuts under different conditions. Although these experiments were not conclusive, they did provide insight into the process.

Cylindrical specimens were machined in mild steel with a diameter of 1 in. and a length of 0.5 in. They were bored through with a 0.08 in. drill and countersunk on both sides. Each specimen was cleaned and weighed to the nearest 0.01 g. The mean weight was 50 g.

To cut these specimens with the laser, a jig was designed which would insulate the workpieces as well as possible (see figure [40]). The specimens were turned by a three-edged countersink mounted on the motor chuck, and they spun on a live center with a hollow ceramic "fish-spine" bead as a point. A 0.06 in. diameter thermocouple (type K) was inserted through the live center into the hole in the workpiece such that the workpiece turned on the stationary thermocouple and thermal contact was maintained. Several experiments were done, however only one series will be discussed because the others provided no additional useful information.

The gas nozzle was configured as shown in figure [30]. Specimens were rotated at 75 rpm, giving a surface speed of 10 cm/sec. Argon was blown through the nozzle at 500 psi. The pressure of the coaxial jet was 10 psi of air. The 1000 W laser beam was focused with a 5 in. objective to a spot size of 0.016 cm. Cuts were made in a logarithmic sequence, using 1, 2, 5, 10, 20, 50, and 100 passes over a given point. The temperature was measured before the laser was started, and the high pressure nozzle was cut off simultaneously with the laser. The peak temperature rise was recorded for each cut, and usually occured roughly 2 sec after the laser was shut off. These measured temperature rises are plotted in figure [41] as ΔT vs. Energy = $P \times t_{on}$.
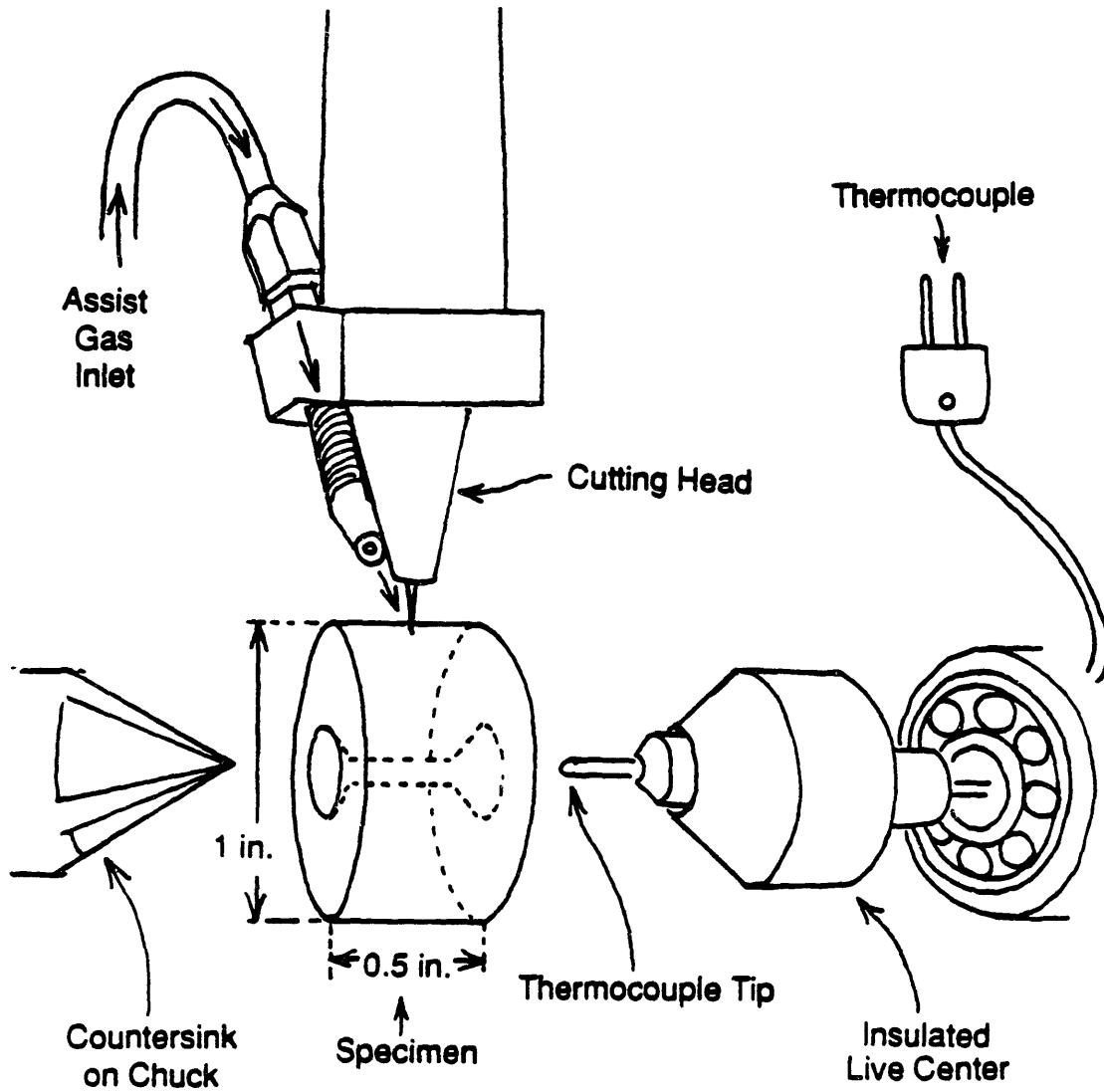
Figure 40. Experimental configuration for calorimetry tests performed of August 1, 1986.
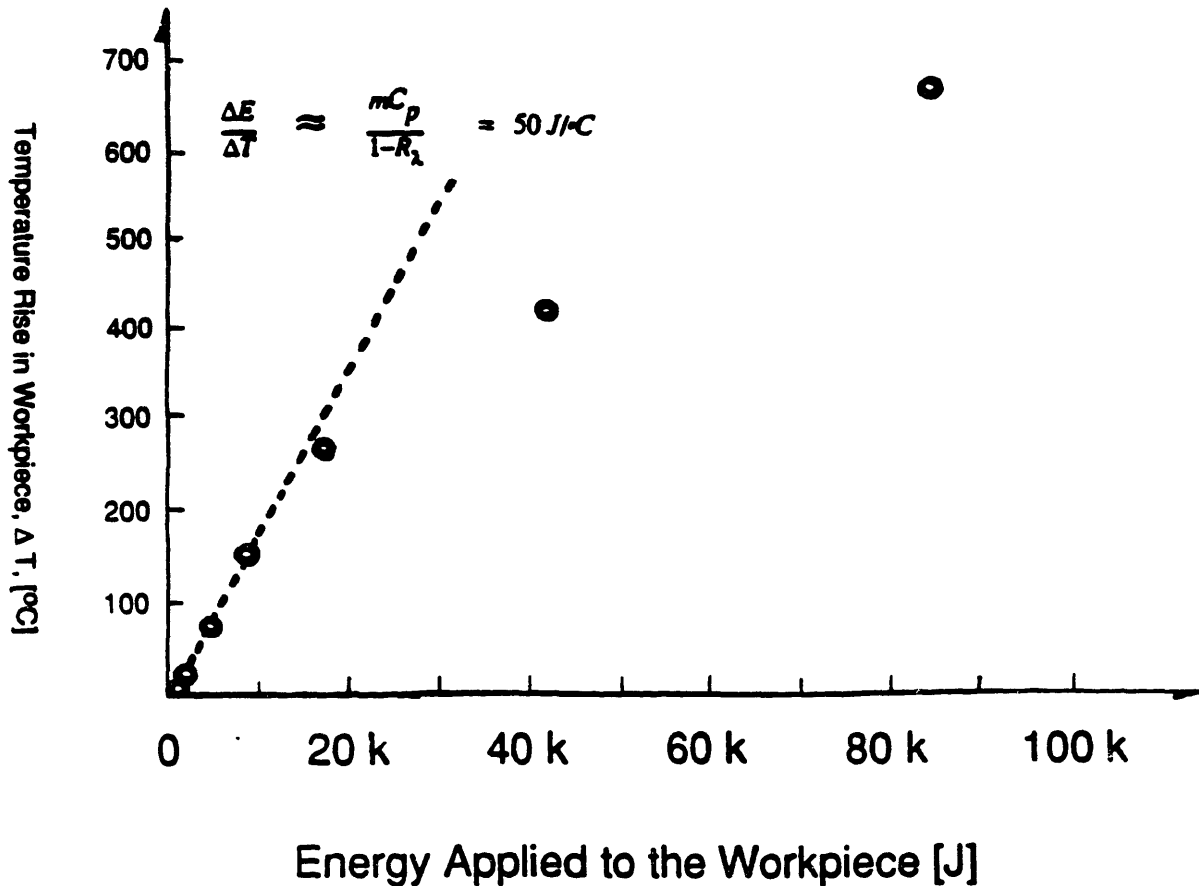
$$\frac{\Delta E}{\Delta T} \approx \frac{m c_p}{1-R_\lambda} = 50 \, J/{}^\circ C$$

Figure 41. Temperature rise, Δ T, vs. Laser energy, P x t, in 50 g mild steel specimens. Conditions: P = 1000 W, V = 10 cm/sec, d = .016 cm, Assist = Argon, 500 psi.

The cooling rate from the gas nozzle was measured in the 100-pass cut. The assist nozzle was cut off simultaneously with the laser to read the peak temperature (700°C). Then the nozzle was turned back on to cool the workpiece. Temperatures were read at five second intervals during a cooling period of two minutes until the cooling rate was less than 0.5° per second. This cooling curve is shown in figure [42]. The cooling power of the gas nozzle was calculated as a function of temperature from this cooling curve by multiplying the cooling rate by the specific heat of the specimen (22.5 J/°C). A graph of cooling power vs. temperature is shown in figure [43].

The weight change of each specimen was measured. The assumption was made that
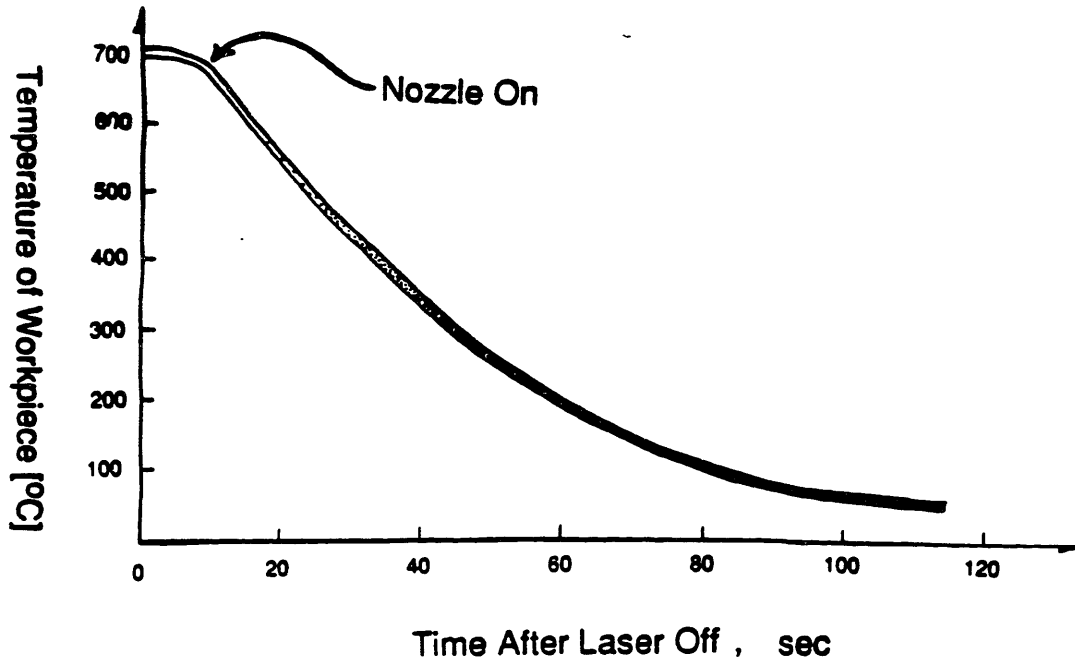
Figure 42. Cooling curve for specimen #27 after laser off. Maximum temperature: 696°C.
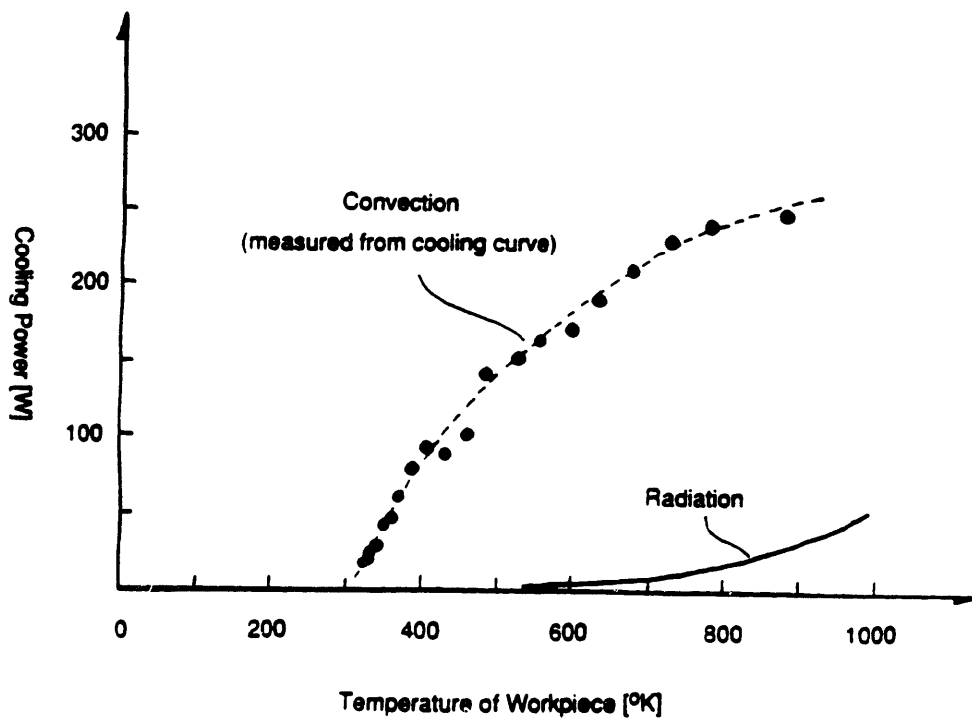
Figure 43. Cooling power vs. Temperature calculated from cooling curve in figure 42.

material left the specimen at its melting point, and the rate of heat extracted due to material removal was calculated.

The calculated cooling power of the assist nozzle was measured without the laser on. When the nozzle blows over the heated cutting front under the laser, a certain quantity of heat must necessarily be lost from that point, and it is impossible to estimate exactly what it is. It is assumed that this quantity of heat is negligible, because the heated area under the laser spot is much smaller than the exposed area of the workpiece. The amount of heat lost due to the assist nozzle blowing on the heated bulk of the workpiece is estimated by integrating the calculated cooling power from room temperature to the temperature in question, and multiplying by the total cutting time for a given specimen.

$$Q_{conv}(T) = \int_0^t P_{cooling}(T)\, \partial t$$

$$\approx t \int_{T_0}^T P_{cooling}(T)\, \partial T \quad \text{(Assuming } \frac{\partial T}{\partial t} \text{ is constant)}$$

197

Since the observed cooling power of the assist nozzle is zero when the workpiece is at room temperature, and the heat extracted due to material removal is negligible, it is possible to estimate the fraction of heat reflected from the workpiece from the relation:

$$\frac{mC_p}{1-R_\lambda} = \frac{\partial E}{\partial T}$$

198

where:

mC_p = 22.5 J/°C = Specific heat of specimen

R_λ = Reflectivity

E = Energy applied from laser

T = Measured temperature of the specimen

This quantity corresponds to the reciprocal of the slope of the line in figure [41]. It is almost exactly 50 J/°C, resulting in an estimate of 0.5 for the reflectivity.

The sums of all of the various measured and calculated heat contributions are plotted in figure [44]. It can be seen that the temperature rise of the workpiece is the dominant mode of heating. Convective losses are negligible, except when the workpiece becomes very hot, and heat loss due to material removal is negligible except in a single pass cut. The calculated radiative heat loss is negligible, and the factor of 0.5 is found to be uniform throughout the experiment. Only one-half of the energy applied by the laser arrived at the workpiece. Some of this heat could have been removed by convection of the assist gas against the laser spot, but it is more likely due to the reflectivity of the steel.

5.7 Summary of Conclusions of Phase III Experimentation

The purpose of the third phase of the experimental program was to test the most promising development from Phase II and optimize it for laser blind cutting. This development was a high-impulse gas nozzle which mounted on the focusing head of the laser and aimed at the kerf. Once the nozzle holder had been built, different nozzles were tested with different gases to determine their effectiveness.

1. The nozzle which had the best effect on the cutting rate had the largest orifice. Of the different gasses and pressures tried, compressed air at 100 psi pressure or higher peformed the best.

2. In the cutting of ceramics, the high-impulse nozzle was able to make cuts in aluminum oxide to depths of 1/4 in. or more with no clogging. Silicon nitride was another material which behaved well under the laser, although this material was not studied as extensively as alumina.

3. Porous ceramics always machine more easily than dense ceramics. This is undoubtedly due to the fact that porous ceramics are tougher than dense ones. Dense ceramics could be machined with precautions to make relatively shallow cuts which did not overheat the workpiece.
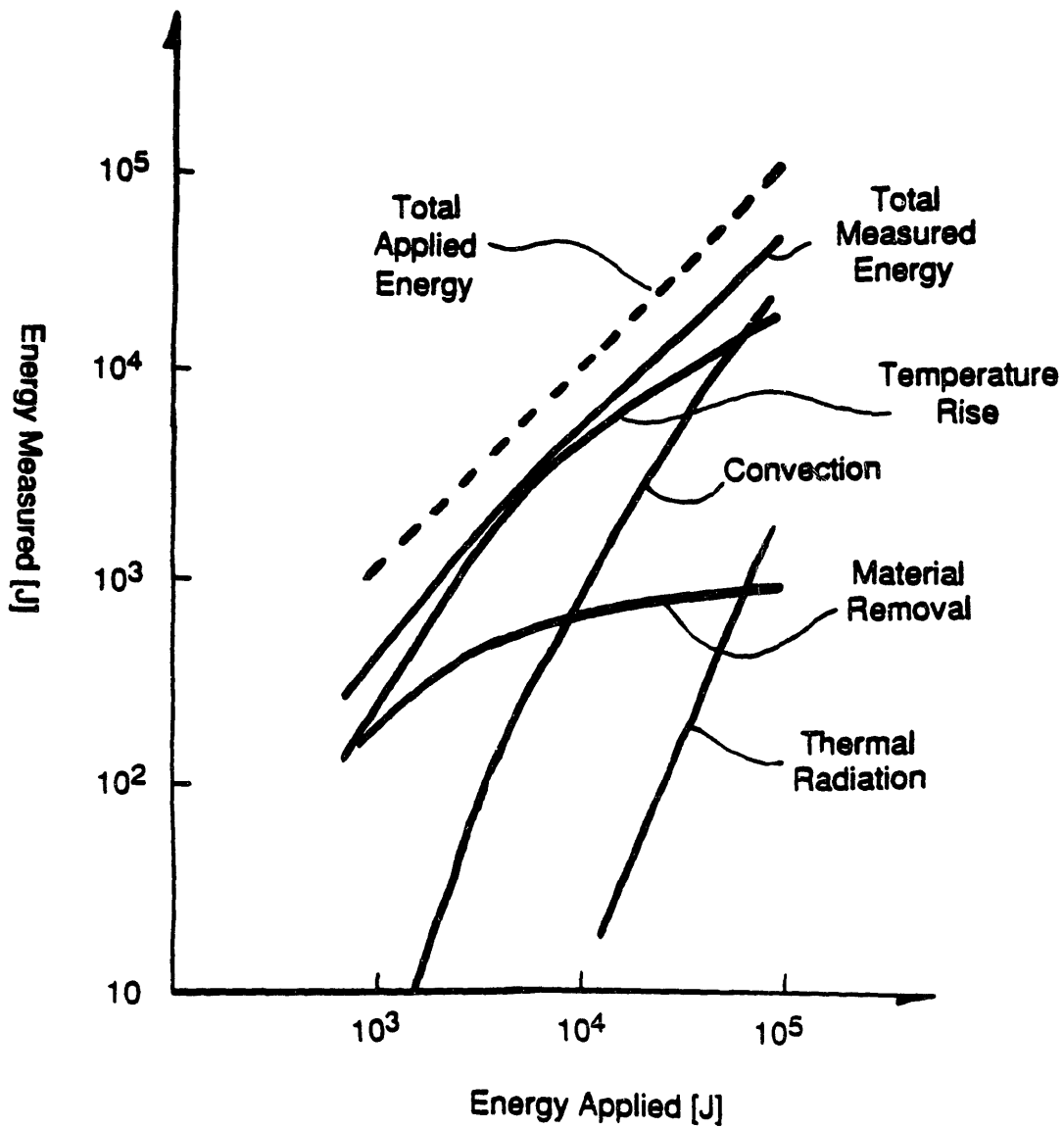
Figure 44. Contributions of various forms of heat loss in laser blind cutting of mild steel calculated from calorimetry data.

4. Metals cut roughly an order of magnitude slower than ceramics. Since metals have roughly ten times the thermal conductivity of ceramics, one would expect metals to dissipate heat into the bulk of the workpiece ten times as quickly as ceramics. This is certainly true, however it appears that there is some other large mode of heat dissipation which is not accounted for in heat conduction models. The heat loss could possibly be due to vaporization of material ejected from the kerf.

5. Oxidizing asist gases provide a detectable improvement in laser cutting of steel. Under the very best conditions, an oxygen or compressed air jet allows the laser to cut steel roughly twice as fast as an argon jet. Pure oxygen damages the workpiece somewhat by producing wide, uneven kerfs. Workpieces were observed to ignite and burn in the oxygen jet even after the laser was turned off. Compressed air produced straight, narrow kerfs in steel as quickly as oxygen, but with none of the problems.

6. The cutting efficiency of the laser in steel is very sensitive to surface speed. A 1500 W focused laser beam cuts optimally at 10 cm/sec, while a 500 W focused laser beam cut optimally at 2 cm/sec with the same energy efficiency as the 1500 W beam.

7. The optimum machining conditions in steel seemed to be more dependent on J/V H, the normalized energy density per pass. For steel, optimum conditions occured for J/V H between 50 and 100. Above 200, the kerf became clogged with resolidified material, and below 50 the cutting efficiency diminished.

8. The cooling power of the assist gas nozzle is insignificant until the temperature of the workpiece becomes excessively high. At 700°C, the asist gas nozzle operating at 500 psi provided 250 W of cooling. At this temperature, the cooling power is roughly 150 W.

9. Roughly half of the heat delivered to a steel workpiece during laser machining is dissipated as a temperature rise in the workpiece. It is hardly surprising that so much heat is conducted away. The surprising result of the calorimetry experiments was that roughly one-half of the heat delivered by the laser is disspated or scattered without entering the workpiece. The most likely explanation of this is that the light is reflected

from the kerf. An experiment to detect this radiation would not be difficult to perform, considering the quantity of energy that is thrown off.

10. A pulsed laser tends to cut with a higher energy efficiency than a CW laser with the same average power. This is slightly deceptive, because a laser which can pulse at 700 W average power and 1500 W peak power can operate in CW mode at something more than 700 W, perhaps even as high as 1500 W CW. Pulsed CO_2 lasers do not ordinarily have peak powers much higher than their maximum CW power. YAG lasers, on the other hand, have peak powers as high as 50 kW for a 250 W average power beam.

6. Conclusion

The theoretical and experimental work presented in this thesis has been performed specifically for the purpose of assisting in the design of the laser lathe. This new machine tool promises to greatly ease many of the problems encopuntered in manufacturing with advanced materials. Before the process can be successful, however, the quality of the cuts must be improved and the cutting process must be controlled to improve dimensional accuracy.

Overall, the feature of the cutting tool which has the greatest effect on performance is the gas jet. During this experimental program, several prototype jets were built, each one with a larger flow rate than the last. Each new jet, in turn, improved the process dramatically. Therefore, it is of primary importance to increase the impulse of the gas jet and obtain cuts of the highest possible quality. Another improved gas jet was used by two students, Alexandra Linde and George Capek for their bachelor's thesis work (MIT S.B. 5/87) which had the following features.

The coaxial nozzle had a taper of 19° and the side jet was oriented almost vertically. The side jet consisted of a 1/4" copper tube, flattened to make a 0.02"x0.25" flat orifice. The orifice was aligned in the same way as the nozzle in figure 30, except it was placed more closely to the laser beam axis at a nearly vertical orientation. This nozzle carried compressed air at 120 psi or oxygen. This nozzle produced cuts of strikingly high quality, better than the cuts produced in this thesis.

There is every reason to expect that further advances are obtainable with more powerful gas jets.

The experimental program has shown that some materials are particularly well suited to laser machining. Ceramics, because of their low thermal conductivity, cut much faster than metals. Ceramics which decompose into vaporous products under laser radiation resist cracking to a higher degree than ceramics which melt in the laser beam. This phenomenon is the most important feature which determines the machinability of a ceramic with lasers.

Metals can be machined using this method, although the cutting rate is slower than for ceramics. The high thermal conductivity of metals allows them to overheat during cutting. If proper coolant is provided, the temperature of the workpiece can be kept down; and parts can be machined. Nevertheless, the slow cutting rate and poor tolerance limits this process to rough machining of very hard metals, unless substantial improvements are made over the results obtained in this thesis.

There is much room for further experimentation. This thesis was limited in scope to cutting with a continuous-wave beam. As of this writing, experiments have been done to show that pulsed laser beams cut faster than CW beams of the same average power. Controlled cracking of brittle materials showed promise, but was not investigated further. No experimentation was performed to determine if oxygen enhances the cutting rate in non-oxide ceramics such as silicon carbide. These are the subjects of future experiments for other students working in the continuation of this project.

This project has been very successful. The purpose of this thesis was to determine the feasibility of the concept of a machine tool based on blind cutting with lasers. The conclusdion is that the laser lathe is feasible, and the work has attracted enough interest both from sponsors and students to keep it advancing.

6.1 Acknowldgements

This project has been funded by two major sponsors.

• Ford Motor Company, Transmission and Chassis Division, and

• Coherent General, Inc.

have my thanks for making this research project possible.

I would like to thank my thesis advisor, Dr. George Chryssolouris, for all of his motivation and direction, and for inventing the laser lathe in the first place.
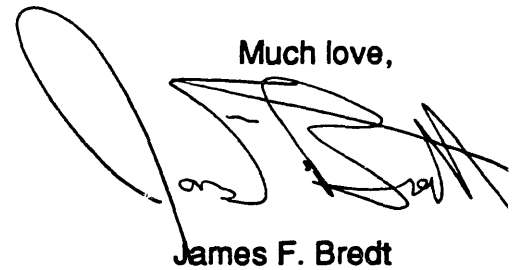
The Laboratory for Manufacturing and Productivity is a very nice community in which I have felt very comfortable for my two and a half year stay with the mechanical

engineers. I would also like to thank my old friends in materials science for giving me a place to hide when I needed to.

My parents have given me a lot of support, but the best thing they've done for me is tell me that a Master's degree is enough.

I also owe a very special thanks to a very good friend of mine named Fred without whose companionship my eight years at MIT would have been unbearable.

Much love,

James F. Bredt

I. BIBLIOGRAPHY FOR LASER MACHINING

Anthony, T.R.: 'The Random Walk of a Drilling Laser Beam' J. Appl. Phys. 51, #12, 1980, 1170-1175, 7 Refs

Babenko, V.P.; Tychinskii, V.P. 'Gas-Jet Laser Cutting (Review)' Soviet J. Quan. Electron. 2, #5, 1973, 399-410, 26 Refs

Bar-Isaac, C.; Korn, U.: 'Moving Heat Source Dynamics in Laser Drilling', Appl. Phys., 3, 1974, 45-54, 24 Refs

Brugger, K.: 'Exact Solutions for the Temperature Rise in a Laser- Heated Slab', J Appl. Phys. 43, #2, 1972, 577-583, 18 Refs

Bunting, K.A.; Cornfield, G.: 'Toward a General Theory of Cutting: A Relationship Between the Incident Power Density and the Cut Speed', Trans. ASME, Feb. 1975

Carslaw, H.S.; Jaeger, J.C.; _Conduction of Heat in Solids_, 2nd Ed. Oxford Univ. Press, Lon. 1959.

Chande, T.; Mazumder, J.: 'Two Dimensional, Transient Model for Mass Transport in Laser Surface Alloying' J. Appl. Phys. 57, #6, 1985, 2226-2232, 11 refs

Chryssolouris, G.: 'Stock Removal by Laser Cutting', U.S. Patent Application Serial No. 640764, Aug. 1984

Chryssolouris, G.; Bredt, J.; Kordas, S: ' Laser Turning for Difficult to Machine Materials', in 'Machining of Ceramic Materials and Components', Proc. PED Vol. 17, Winter Annual Meeting of ASME, 11/85, pp 9-19, 7 refs

Chryssolouris, G.; Bredt, J.; Kordas, S.: 'A New Machine Tool Concept Based on Lasers', NAMRC, May, 1986, 12 refs

Chryssolouris, G.; Bredt, J.; Kordas, S.; Wilson, E.: 'Theoretical Aspects of a Laser Machine Tool'

Chun, M.K.; Rose, K.: 'Interaction of High Intensity Laser Beams with Metals' J. Appl.

Phys. 41 #2, 1970, 614-620, 10 Refs

Cline, H.E.; Anthony, T.R.: ' Heat Treating and Melting Material with a Scanning Laser or Electron Beam', J. Appl. Phys. 48, #9, 1977, 3895-3900, 17 Refs

Cohen, M.I.; Epperson, J.P.; 'Applications of Lasers to Micro- electronic Fabrication', in _Advances in Electronics and Electron Physics_ Marton, El-Kareh Eds, V. 4, 1968

Copley, S.M.; Bass, M.: Wallace, R.G.: 'Shaping Silicon Compound Ceramics with a Continuous Wave Carbon Dioxide Laser', in _Lasers in Materials Processing_ E.A. Hetzbower, Ed. 1983 ISBN 0-87170-173-1, 97-105, 4 Refs

Dabby, F.W.; Paek, U-C. 'High Intensity Vaporization and Explosion of Solid Material', IEEE J. Quan. Electron. QE-8, #2, 1972, 107-111, 10 Refs

Decker, I.; Ruge, J.; Atzert, U.: 'Physical Models and Technological Aspects of Laser Gas Cutting', Proc. SPIE, Sept, 1983, 81-87

Dowden, J.; Davis, M.; Kapadia, P.: 'The Flow of Heat and the Motion of the Weld Pool in Penetration Welding with a Laser' J. Appl. Phys., 57, #9, 1985, 4474-4479, 11 refs

El-Adawi, M.K.; Shalaby, S.A.:'Laser Melting of Solids- An Exact Solution for Time Intervals Greater Than the Transit Time' J. Appl. Phys., 60, #7, 1986, 2260-2265, 23 refs

El-Adawi, M.K.: 'Laser Melting of Solids- An Exact Solution for Time Intervals Less or Equal to the Transit Time', J. Appl. Phys., 60, #7, 1986, 2256-2259, 15 refs

El-Adawi, M.K.; Elshehawey, E.F.: 'Heating a Slab Induced by a Time-Dependent Laser Irradiance- An Exact Solution', J. Appl. Phys. 60, #7, 1986, 2250-2255, 21 refs

Foote, G.B.: 'A Model of Deep-Penetration Electron-Beam and Laser Welding', PhD. Thesis, MIT Mech.E., 1976

Hablanian, M.H.: 'A Correlation of Welding Variables' in Proc. 4th Symp. Elect. Beam

146

Tech., 1962, 262-268, 5 Refs

Hella, R.A.: 'Laser Beam Interaction with Metal', S.M. Thesis, MIT Mech.E., Jan. 1974, 11 Refs

Klemens, P.G.: 'Heat Balance and Flow Conditions for Electron Beam and Laser Welding', J. Appl. Phys., 45, #5, 1976

Kocher, E.; Tschudi, L.; Steffen, J; Herziger, G.: 'Dynamics of Laser Processing in Transparent Media' IEEE J. Quan. Electron. QE-8, #2, 1972, 120-125, 27 Refs

Mazumder, J.; Steen W.M.: ' Heat Transfer Model for CW Laser Processing', J. Appl. Phys., 51, #2, 1980, 941-947 42 Refs

Mecholsky, J.J.: 'Fracture of Ceramics by Single-Pulse 10.6 um Irradiation' J Appl. Phys. 50, #8, 1979, 5488-5491, 20 Refs

Miyazaki, T; Geidt, W.H.: 'Heat Transfer from an Elliptical Cylinder Moving Through an Infinite Plate Applied to Electron Beam Welding', Int. J. Heat & Mass Transf., 25, #6, 1982, 807-814

Modest, M.F.; Abakians, H.: 'Heat Conduction in a Moving Semi- infinite Solid Subjected to Pulsed Laser Irradiation' Trans. ASME J. Heat Transf., 108, #8, 1986, 597-601, 12 refs

Modest, M.F.; Abakians, H.:'Evaporative Cutting of a Semi-infinite Body With a Moving CW Laser', Trans. ASME J. Heat Transf., 108, #8, 1986, 602-607, 20 refs

Paek, U-C.; Gagliano, F.P. 'Thermal Analysis of Laser Drilling' IEEE J. Quan. Electron. QE-8, #2 1972, 112-119, 15 Refs

Ready, J.F. 'Effects Due to Absorbtion of Laser Radiation' J Appl. Phys. 36, #2, 1965, 462-468, 20 Refs

Rosenthal, D. 'The Theory of Moving Sources of Heat and Its Appli- cation to Metal Treatments' Trans ASME 1946, 849-866, 20 Refs

Schoucker, D.; Abel, W.: 'Material Removal Mechanism of Laser Cutting', Proc. SPIE, Sept 1983, 88-95

Schvan, P.; Thomas, R.E.: ' Time Dependant Heat Flow Calculation of CW Laser-induced Melting of Silicon', J. Appl. Phys. 57, #10, 1985, 4738-4741

Scruby, C.B.; Dewhurst, R.J.; Hutchins, D.A.; Palmer, S.B: ' Quan- titative Studies of Thermally Generated Elastic Waves in Laser Irradiated Metals' J. Appl. Phys. 51, #12, 1980, 6210-6216, 29 refs

Sturmer, E.; von Allmen, M.: 'Influence of Laser-Supported Detonation Waves on Metal Drilling with Pulsed CO2 Lasers', J Appl. Phys. 49, #11, 1978, 5648-5664, 37 Refs

Swift-Hook, D.T.; Gick, A.E.F: 'Penetration Welding with Lasers', Welding Research Suppl., Welding, Nov. 1973, 492-s-499-s, 12 refs

Takamoto, K.; Nakayama, S.: 'Machining of Thin Metal Films with a Deflected Laser Beam' Review of Elec. Comm. Labs, 23, #3-4, 1975, 353-359, 3 Refs

Wagner, R.E. 'Laser Drilling Mechanics' J. Appl. Phys. 45, #10, 1974, 4631-4637, 10 Refs.

II. . Experimental Data

II.1 . PHASE I EXPERIMENTAL DATA

Al_2O_3 Moving Tests Single Pass Cuts numbered I-S#

d = 0.005

DATE: 8/17/84

Cut Number	Laser Power [W]	Surface Speed [in/sec]	Energy Density [J/in2]	Depth of Cut [in]	D/d [ ]	ED/d [J/in3]	ED/d [J/cm3]
1	756	.417	363k	.134	26.8	72.6 M	4.43 M
2	' '	' '	' '	.148	29.6	' '	' '
3	' '	' '	' '	.193	38.6	' '	' '
4	' '	' '	' '	.202	40.4	' '	' '
5	' '	' '	' '	.200	40.0	' '	' '
6	' '	0.834	181 k	.136	27.2	36.2 M	2.21 M
7	' '	' '	' '	.117	23.4	' '	' '
8	' '	' '	' '	.131	26.2	' '	' '
9	' '	' '	' '	.135	27.0	' '	' '
10	' '	' '	' '	.142	28.4	' '	' '
11	' '	1.25	121 k	.094	18.8	24.2 M	1.48 M
12	' '	' '	' '	.097	19.4	' '	' '
13	' '	' '	' '	.099	19.8	' '	' '
14	' '	' '	' '	.101	20.2	' '	' '
15	' '	' '	' '	.095	19.0	' '	' '
16	' '	1.42	106 k	.084	16.8	21.2 M	1.29 M
17	' '	' '	' '	.095	19.0	' '	' '
18	' '	' '	' '	.086	17.2	' '	' '
19	' '	' '	' '	.091	18.2	' '	' '
20	' '	' '	' '	.078	15.6	' '	' '
21	' '	1.67	91 k	.081	16.2	18.2 M	1.11 M
22	' '	' '	' '	.081	16.2	' '	' '
23	' '	' '	' '	.082	16.4	' '	' '
24	' '	' '	' '	.079	15.8	' '	' '
25	' '	' '	' '	.081	16.2	' '	' '

DATE: 8/17/84   spot size: .005 in.

Cut Number	Laser Power [W]	Surface Speed [in/sec]	Energy Density [J/in2]	Depth of Cut [in]	D/d [ ]	ED/d [J/in3]	ED/d [J/cm3]

26	1000	.192	1.04 M	.414	82.8	208 M	12.69 M
27	700	′′	730 k	.273	54.6	156 M	9.51 M
28	500	′′	520 k	.145	29.0	104 M	6.34 M
29	300	′′	310 k	.122	24.4	62 M	3.78 M
30	1000	.417	480 k	.176	35.2	96 M	5.85 M
31	700	′′	330 k	.147	29.4	66 M	4.02 M
32	500	′′	240 k	.100	20.0	48 M	2.93 M
33	300	′′	140 k	.065	13.0	20 M	1.22 M

DATE: Augustne Kim, undated   d = .005 in.

Cut Number	Laser Power [W]	Surface Speed [in/sec]	Energy Density [J/in2]	Depth of Cut [in]	D/d [ ]	ED/d [J/in3]	ED/d [J/cm3]
34	300	6	10 k	.0043	0.86	2 M	120 k
35	′′	3	20 k	.0104	2.08	4 M	240 k
36	′	1.2	50 k	.0235	4.70	10 M	610 k
37	′′	.6	100 k	.0451	9.02	20 M	1.22 M
38	500	10	10 k	.0042	.84	2 M	120 k
39	′′	5	20 k	.0091	1.82	4 M	240 k
40	′′	2	50 k	.0235	4.70	10 M	610 k
41	′′	1	100 k	.0498	9.96	20 M	1.22 M
42	′′	0.5	200 k	.1024	20.48	40 M	2.44 M
43	100	20	10 k	.0037	.74	2 M	120 k
44	′′	10	20 k	.0106	2.12	4 M	240 k
45	′′	4	50 k	.0174	3.48	10 M	610 k
46	′′	2	100 k	.0361	7.22	20 M	1.22 M
47	′′	1	200 k	.0642	12.84	40 M	2.44 M

DATE: 11/30/84   d = .04 in.

Cut Number	Laser Power [W]	Surface Speed [in/sec]	Energy Density [J/in2]	Depth of Cut [in]	D/d [ ]	ED/d [J/in3]	ED/d [J/cm3]
48	150	.17	22.5 k	.0508	1.27	563 k	34.3 k
49	′′	.33	11.3 k	.0284	.71	283 k	17.26 k
50	250	.17	37.5 k	.0703	1.76	940 k	57.32 k
51	′′	.42	15 k	.0270	.675	375 k	22.87 k
52	′′	.84	7.5	.0112	.28	187 k	11.40 k
53	′′	1.26	5.0 k	.0125	.31	125 k	7,62 k
54	′′	1.67	3.75 k	.0064	.16	94 k	5.73 k
55	′′	.17	37.5 k	.0756	1.92	940 k	57.32 k

DATE: 12/18/84   d = .04 in.

Cut Number	Laser Power [W]	Surface Speed [in/sec]	Energy Density [J/in2]	Depth of Cut [in]	D/d [ ]	ED/d [J/in3]	ED/d [J/cm3]
74	150	.17	22.5	.036	.9	562 k	34.27 k
75	250	.17	37.5 k	.057	1.43	940 k	57.32 k
76	′′	.42	15 k	.047	1.17	375 k	22.87 k
77	500	.17	75 k	.164	4.10	1.87 M	110 k
78	′′	.42	30 k	.092	2.30	750 k	45.7 k
79	′′	.83	15k	.046	1.15	375 k	22.87 k
80	′′	1.67	7.5 k	.025	.63	187 k	11.4 k
81	1000	.42	30 k	.092	2.30	750 k	45.7 k
82	′′	.83	30 k	.107	2.68	750 k	45.73 k
83	′′	1.67	15 k	.052	1.30	375 k	22.87 k

DATE: 12/18/84   d = .02 in.

Cut Number	Laser Power [W]	Surface Speed [in/sec]	Energy Density [J/in2]	Depth of Cut [in]	D/d [ ]	ED/d [J/in3]	ED/d [J/cm3]
84	1000	1.67	30 k	.093	4.65	1.5 M	90 k
85	′′	.42	120 k	.220	11.00	6.0 M	370 k
86	250	.42	30 k	.062	3.10	1.5 M	90 k

DATE: 11/12/85   d = 0.05 in.

Cut Number	Laser Power [W]	Surface Speed [in/sec]	Energy Density [J/in2]	Depth of Cut [in]	D/d [ ]	ED/d [J/in3]	ED/d [J/cm3]
87	1000	.47	420 k	.204	40.8	84 M	5.1 M
88	′′	′′	′′	.193	38.6	84 M	5.1 M

****

Al$_2$O$_3$ Moving tests, Multiple pass

Cuts numbered I-M#

DATE: 11/30/84   .04 in.

Cut Number	Laser Power [W]	Surface Speed [in/sec]	Number of Passes	Energy Density [J/in2]	Depth of Cut [in]	D/d [ ]	ED/d [J/in3]
15	150	.17	2	45k	.0645	1.61	1.13M
16	''	.33	''	22.5k	.0460	1.15	560 k
17	250	.17	''	75 k	.1033	3.32	1.88 M
18	''	.42	''	30 k	.0537	1.34	750 k
19	''	.84	''	15 k	.0264	.66	375 k
20	''	1.26	''	10 k	.0154	.385	250 k
21	''	1.67	''	7.5 k	.0032	.08	188 k
22	''	.17	''	75 k	.0885	2.22	1.88 M

DATE: 12/18/84   d = .04 in.

Material : Al2O3

Cut Number	Laser Power [W]	Surface Speed [in/sec]	Number of Passes	Energy Density [J/in2]	Depth of Cut [in]	D/d [ ]	ED/d [J/in3]
41	150	.17	5	112.5k	.220	5.5	3.12 M
42	250	.17	8	300 k	.387	9.7	7.5 M
43	''	.42	9	135k	.268	6.7	3.37 M
44	500	.17	9	675 k	.571	14.3	16.9 M
45	''	.42	9	270 k	.400	10.0	6.75 M
46	''	.83	9	135 k	.298	7.45	3.37 M
47	''	1.67	9	67.5 k	.189	4.7	1.69 M
48	1000	.42	9	540 k	.697	17.4	13.5 M
49	''	.83	9	270 k	.597	14.9	6.75 M
50	''	1.67	9	135 k	.370	9.25	3.38 M

DATE: 12/18/84   d = .02 in.

Material : Al2O3

Cut Number	Laser Power [W]	Surface Speed [in/sec]	Number of Passes	Energy Density [J/in2]	Depth of Cut [in]	D/d [ ]	ED/d [J/in3]
51	1000	.42	9	1.08 M	.677	38.8	54 M

```
52        250        .42        8           240 k     .222      11.1      12 M
```

DATE: 11/12/85   d = .005 in. P = 1000 W

Material: Al2O3 With supersonic nozzle

Cut Number	Surface Speed [in/sec]	Number of Passes	Energy Density [J/in2]	Depth of Cut [in]	D/d [ ]	ED/d [J/in3]	Nozzle
54	.79	2	420 k	.254	50.8	84 M	−
55	′′	′′	′′	.169	33.8	′′	+
56	1.57	3	′′	.176	35.2	′′	+
57	′′	′′	′′	.149	29.8	′′	−
58	3.92	8	′′	.107	21.4	′′	−
59	′′	8	′′	.179	35.8	′′	+
60	7.85	17	′′	.128	25.6	′′	−
61	′′	′′	′′	.168	33.6	′′	+
62	22.8	48	′′	.109	21.8	′′	+
63	′′	′′	′′	.090	18.0	′′	+
64	′′	′′	′′	.062	12.4	′′	−
65	53	112	′′	.071	14.2	′′	+
66	169	278	′′	.058	11.6	′′	+

DATE: 11/12/85   d = .005 in.

MATERIAL: Mild Steel with supersonic nozzle

Cut Number	Laser Power [W]	Surface Speed [in/sec]	Number of Passes	Energy Density [J/in2]	Depth of Cut [in]	D/d [ ]	ED/d [J/in3]
67	1000	.45	1	440 k	.067	13.4	88 M
68	′′	.75	1	275 k	.040	8.0	53 M
69	′′	1.5	3	400 k	.091	18.2	80 M
70	′′	3.75	8	430 k	.109	21.8	86 M
71	′′	7.5	16	430 k	.054	10.8	86 M
72	500	4.5	30	660 k	.029	5.8	132 M
73	′′	′′	20	440 k	.051	10.2	88 M
74	′′	′′	10	220 k	.038	7.6	44 M
75	′′	′′	6	132 k	.029	5.8	27.5 M
76	′′	′′	4	88 k	.027	5.4	17.5 M
77	′′	′′	2	44 k	.010	2.0	8.8 M
78	′′	′′	1	22 k	.014	2.8	4.4 M
79	1000	′′	30	1.32 M	.086	17.2	264 M

80	''	''	20	880 k	.084	16.8	176 M
81	''	''	10	440 k	.080	16.0	88 M
82	''	''	6	264 k	.054	10.8	53 M
83	''	''	4	176 k	.034	6.8	35 M
84	''	''	2	88 k	.044	8.8	17.6 M
85	''	''	1	44 k	.026	5.2	8.8 M
86	''	21.4	47	440 k	.029	5.8	88 M
87	''	48.6	108	440 k	.034	6.8	88 M
88	''	82.7	184	440 k	.024	4.8	88 M
89	''	158.3	351	440 k	<.002	<.4	88 M

****

II.2 . Phase I Stationary Tests

Date: 7/13/84

Laser Energy [J]	Energy Density [J/in2]	ED/d [J/in3]	Depth [in]	D/d [ ]
10.1	520k	104 M	.0283	5.66
20.1	1.02M	204M	.0405	8.10
30.1	1.52 M	304 M	.0688	13.76
40.1	2.02 M	404 M	.0537	10.74
50.1	2.52 M	504 M	.0532	10.64
60.1	3.02 M	604 M	.0692	13.84
70.1	3.52 M	704 M	.0622	12.44
80.1	4.02 M	804 M	.0711	14.22
10.1	520 K	104 M	.0102	2.04
20.2	1.04 M	208 M	.035	7.0
30.3	1.56 M	312 M	.0377	7.54
40.4	2.08 M	416 M	.0458	9.16
50.5	2.60 M	520 M	.0525	10.5
60.6	3.12 M	624 M	.0514	10.28
70.7	3.64 M	728 M	.0620	12.4
80.8	4.16 M	832 M	.0556	11.1
90.9	4.68 M	936 M	.0575	11.5
101	5.20 M	1.04 B	.0840	16.8
202	10.4 M	2.08 B	.1220	24.4
404	20.8M	4.16 B	.1147	22.9
505	26.0 M	5.20 B	.1604	32.0
606	31.2 M	6.24 B	.1440	28.8
707	36.4 M	7.28 B	.1451	29.0
808	41.6 M	8.32 B	.1490	29.8
909	46.8M	9.36 B	.1605	32.1
1010	52 M	10.4 B	.1531	30.6

2020	104 M	20.8 B	.1751	34.1
3030	156 M	31.2 B	.1895	37.9
4040	208 M	41.6 B	.2626	27.9
5050	260 M	52.0 B	.2414	48.3
60.1	3.06 M	612 M	.0553	11.6
120.2	6.12 M	1.224 B	.0686	13.7
180.3	9.18 M	1.836 B	.075	15.0
240.4	12.24M	2.448 B	.1169	23.4
300.5	15.30M	3.060 B	.1041	20.8
360.6	18.36 M	3.672 B	.1218	24.4
420.7	21.42 M	4.284 B	.1293	25.8
480.8	24.48 M	4.896 B	.1601	32.0
540.9	27.54 M	5.508 B	.1523	30.4
601.0	3.060 M	6.120 B	.1627	32.5
1202	61.2 M	12.24 B	.1523	30.4
601.0	30.6 M	6.12 B	.1627	32.5
1202	61.2 M	12.24 B	.1564	31.2
1803	91.8 M	18.56 B	.1605	32.1
2404	122.4 M	24.48 B	.1902	38.0
3005	153 M	30.6 B	.2066	41.7
3606	183.6 M	36.7 B	.1886	37.7
4207	214.2 M	42.8 B	.1659	33.2
4808	244.8 M	49.0 B	.1973	39.4
5409	275.4 M	55 B	.1808	36.2
6010	306 M	61.2 B	.2688	53.7
12020	612 M	122.4 B	.2479	49.5
18030	918 M	183.6 B	.1878	37.5
24040	1.224 B	244.8 B	perforated	

Date: 3/23/84   Material: Mild Steel

Laser Energy [J]	Energy Density [J/in2]	ED/d [J/in3]	Depth [in]	D/d [ ]
1.27	65 k	13 M	.011	2.2
1060	54 M	10.8 B	.1557	31.1
6.5	330 k	66 M	-	-
65	3.3M	660 M	.023	4.6
130	6.6 M	1.33 B	.049	9.8
195	9.9 M	1.99 B	.052	10.4
260	13.3 M	2.66 B	.103	20.6
325	16.6 M	3.33 B	.109	21.8
390	19.9 M	3.99 B	.133	26.6
455	23.3 M	4.66 B	.140	28.0
520	26.6 M	5.33 B	.115	23.0
585	29.9 M	5.99 B	.121	24.2
650	33.3 M	6.66 B	.126	25.2

```
1300      66 M      13.3 B    .123      24.6
1950      99 M      19.9 B    .123      24.6
2600      133 M     26.6 B    .126      25.2
3250      166 M     3.33 B    .152      30.4
50        2.55 M    510 M     .054      10.8
''        ''        ''        .0425     8.5
''        ''        ''        .0472     9.4
''        ''        ''        .0473     9.4
''        ''        ''        .0393     7.8
''        ''        ''        .0378     7.5
''        ''        ''        .0495     9.9
''        ''        ''        .0412     8.2
```

Date: 3/23/84

Material: 304 Stainless Steel

Laser Energy	Energy Density	ED/d	Depth	D/d
[J]	[J/in2]	[J/in3]	[in]	[ ]
1.26	64 k	12.8 M	.006	1.2
970	49.5 M	9.9 B	.075	15
.65	33 k	6.6 M	.026	5.2
1.30	66 k	13.3 M	-	-
1.95	99 k	19.9 M	.0167	3.3
2.60	133 k	26.6 M	-	-
3.25	166 k	33.3 M	.0262	5.2
3.90	199 k	39.9 M	.0249	4.9
4.55	233 k	46.6 M	.0269	5.3
6.5	330 k	66 M	.009	1.8
65	3.3 M	660 M	.02	4.0
130	6.6 M	1.33 B	.032	6.4
195	9.9 M	1.99 B	.0335	6.7
260	13.3 M	2.66 B	.042	8.4
325	16.6 M	3.33 B	.0597	11.9
390	19.9 M	3.99 B	.054	10.8
455	23.3 M	4.66 B	.224	44.8
520	26.6 M	5.33 B	.213	42.6
585	29.9 M	5.99 B	.224	44.8
650	33.3 M	6.66 B	.2618	52.4

Date: 8/10/84   **Material:** Al_2O_3

Average Power	Laser Energy	Energy Density	ED/d	Depth	D/d

[w]	[J]	[J/in2]	[J/in3]	[in]	[ ]
1000	.7	28 k	5.6 M	.012	2.4
''	1.4	56 k	11.2 M	.034	7.8
''	2.1	84 k	16.8 M	.055	11.0
''	2.8	112 k	22.4 M	.052	10.4
''	3.5	140 k	28.0 M	.063	12.6
''	4.2	168 k	33.6 M	.060	12.0
''	4.9	196 k	39.2	.076	15.2
''	5.6	224 k	44.8 M	.112	22.4
''	6.3	252 k	50.4 M	.107	21.4
''	7.0	280 k	56.0 M	.139	27.8
500	.35	14 k	2.8 M	-	-
''	.70	28 k	5.6 M	.0213	4.26
''	1.05	42 k	8.4 M	.0397	7.94
''	1.40	56 k	11.2 M	.0500	10.0
''	1.75	70 k	14 M	.0487	9,74
''	2.10	84 k	16.8 M	.0509	10.18
''	2.45	98 k	19.6 M	.0756	15.12
''	2.80	112 k	22.4 M	.0690	13.8
''	3.15	126 k	25.2 M	.0758	14.76
''	3.50	140 k	28.0 M	.0990	19.8
100	0.4	16 k	3.2 M	.0098	1.96
''	1.0	40 k	8 M	.0285	5.7
''	2.0	80 k	16 M	.0417	8.34
''	4.0	160 k	32 M	.0525	10.5
''	10.0	400 k	80 M	.0641	12.82
300	0.42	16.8 k	3.36 M	.0067	1.34
''	1.02	40.8 k	8.12 M	.0319	6.38
''	2.04	81.6 k	16.32 M	.0526	10.52
''	4	160 k	32 M	.1047	20.94
''	10	400 k	80 M	.1431	28.62
500	.45	18 k	3.6 M	.0092	1.84
''	1.05	42 k	8.4 M	.0390	7.8
''	2.05	82 k	16.4 M	.0698	13.96
''	4.05	122 k	24.4 M	.0856	17.2
''	10.05	402 k	80.4 M	.1567	31.34
1000	1.1	44 k	8.8 M	.0221	4.42
''	2.1	84 k	16.8M	.0445	8.90
''	4.1	164 k	32.8 M	.0808	16.16
''	10.1	404 k	80.8 M	.1032	20.64

Date: 3/23/84

Material: Al O
             2 3

Laser Energy [J]	Energy Density [J/in2]	ED/d [J/in3]	Depth [in]	D/d [ ]

.46	18.4 k	3.6 M	.0016	.32
.74	29.6	5.92	.0033	.66
.96	38.5 k	7.7 M	.0043	.86
1.10	44 k	8.8 M	.0168	3.36
1.26	50.2 k	10.04 M	.0214	4.28
1.3	52 k	10.4 M	.0252	5.04
1.95	78 k	15.6 M	.0422	8.44
2.6	104 k	20.8 M	.0581	11.62
3.25	130 k	26 M	.0778	15.56
3.9	156 k	31.2 M	.0890	17.80
4.55	182 k	36.4 M	.1049	20.98
5.2	208 k	41.6 M	.1075	21.50
5.85	234 k	46.8 M	.1241	24.82
6.5	260 k	52 M	.1344	26.88
65	2.6 M	520 M	.3246	64.92

Date: 8/17/84   **Material:** Al O
                                                      2 3

Laser Energy [J]	Energy Density [J/in2]	ED/d [J/in3]	Depth [in]	D/d [ ]
8.64	346 k	69.2 M	.1281	25.62
7.7	308 k	61.6 M	.1009	20.18
6.3	252 k	50.4 M	.0974	19.48
5.95	238 k	47.6 M	.1105	22.1
5.6	224 k	44.8 M	.1229	24.58
5.25	210 k	42.0 M	.0924	18.48
4.9	196 k	39.2 M	.0917	18.34
4.55	18.2 k	36.4 M	.0665	13.30
8.415	337 k	67.4 M	.1387	27.74
7.695	308 k	61.6 M	.1530	30.6
7.65	306 k	61.2 M	.1162	23.24
7.20	288 k	57.6 M	.1317	26.34
6.753	270 k	54.0 M	.1105	22.1
6.3	252 k	50.4 M	.1102	22.04
5.85	234 k	46.8 M	.0986	19.72
3.24	130 k	26 M	.0773	15.46
7.20	288 k	57.6 M	.1442	28.84
10.8	432 k	86.4 M	.1623	32.43
12.6	504 k	108 M	.1640	32.8
19.8	798 k	159.6 M	.1707	34.14
2.88	115 k	23 M	.0870	17.4
3.60	144 k	28.8 M	.1089	21.78

II.3 . PHASE III Experimentation

These experiments were performed between July and September 1986 at Coherent General in Sturbridge. A model 51 CO_2 laser was used. The spot size was 0.016 cm unless noted. Focal length was 5 in unless noted.

The nozzle used in this section had a 0.25 in. diam. circular orifice held 0.25 in. from the focal point 45° inclination

Date: 7/11/86   Material: Porous SiC

Power : 1000 w   Surface Speed:5 cm/sec   Assist: Ar 500psi

Cut Number	Number Scans	Depth of Cut [in]	Width of Cut [in]	Energy Density [J/cm2]
5	1	.035	.024	12 k
6	2	.060	.013	24 k
7	5	.124	.006	60 k
8	10	.077	.022	120k

Surface Speed: 10 cm/sec

9	1	.039	.030	6 k
10	2	.054	.013	12 k
11	5	.089	.014	30 k
12	10	.086	.033	60 k

Surface Speed: 20 cm/sec

13	1	.018	.022	3 k
14	2	.022	.005	6 K
15	5	.042	.005	15 K

Surface Speed: 33 cm/sec

19	1	.010	.016	2 K
20	2	.008	.014	4 K
21	5	.022	.016	10 K
22	10	.037	.014	20 K
23	16	.038	.011	30 K
24	33	.045	.023	60 K
25	66	.103	.027	120 K

Date: 7/11/86   Material: POROUS AL2O3

Power : 1000 w Surface Speed: 10 cm/sec Assist: Ar 500psi

Cut Number	Number Scans	Depth of Cut [in]	Width of Cut [in]	Energy Density [J/cm2]
25.5	1	.031	.007	6 k
26	1	.053	.011	6 k
27	2	.100	.009	12 k
28	5	.179	.008	30 k
29	8	.198	.008	48 k
30	10	.242	.008	60 k
31	20	.250	.008	120 k
32	50	.294	.012	300 k

* no nozzle

* with nozzle

Surface Speed: (number of scans) cm/sec

Cut Number	Number Scans	Depth of Cut [in]	Width of Cut [in]	Energy Density [J/cm2]
33	3	.235	.008	60 k
34	5	.200	.008	60 k
35	8	.208	.007	"
36	15	.223	.008	"
37	15	.257	.007	"
38	20	.231	.008	"
39	30	.231	.006	"
40	50	.158	.010	"
41	120	.087	.007	"
42	90	.089	.007	"
43	200	.081	.006	"
44	400	.050	.007	"

Date: 7/11/86   Material: Porous Al2O3

Power : 1500 w   Assist: Ar 500psi

Cut Number	Speed [cm/sec]	Number Scans	Depth of Cut [in]	Width of Cut [in]	Energy Density [J/cm2]
45	10	7	.200	.014	63 k
46	15	10	.193	.009	60 k
47	30	20	.161	.007	60 k
48	45	30	.164	.009	"
49	60	40	.143	.009	"
50	60	1	.009	.010	1.5 k
51	60	2	.021	.013	3 K
52	"	5	.033	.012	7.5 k
53	"	10	.073	.009	15 k
54	"	20	.109	.008	30 k
55	"	100	.177	.010	150 k

Date: 7/11/86   Material: Porous A1203
Surface Speed: 10 cm/sec   Power : 1000 W
Number of scans: 10

Cut Number	Nozzle Press. [psi]	Depth of Cut [in]	Width of Cut [in]	Energy Density [J/cm2]
56	500	.225	.008	60 k
57	400	.229	.009	"
58	300	.206	.010	"

Date: 7/17/86   Material: Mild Steel
Power : 1000 w   Surface Speed: 10 cm/sec   Assist: Ar 500psi

Cut Number	Number Scans	Depth of Cut [in]	Width of Cut [in]	Energy Density [J/cm2]
59	1	.039	.007	6 k
60	2	.040	.005	12 k
61	5	.075	.010	30 k
62	10	.110	.008	60 k
63	20	.099	.008	120 k
64	50	.101	.009	300 k
65	100	.133	.013	600 k

Date: 7/17/86   Material: AMS 5613 Stainless
Power : 1000 w   Assist: Ar 500psi   Surface Speed: 10 cm/sec

Cut Number	Number Scans	Depth of Cut [in]	Width of Cut [in]	Energy Density [J/cm2]
66	1	.061	.011	6 k
67	2	.048	.010	12 k
68	5	.076	.009	30 k
69	10	.100	.009	60 k
70	20	.123	.010	120 k
71	50	.141	.009	300 k
72	100	.161	.007	600 k

Date: 7/17/86   Material: 303 Stainless
Power : 1000 w   Assist: Ar 500psi   Surface Speed: 10 cm/sec

Cut Number	Number Scans	Depth of Cut [in]	Width of Cut [in]	Energy Density [J/cm2]
73	1	.033	.009	6 k
74	2	.059	.008	12 k
75	5	.085	.009	30 k
76	10	.108	.006	60 k
77	20	.150	.008	120 k
78	50	.190	.007	300 k
79	100	.190	.008	600 k

Date: 7/17/86   Material: Invar
Power : 1000 w   Assist: Ar 500psi   Surface Speed: 10 cm/sec

Cut Number	Number Scans	Depth of Cut [in]	Width of Cut [in]	Energy Density [J/cm2]
80	1	.037	.013	6 k
81	2	.061	.009	12 k
82	5	.062	.010	30 k
83	10	.076	.010	60 k
84	20	.120	.013	120 k
85	50	.125	.009	300 k
86	100	.163	.011	600 k

Date: 7/17/86   Material: Nickel
Power : 1000 w   Assist: Ar 500psi   Surface Speed: 10 cm/sec

Cut Number	Number Scans	Depth of Cut [in]	Width of Cut [in]	Energy Density [J/cm2]
87	1	.013	.005	6 k
88	2	.026	.007	12 k
89	5	.046	.008	30 k
90	10	.044	.007	60 k
91	20	.045	.008	120 k
92	50	.044	.008	300 k
93	100	.046	.011	600 k

Surface Speed: 2 cm/sec

94	1	.074	.008	30 k
95	2	.057	.008	60 k
96	5	-	-	150 k

97	10	.013	.006	300	k

Date: 7/17/86   **Material: Inconel**

Power : 1000 w   **Assist: Ar 500psi**   **Surface Speed: 10 cm/sec**

Cut Number	Number Scans	Depth of Cut [in]	Width of Cut [in]	Energy Density [J/cm2]	
101	1	.033	.010	6	k
102	2	.072	.008	12	k
103	5	.079	.011	30	k
104	10	.104	.008	60	k
105	20	.122	.006	120	k
106	50	.164	.011	300	k
107	100	.168	.012	600	k

Date: 7/17/86   **Material: Titanium**

Power : 1000 w   **Assist: Ar 500psi**   **Surface Speed: 10 cm/sec**

Cut Number	Number Scans	Depth of Cut [in]	Width of Cut [in]	Energy Density [J/cm2]	
108	1	.026	.011	6	k
109	2	-	.009	12	k
110	5	.052	.009	30	k
111	10	.114	.009	60	k
112	20	.163	.011	120	k
113	50	.079	.014	300	k
114	100	.154	.008	600	k

Date: 7/17/86   **Material: Mild Steel**

Power : 1000 w   **Assist: O_2 100psi**   **Surface Speed: 10 cm/sec**

Cut Number	Number Scans	Depth of Cut [in]	Width of Cut [in]	Energy Density [J/cm2]	
115	1	.022	.012	6	k
116	2	.039	.013	12	k
117	5	.074	.014	30	k
118	10	.119	.012	60	k
119	20	.185	.017	120	k

120	50	.212	.015	300 k
121	100	.235	.026	600 k
122	20	.119	.012	60 k

Surface Speed: 5 cm/sec

123	3	.174	.016	36 k
124	1	.203	.027	12 k

Surface Speed: 20 cm/sec

125	1	.031	.019	3 k
126	2	.064	.015	6 k
127	3	.068	.017	9 k
128	5	.101	.016	15 k
129	10	.120	.017	30 k
130	20	.135	.020	60 k
131	50	.158	.019	150 k
132	100	.221	.015	300 k

Date: 7/17/86   Material: Dense Silicon Nitride
Power : 1000 w   Assist: Ar 500psi   Surface Speed: 10 cm/sec

Cut Number	Number Scans	Depth of Cut [in]	Width of Cut [in]	Energy Density [J/cm2]
149	1	.018	–	6 k
150	2	.032	–	12 k
151	5	.056	–	30 k
152	10	.090	–	60 k

Date: 7/25/86   Material: Mild Steel
Power : 1000 w   Surface Speed: 10 cm/sec   Assist: Ar 500psi
Focal Length : 10 in.

Cut Number	Number Scans	Depth of Cut [in]	Width of Cut [in]	Energy Density [J/cm2]
153	1	.003	.013	6 k
154	2	.006	.015	12 k
155	5	.027	.015	30 k
156	10	.053	.013	60 k
157	20	.075	.012	120 k
158	50	.097	.011	300 k

```
159        100        .116        .015        600 k
```

Assist: O$_2$ 50psi

```
160        1          .040        .045        6 k
161        2          .071        .040        12 k
162        5          .115        .042        30 k
163        10         .141        .042        60 k
164        20         .209        .050        120 k
165        50         .326        .052        300 k
166        100        .366        .050        600 k
```

Date: 7/25/86   Material: Cemented Tungsten Carbide (WC)
Assist: Ar 500psi   Surface Speed: 5 cm/sec   Power : 1000 w

Cut Number	Number Scans	Depth of Cut [in]	Width of Cut [in]	Energy Density [J/cm2]
167	1	.003	.010	12 k
168	2	.003	.009	24 k
169	5	.035	.014	60 k
170	10	.108	-	120 k
171	20	.024	.013	240 k

Date: 7/25/86   Material: Monel

Cut Number	Number Scans	Depth of Cut [in]	Width of Cut [in]	Energy Density [J/cm2]
172	1	.017	.009	30 k
173	2	.029	.015	60 k
174	5	.038	.014	150 k
175	10	.076	.011	300 k
176	20	.135	.009	600 k

Date: 7/25/86   Material: Molybdenum
Assist: Ar 500psi   Surface Speed: 2 cm/sec   Power : 1000 w

Cut Number	Number Scans	Depth of Cut [in]	Width of Cut [in]	Energy Density [J/cm2]
1	\			
2	\			

```
 5    \
10     \  All Cuts  < .002 in. deep
20     /
50    /
100  /
```

II.4 . Phase III: Calorimetry Tests

The nozzle used in this section had a 0.25 in. diam. circular orifice held 0.25 in. from the focal point 45° inclination

Date: 8/1/86   Material: Mild Steel
Assist: Ar 500psi   Surface Speed: 10 cm/sec   Power : 1000 w

In these tests, a thermocouple was incorporated into the experime specimens. Temperature rises and weight changes before and after were measured and are given in the following table.

Cut Number	Number on Specimen	Number Scans	Depth of Cut [mm]	Width of Cut [mm]	Energy Density [J/cm2]	D/d
177	1	1	.18	.31	6 k	1.0
178	2	2	.41	.28	12 k	2.3
179	3	5	.74	.36	30 k	4.1
180	4	10	1.83	.28	60 k	10.2
182	6	20	3.05	.48	120 k	17.0
183	7	50	3.53	.48	300 k	19.7
184	8	100	5.64	.61	600 k	31.4

Assist: O_2 100psi

185	9	1	.18	.23	6 k	1.0
186	10	1	.20	.25	6 k	1.1
187	11	2	.36	.66	12 k	2.0
188	12	5	.71	.56	30 k	4.0
189	13	6	1.63	.38	36 k	9.1
190	14	5	1.25	.31	30 k	6.9
191	15	10	1.37	.43	60 k	7.6
192	16	20	1.55	.51	120 k	8.6
193	17	50	3.91	.76	300 k	21.8
194	18	100	7.19	.53	600 k	40.0

Assist: Ar 500psi

195	21	1	.18	.36	6 k	1.0

196	22	2	.74	.36	12 k	4.1
197	23	5	1.42	.33	30 k	7.9
198	24	10	1.58	.28	60 k	8.8
199	25	20	1.40	.49	120 k	7.8
200	26	50	3.84	.53	300 k	21.4
201	27	100	4.17	.43	600 k	23.2

Assist: Ar 500psi   Surface Speed: (number of scans) cm/sec

202	19	10	2.41	.38	60 k	13.4
204	28	16	1.60	.38	60 k	8.9
205	29	5	1.04	.89	"	5.8
206	30	3	1.25	.33	"	6.9

Assist: none

207	32	10	.20	.31	"	1.1

Assist: Ar 500psi   Surface Speed: 6 cm/sec
AXIAL CUTS: .62" diam. trace

209	33	1	.64	.36	10 k	3.5
210	34	2	.74	.38	20 k	4.1
211	35	5	2.90	.97	50 k	16.1
212	36	10	2.95	.38	100 k	16.4
213	37	20	3.58	1.19	200k	19.9
214	38	50	4.83	.86	500 k	26.9
215	39	100	3.61	.83	1.0 M	20.1

Assist: O$_2$ 100psi   (AXIAL CUTS)

216	40	1	.64	.28	10 k	3.5
217	41	2	1.91	.36	20 k	10.6
218	42	5	2.52	.48	50 k	14.0
219	43	10	2.49	.81	100 k	13.9
220	44	20	3.58	1.09	200 k	19.9
221	45	50	2.95	.91	500 k	16.4
222	46	100	4.01	.86	1.0 M	22.3

SPECIMEN WEIGHTS AND TEMPERATURES.

Number on Specimen	Weight Before [g]	Weight After [g]	Temp. Before [C]	Temp. After [C]	Nozzle Time [sec]
1	49.41	49.39	19	24	7
2	50.35	50.15	25	42	4
3	49.60	49.50	25	77	9

4	49.07	48.83	24	153	15
5	49.41	49.26			
6	50.76	50.56	25	272	20
7	50.71	50.34	25	497	45
8	49.75	49.23	27	663	83
9	48.21	48.13	26	32	18
10	48.46	48.40	25	33	5
11	50.26	50.16	24	44	5
12	49.67	49.52	25	95	5
13	48.58	49.40	24	117	11
14	49.44	49.21	25	102	9
15	49.34	49.03	25	184	15
16	51.00	50.49	25	333	20
17	50.19	49.25	27	581	46
18	49.26	47.71	29	778	83
19	49.92	49.61	26	198	15
20	49.14	48.77			
21	50.47	50.23	25	30	4
22	49.84	49.60	24	44	6
23	49.83	49.46	25	97	9
24	49.59	49.22	25	179	16
25	48.08	47.63	25	299	20
26	49.30	48.56	28	454	45
27	50.14	48.88	27	696	82
28	49.92	49.31	26	154	15
29	48.00	47.21	27	160	14
30	49.66	49.16	26	201	11
31	47.46	47.24			
32	50.04	49.59	25	135	0
33	49.62	49.27	25	28	
34	51.14	50.88	23	36	
35	47.33	47.12	23	62	
36	50.14	49.78	24	102	
37	47.67	48.81	26	118	
38	48.44	48.18	25	242	
39	48.29	47.98	30	340	
40	48.62	48.32	29	45	3
41	51.00	50.68	28	53	5
42	51.11	50.81	26	130	11
43	48.62	48.32	26	189	10
44	49.00	48.22	28	222	18
45	49.91	49.22	28	503	25
46	49.00	46.80	29	550	54

COOLING CURVE FOR   CUT #201 (specimen #27)
Assist: Argon 500psi   Depth of cut: 0.164 in.

Time | Temp
After |

```
Laser |
 off  |
[sec]    [C]

0        696  \
5        690   Nozzle off
10       673  /

         Nozzle on:
15       603
20       559
25       505
30       451
35       401
40       357
45       318
50       279
55       244
60       208
65       180.
70       153
75       130
80       111
85        94
90        83
95        73
100       64
105       58
110       53
115       49
```

II.5 . Continuation of Phase III Experiments

This section was performed using the assist nozzle with a 0.02 x 0.10 in. orifice, held

0.25 in. from the focal point at 45° orientation.

Date: 8/8/86   Material: Mild Steel
Power: 1000 w   Surface Speed : 10 cm/sec   Assist: Ar 500psi

Cut Number	Number Scans	Depth of Cut [in]	Width of Cut [in]	Energy Density [J/cm2]
235	1	.010	.015	6 k
236	2	.030	.013	12 k
237	5	.067	.012	30 k
238	10	.110	.012	60 k

239   20   .120   .011   120 k

Surface Speed: 20 cm/sec   Assist: Ar 400psi

240   1   .010   .013   3 k
241   2   .029   .012   6 k
242   5   .054   .008   15 k
243   10   .068   .010   30 k
244   20   .073   .012   60 k

Surface Speed: 10 cm/sec   Assist: Ar 300psi

245   1   .006   .014   6 k
246   2   .007   .015   12 k
247   5   .023   .008   30 k
248   10   .103   .015   60 k
249   20   .126   .011   120 k

Surface Speed: 10 cm/sec   Assist: Ar 200psi

250   1   .003   .012   6 k
251   2   .005   .013   12 k
252   5   .017   .011   30 k
253   10   .030   .010   60 k
254   20   .056   .006   120 k

Date: 8/8/86   Material: 303 Stainless Steel
Power: 1000 w   Surface Speed: 10 cm/sec   Assist: Ar 500psi

Cut Number	Number Scans	Depth of Cut [in]	Width of Cut [in]	Energy Density [J/cm2]	D/d	ED/d [J/cm3]
255	1	.025	.009	6 k		
256	2	.048	.011	12 k		
257	5	.095	.013	30 k		
258	10	.065	.014	60 k		
259	20	.107	.017	120 k		

Surface Speed: 5 cm/sec

260   1   .054   .012   12 k
261   2   .073   .015   24 k
262   5   .104   .018   60 k
263   10   .117   .017   120 k

Surface Speed: 2 cm/sec

265	1	.105	.017	30 k
266	2	.116	.020	60 k
267	5	.090	.019	150 k

Surface Speed: 50 cm/sec

268	1	.003	.012	1.2 k
269	2	.004	.012	2.4 k
270	5	.013	.011	6 k
271	10	.021	.010	12 k
272	20	.024	.009	24 k
273	50	.055	.019	60 k
274	100	.068	.010	120 k
275	200	.079	.010	240 k

Surface Speed: 100 cm/sec

276	1	<.002	–	600
277	2	<.002	–	1.2 k
278	5	<.002	–	3 k
279	10	.003	.011	6 k
280	20	.006	.008	12 k
281	40	.012	.003	24 k
282	100	.029	.007	60 k
283	200	.031	.009	120 k
284	400	.042	.014	240 k

Date: 8/8/86   Material: Mild Steel
Power: 1000 w   Surface Speed: 10 cm/sec   Assist: O_2 20psi

Cut Number	Number Scans	Depth of Cut [in]	Width of Cut [in]	Energy Density [$J/cm2$]	D/d	ED/d [$J/cm3$]
289	1	.010	.023	6 k		
290	2	.027	.020	12 k		
291	5	.048	.029	30 k		
292	10	.114	.020	60 k		
293	20	.130	.017	120 k		
294	50	.231	.018	240 k		

Assist: O_2 20-90 psi steadily increasing

295	120	.329	.021	720 k

Power: 1500 w   Surface Speed: 10 cm/sec   Assist: O_2 20psi

296	1	.015	.028	9 k

297	2	.028	.038	18 k	
298	5	.062	.031	45 k	
299	10	.111	.051	90 k	
300	20	.229	.054	180 k	

Power: 1500 w   Assist: O_2 30psi

301	50	.280	.050	450 k	
302	60	.372	.047	540 k	

Date: 8/22/86   **Material: Mild Steel**
Surface Speed: 10 cm/sec   Assist: Argon 200psi

Cut Number	Number Scans	Depth of Cut [in]	Width of Cut [in]	Energy Density [J/cm2]	D/d	ED/d [J/cm3]

Power: 1000 w

303	1	.021	.008	6 k		
304	10	.076	.008	60 k		
305	50	.116	.007	300 k		

Power: 700 w

306	1	.011	.007	4.2 k		
307	10	.051	.007	42 k		
308	50	.093	.007	210 k		

Power: 500 w

309	1	.003	.004	3 k		
310	10	.024	.007	30 k		
311	50	.049	.007	150 k		

Power: 300 w

312	1	.002	.004	1.8 k		
313	10	.004	.004	18 k		
314	50	.027	.004	90 k		

Date: 8/22/86   **Material: Mild Steel**
Surface Speed: 2 cm/sec   Assist: Argon 200psi

Cut Number	Number Scans	Depth of Cut [in]	Width of Cut [in]	Energy Density [J/cm2]	D/d	ED/d [J/cm3]

Power: 1000 w

| 315 | 1 | .095 | .011 | 30 k |
| 316 | 10 | .045 | .009 | 300 k |

Power: 700 w

| 317 | 1 | .042 | .008 | 21 k |
| 318 | 10 | .071 | .010 | 210 k |

Power: 500 w

| 319 | 1 | .046 | .010 | 15 k |
| 320 | 10 | .092 | .007 | 150 k |

Power: 300 w

| 321 | 1 | .002 | .004 | 9 k |
| 322 | 10 | .067 | .008 | 90 k |

Date: 8/22/86   Material: Mild Steel
Surface Speed: 10 cm/sec   Assist: O_2 25psi

Cut Number	Number Scans	Depth of Cut [in]	Width of Cut [in]	Energy Density [J/cm2]	D/d	ED/d [J/cm3]

Power: 1000 w

323	1	.016	.010	6 k
324	10	.053	.010	60 k
325	50	.137	.011	300 k

Power: 700 w

326	1	.006	.008	4.2 k
327	10	.024	.013	42 k
328	50	.093	.010	210 k

Power: 500 w

329	1	.008	.006	3 k
330	10	.014	.011	30 k
331	50	.051	.010	150 k

Power: 300 w

| 332 | 1 | <.002 | - | 1.8 k |

```
333      10      .004    .011    18 k
334      50      .024    .008    90 k
```

Power: 300 w   Surface Speed: 2 cm/sec

```
335      1       .045    .015    9 k
336      10      .061    .007    90 k
```

Date: 8/22/86   Material: Mild Steel
Surface Speed: 10 cm/sec Power: 1000 w   Number of Scans: 50

Cut Number	Oxygen Press. [psi]	Depth of Cut [in]	Width of Cut [in]	Energy Density [J/cm2]	D/d	ED/d [J/cm3]
342	25	.095	.011	300 k		
343	40	.225	.012	"		
344	50	.197	.011	"		
345	60	.216	.015	"		

Number of Scans : One

```
346      75      .076    .027    6 k
```

Number of Scans: 75

```
347      75      .324    .019    450 k
```

Power: 500 w   Surface Speed: 10 cm/sec   Number of Scans: 50

```
348      25      .026    .008    150 k
349      40      .106    .007    "
350      50      .160    .006    "
351      60      .207    .008    "
352      75      .209    .005    "
353      100     .204    .008    "
```

Date: 8/22/86   Material: Mild Steel
Surface Speed: 10 cm/sec

Cut Number	Number Scans	Argon Press. [psi]	Depth of Cut [in]	Width of Cut [in]	Energy Density [J/cm2]	D/d	ED/d [J/cm3]

Power: 1000 w

```
354      1       1000    .019    .008    6 k
```

355	10	"	.076	.009	60 k
356	50	"	.091	.007	300 k
357	1	500	.022	.007	6 k
358	10	"	.072	..007	60 k
359	50	"	.117	.009	150 k

Power: 300 w

360	1	500	<.002	-	1.8 k
361	10	"	.013	.005	18 k
362	50	"	.026	.005	90 k

Power: 500 w

363	1	500	.006	.005	3 k
364	10	"	.024	.008	30 k
365	50	"	.055	.004	150 k
366	50	200	.079	.005	150 k

Date: 8/22/86   Material: Mild Steel
Power: 1000 w   Surface Speed: 10 cm/sec   Assist: Argon 200psi
Number of scans: 10

Cut Number	Pos. of Focal Pt [in] Above Surface	Depth of Cut [in]	Width of Cut [in]	Energy Density [J/cm2]	D/d	ED/d [J/cm3]
367	+.050	.075	.008	60 k		
368	.040	.075	.008	"		
369	.030	.075	.009	"		
370	.020	.082	.007	"		
371	+.010	.068	.008	"		
372	.000	.086	.008	"		
373	-.010	.086	.005	"		
374	.020	.094	.007	"		
375	.030	.111	.005	"		
376	.040	.101	.005	"		
377	.050	.102	.008	"		
378	.060	.096	.008	"		
379	.070	.098	.007	"		
380	.080	.100	.006	"		
381	.090	.095	.006	"		
382	-.100	.034	.008	"		

Date: 8/29/86   Material: Mild Steel

Surface Speed: 10 cm/sec   Assist: Air 200psi

Cut Number	Number Scans	Depth of Cut [in]	Width of Cut [in]	Energy Density [J/cm2]	D/d		ED/d [J/cm3]

Power: 1000 w

383	1	.013	.010	6 k			
384	2	.013	.009	12 k			
385	5	.072	.004	30 k			
386	10	.116	.009	60 k			
387	20	.150	.006	120 k			
388	50	.263	.009	300 k			
389	100	.332	.006	600 k			

Power: 700 w

390	1	<.002	–	4.2 k			
391	2	<.002	–	8.4 k			
392	5	.017	.008	21 k			
393	10	.036	.008	42 k			
394	20	.097	.006	84 k			
395	50	.120	.007	210 k			
396	100	.243	.007	420 k			

Power: 500 w

397	1	<.002	–	3 k			
398	2	.006	.006	6 k			
399	5	.006	.008	15 k			
400	10	.022	.005	30 k			
401	20	.017	.007	60 k			
402	50	.067	.008	150 k			
403	100	.131	.006	300 k			

Power: 300 w

404	1	.002	.004	1.8 k			
405	2	.006	.008	3.6 k			
406	5	.012	.008	9 k			
407	10	.016	.007	18 k			
408	20	.008	.007	36 k			
409	50	.026	.007	90 k			

Date: 8/29/86   Material: Mild Steel
Surface Speed: 10 cm/sec Assist: Air 200psi

Cut Number	Number Scans	Depth of Cut [in]	Width of Cut [in]	Energy Density [J/cm2]	D/d	ED/d [J/cm3]
Power: 1500 w						
410	1	.042	.008	9 k		
411	2	.073	.007	18 k		
412	5	.149	.010	45 k		
413	10	.184	.011	90 k		
414	20	.225	.011	180 k		
415	50	.372	.019	450 k		
416	100	.368	.008	900 k		
Power: 1000 w Assist: Air 100psi						
417	1	.009	.010	6 k		
418	2	.020	.011	12 k		
419	5	.041	.008	30 k		
420	10	.112	.009	60 k		
421	20	.149	.010	120 k		
422	50	.247	.012	300 k		
423	100	.299	.013	600 k		
Power: 700 w Assist: Air 100psi						
424	1	.004	.008	4.2 k		
425	2	.008	.010	8.4 k		
426	5	.028	.006	21 k		
427	10	.041	.006	42 k		
429	20	.159	.009	84 k		
430	50	.199	.011	210 k		
Power: 500 w Assist: Air 100psi						
431	1	<.002	-	3 k		
432	2	.005	.008	6 k		
433	5	.015	.008	15 k		
434	10	.039	.006	30 k		
435	20	.024	.015	60 k		
436	100	.102	.019	300 k		
437	50	.047	.010	150 k		
Power: 300 w Assist: Air 100psi						
437a	1	.002	.003	1.8 k		
438	2	.003	.003	3.6 k		
439	5	.002	.002	9 k		
440	10	.008	.005	18 k		

441	20	.008	.006	36 k
442	50	.013	.005	90 k
443	100	.012	.006	180 k

Power: 150 w   Assist: Air 100psi

444	1 \		
445	2 \		
446	5 \		
447	10 \	<.002	-
448	20 /		
449	50 /		
450	100/		

Power: 1500 w   Assist: Air 100psi

451	1	.064	.006	9 k
452	2	.089	.003	18 k
453	5	.111	.012	45 k
454	10	.147	.007	90 k
455	20	.216	.018	180 k
456	50	.380	.010	450 k
457	100	.400	.018	900 k
458	200	.451	.015	1.8 M

Date: 8/29/86   Material: Mild Steel
Surface Speed: 5 cm/sec   Assist: Air 100psi

Cut Number	Number Scans	Depth of Cut [in]	Width of Cut [in]	Energy Density [J/cm2]	D/d		ED/d [J/cm3]

Power: 1000 w

459	1	.068	.005	12 k
460	2	.090	.010	24 k
461	5	.111	.010	60 k
462	10	.158	.009	120 k
463	20	.193	.008	240 k
464	50	.329	.016	600 k

Power: 700 w

465	1	.038	.003	8.4 k
466	2	.055	.006	16.8 k
467	5	.074	.009	42 k
468	10	.106	.005	84 k

Cut Number	Number Scans	Depth of Cut [in]	Width of Cut [in]	Energy Density [J/cm2]
469	20	.145	.006	168 k
470	50	.163	.005	420 k

Power: 500 w

Cut Number	Number Scans	Depth of Cut [in]	Width of Cut [in]	Energy Density [J/cm2]
471	1	.026	.005	6 k
472	2	.042	.009	12 k
473	5	.056	.008	30 k
474	10	.090	.006	60 k
475	20	.115	.009	120 k
476	50	.181	.015	300 k

Power: 300 w

Cut Number	Number Scans	Depth of Cut [in]	Width of Cut [in]	Energy Density [J/cm2]
477	1	.001	.002	3.6 k
478	2	.002	.004	7.2 k
479	5	.016	.006	18 k
480	10	.028	.005	36 k
481	20	.060	.005	72 k
482	50	.023	.005	180 k

Power: 150 w

Cut Number	Number Scans	Depth of Cut [in]	Width of Cut [in]	Energy Density [J/cm2]
483	1	<.002	-	1.8 k
484	2	<.002	-	3.6 k
485	5	<.002	-	9 k
486	10	.002	.004	18 k
487	20	.007	.002	36 k
488	50	.019	.002	90 k

Power: 1500 w

Cut Number	Number Scans	Depth of Cut [in]	Width of Cut [in]	Energy Density [J/cm2]
489	1	.089	.006	18 k
490	2	.123	.009	36 k
491	5	.150	.007	90 k
492	10	.198	.021	180 k
493	20	.239	.013	360 k
494	50	.344	.013	900 k

Date: 8/29/86   Material: Mild Steel
Surface Speed: 2 cm/sec   Assist: Air 100psi

Cut Number	Number Scans	Depth of Cut [in]	Width of Cut [in]	Energy Density [J/cm2]	D/d		ED/d [J/cm3]

Power: 150 w

495	1	.003	.004	4.5 k
496	2	.003	.004	9 k
497	5	.010	.005	22.5 k
498	10	.013	.004	45 k
499	20	.003	.004	90 k

Power: 300 w

500	1	.006	.005	9 k
501	2	.042	.005	18 k
502	5	.059	.005	45 k
503	10	.080	.007	90 k
504	20	.103	.006	180 k

Power: 500 w

505	1	.070	.008	15 k
506	2	.081	.007	30 k
507	5	.099	.007	45 k
508	10	.126	.008	90 k
509	20	.160	.012	180 k
510	50	.236	.004	750 k

Power: 700 w

511	1	.074	.009	21 k
512	2	.102	.008	42 k
513	5	.130	.009	105 k
514	10	.150	.013	210 k
515	20	.205	.010	420 k
516	50	.327	.010	1.05 M

Date: 8/29/86   Material: Mild Steel
Surface Speed: 24 cm/sec   Assist: O_2 80psi coaxial

Power: 700 w pulsed; 500 Hz; pulse length : 1 ms.

Cut Number	Number Scans	Depth of Cut [in]	Width of Cut [in]	Energy Density [J/cm2]	D/d	ED/d [J/cm3]
517	1	.006	.014	1.75 k		
518	2	.011	.014	3.5 k		
519	5	.027	.009	8.75 k		
520	10	.055	.010	17.5 k		
521	20	.079	.009	35 k		
522	50	.111	.010	87.5 k		

523   100   .157   .013   175 k

****

This concludes the tabulated experimental data of this thesis.

What follows is an atlas of cut profiles traced from optical micrographs.

III. . Cut Atlas

In addition to measuring depths and widths, certain selected cuts were photographed with an optical microscope in order to examine the uniformity of the cuts, and to aid in illustrating the experimental discussion.

The profiles presented in the following section were traced from original photographs. In most cases, there are two contours represented. The outer one is the boundary between resolidified material and unmelted material. The inner boundary is the surface of the cleared out portion of the cut. In some cases, the molten boundary and the cut wall coincide. In some other cases, there is no empty space in the kerf, and the kerf is identical to a weld.

A. Porous Al$_2$O$_3$

Pix No.	Mag. in Figure	Trace Number	Depth of Cut [in]	Energy Density [J/in2]
1	8.5x	I-S1	.146	363 k
2	8.5x	I-S2	.133	363 k
3	8.5x	I-S9	.139	181 k
4	8.5x	I-S10	.143	181 k
5	13.5x	I-S15	.103	121 k
6	13.5x	I-S16	.089	107 k
7	13.5x	I-S24	.089	91 k
8	13.5x	I-S25	.081	91 k
9	13.5x	I-S78	.092	30 k
10	13.5x	I-S79	.046	15 k
11	17x	I-S80	.025	7.5 k
12	6.8x	I-S81	.182	60 k
13	8.5x	I-S82	.107	30 k
14	10.8x	I-S83	.052	15 k
15	10.8x	I-S84	.093	30 k
16	5.4x	I-S85	.220	120 k
17	6.8x	I-M54	.242	420 k
18	3.4x	I-M46	.298	135 k
19	3.4x	I-M45	.400	270 k
20	6.8x	I-M47	.189	67.5 k
21	3.4	I-M49	.597	270 k
22	6.8x	I-M60	.116	420 k
23	6.8x	I-S88	.175	420 k
24	6.8x	I-S87	.230	420 k
25	6.8x	I-M61	.200	420 k
26	6.8x	I-M59	.210	420 k

27	6.8x	I-M58	.150	420 k
28	6.8x	I-M57	.162	420 k
29	6.8x	I-M56	.210	420 k
30	6.8x	I-M55	.174	420 k
31	21.6x	III-26	.039	36 k
32	17x	III-27	.098	72 k
33	8.5x	III-28	.189	180 k
34	6.8x	III-29	.208	288 k
35	5.4x	III-30	.223	360 k
36	5.4x	III-31	.257	720 k
37	4.2x	III-32	.323	1.8 M
38	6.8x	III-33	.217	360 k
39	8.5x	III-34	.177	360 k
40	8.5x	III-35	.200	360 k
41	10.8x	III-36	.164	360 k
42	6.8x	III-37	.204	360 k
43	5.4x	III-38	.243	360 k
44	5.4x	III-39	.219	360 k
45	5.4x	III-40	.165	360 k
46	21.6x	III-41	.085	360 k
47	8.5x	III-42	.081	360 k
48	21.6x	III-43	.081	360 k
49	21.6x	III-44	.050	360 k
50	13.5x	III-45	.180	410 k
51	13.5x	III-46	.191	360 k
52	13.5x	III-47	.164	360 k
53	8.5x	III-48	.145	360 k
54	8.5x	III-49	.126	360 k
55	21.6x	III-50	.011	9 k
56	21.6x	III-51	.021	18 k
57	17x	III-52	.053	45 k
58	17x	III-53	.079	90 k
59	10.8x	III-54	.119	180 k
60	8.5x	III-55	.161	360 k
61	8.5x	III-56	.185	360 k
62	6.8x	III-57	.180	360 k
63	6.8x	III-58	.203	360 k

B. Mild Steel   (All cuts Phase III)

Pix No.	Mag. in Figure	Trace Number III-	Depth of Cut [in]	Energy Density [J/in2]
64	6.8x	132	.221	1.8 M
65	6.8x	131	.158	900 k

66	8.5x	130	.135	360 k
67	10.8x	129	.120	180 k
68	13.5x	128	.101	90 k
69	13.5x	127	.068	54 k
70	17x	126	.064	36 k
71	17x	125	.031	18 k
72	17x	122	.119	720 k
73	6.8x	123	.174	220 k
74	6.8x	124	.203	70 k
75	5.4x	121	.235	3.6 M
76	6.8x	120	.212	1.8 M
77	8.5x	119	.185	720 k
78	17x	117	.074	180 k
79	17x	116	.039	72 k
80	17x	115	.022	36 k
81	10.8x	342	.095	1.8 M
82	5.4x	343	.225	1.8 M
83	5.4x	344	.197	1.8 M
84	5.4x	345	.216	1.8 M
85	13.5x	346	.076	36 k
86	4.2x	347	.324	2.7 M
87	21.6x	348	.026	900 k
88	10.8x	349	.106	900 k
89	6.8x	350	.160	900 k
90	5.4x	351	.207	900 k
91	5.4x	352	.209	900 k
92	5.4x	353	.204	900 k
93	21.6x	383	.013	36 k
94	21.6x	384	.013	72 k
95	17x	385	.072	180 k
96	8.5x	386	.116	360 k
97	8.5x	387	.150	720 k
98	5.4x	388	.263	1.8 M
99	4.2	389	.332	3.6 M
100	21.6x	392	.017	130 k
101	21.6x	393	.036	260 k
102	10.8x	394	.097	520 k
103	6.8	395	.120	1.3 M
104	5.4	396	.243	2.6 M
105	21.6x	399	.006	90 k
106	21.6x	400	.022	180 k
107	21.6x	401	.017	360 k
108	17x	402	.067	900 k
109	8.5	403	.131	1.8 M
110	17x	354	.019	36 k
111	17x	355	.076	360 k
112	10.8x	356	.091	1.8 M
113	17x	357	.022	36 k
114	13.5	358	.072	360 k

115	10.8x	359	.117	1.8 M
116	21.6	361	.013	120 k
117	17x	362	.026	600 k
118	17x	364	.024	180 k
119	17x	365	.055	900 k
120	17x	366	.079	1.8 M
121	17x	357	.075	360 k
122	17x	368	.075	360 k

13   14   15   16

17   18   19   20

21   22   23   24
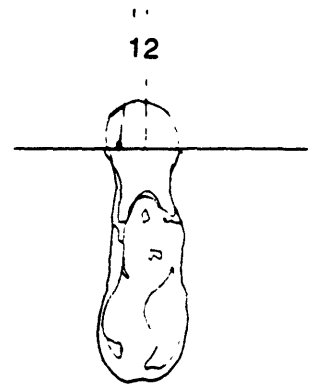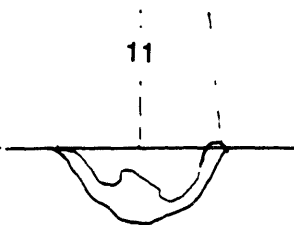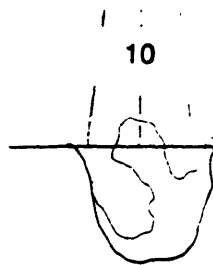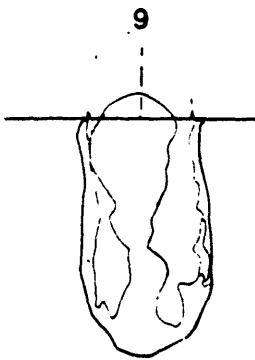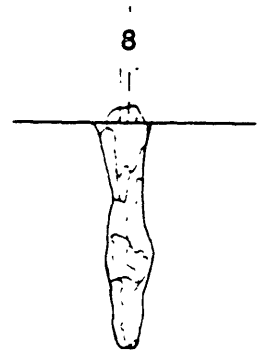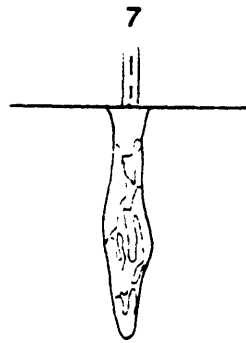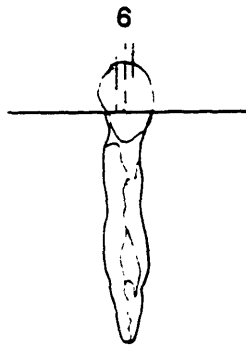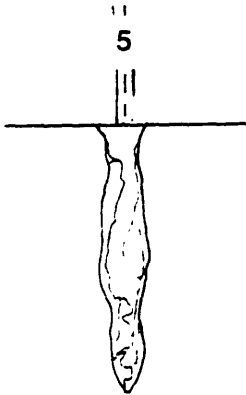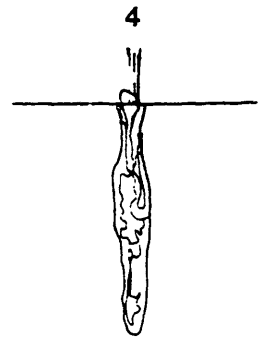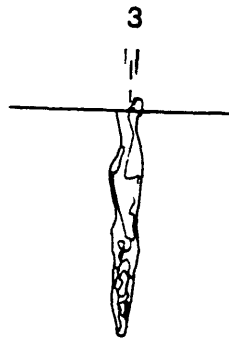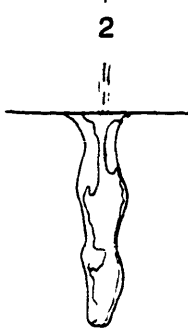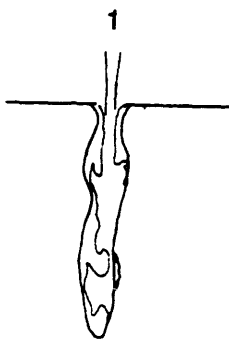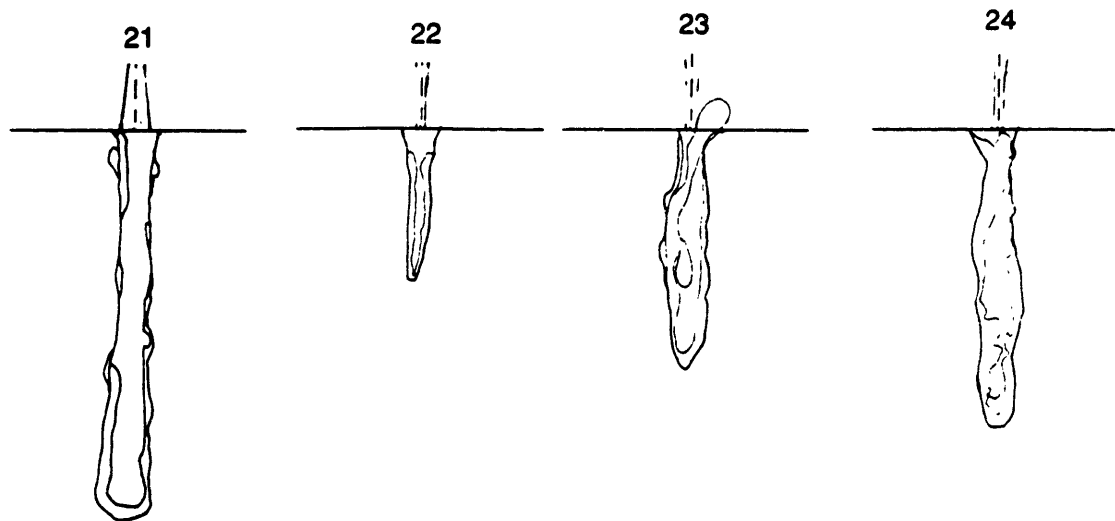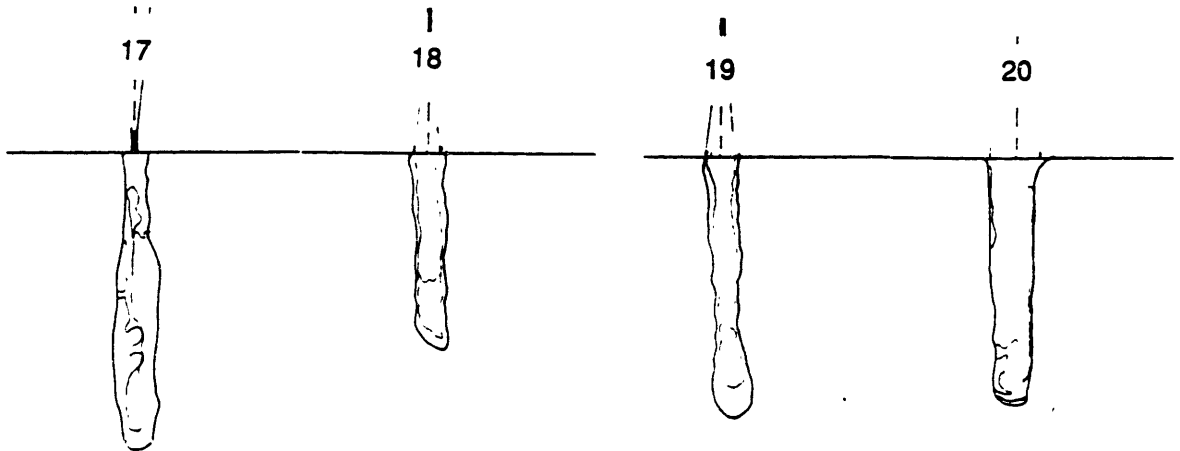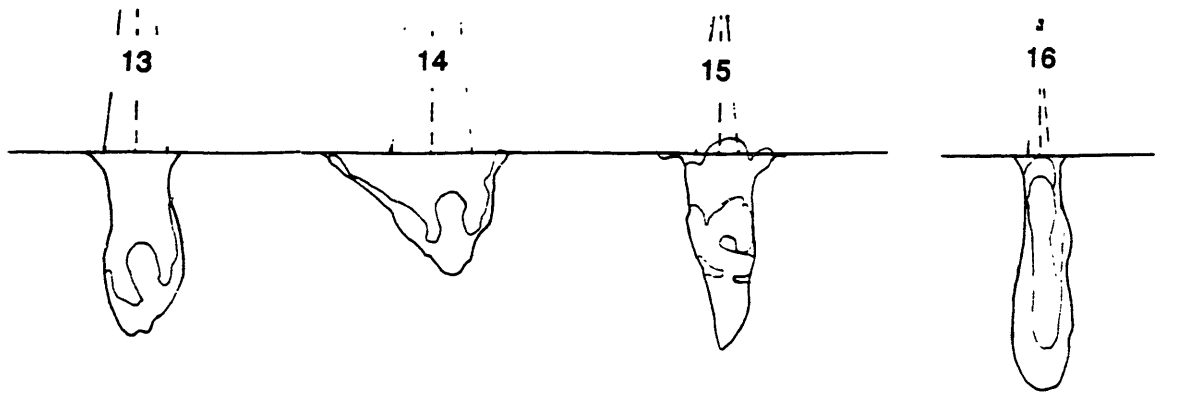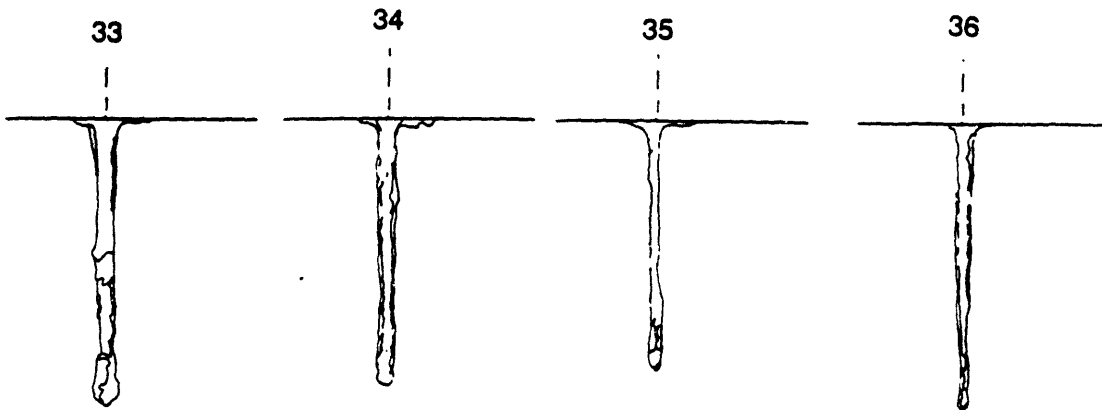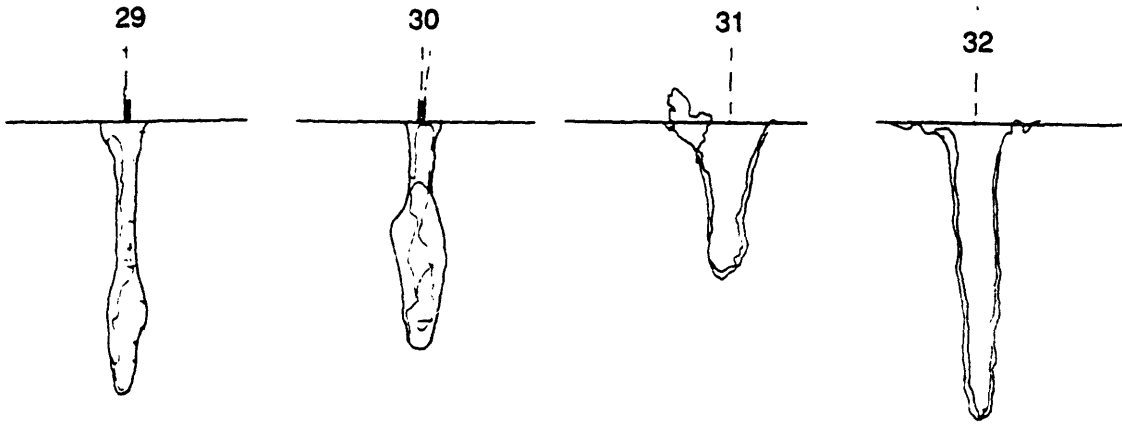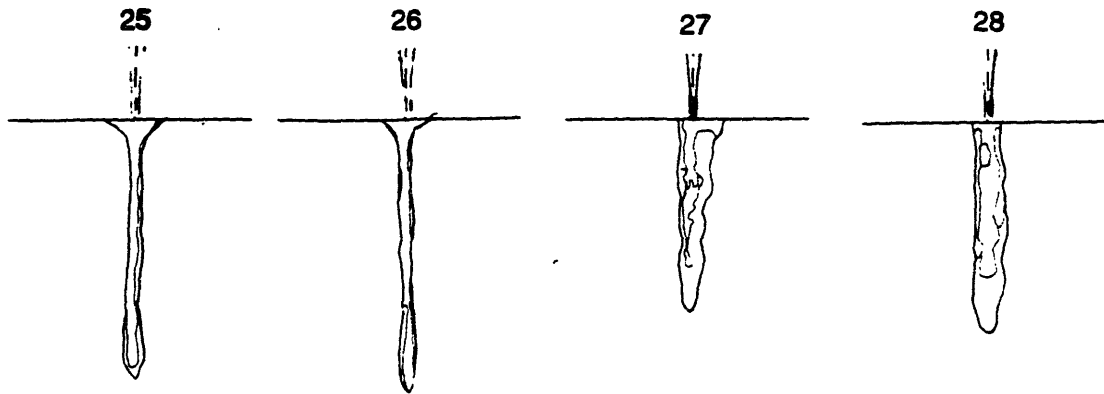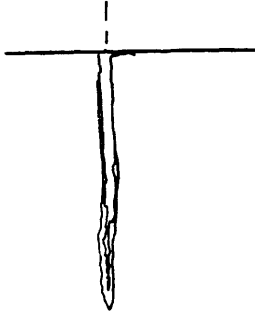
37 38 39 40

41 42 43 44

45 46 47 48

61   62   63

64

65

66

67

68

69

70

71

72

73

74

75
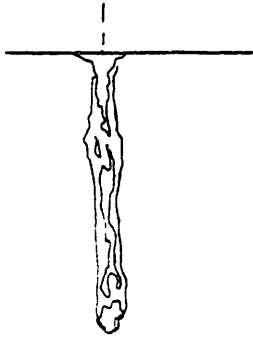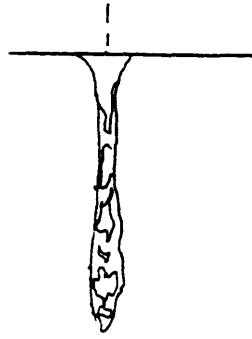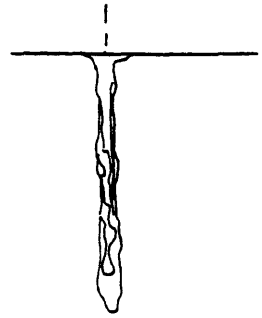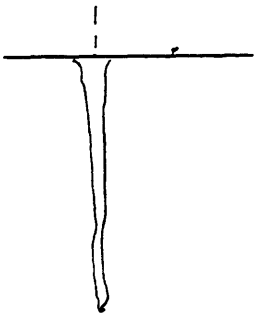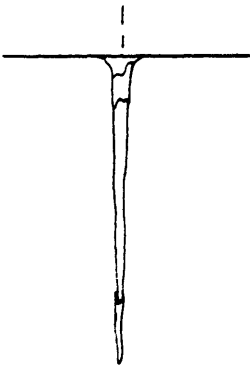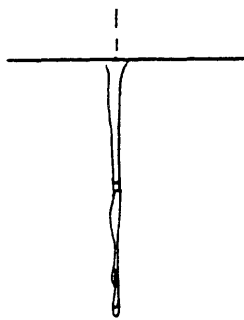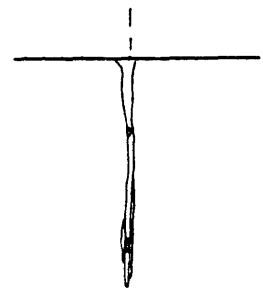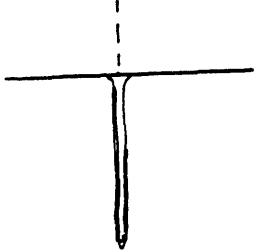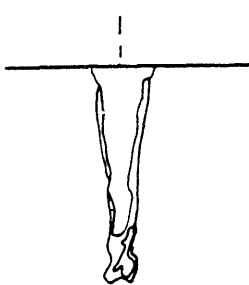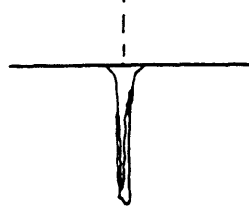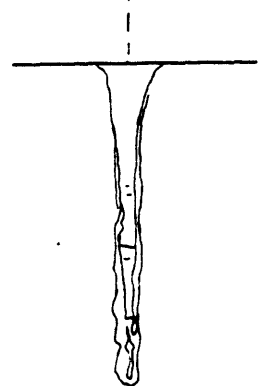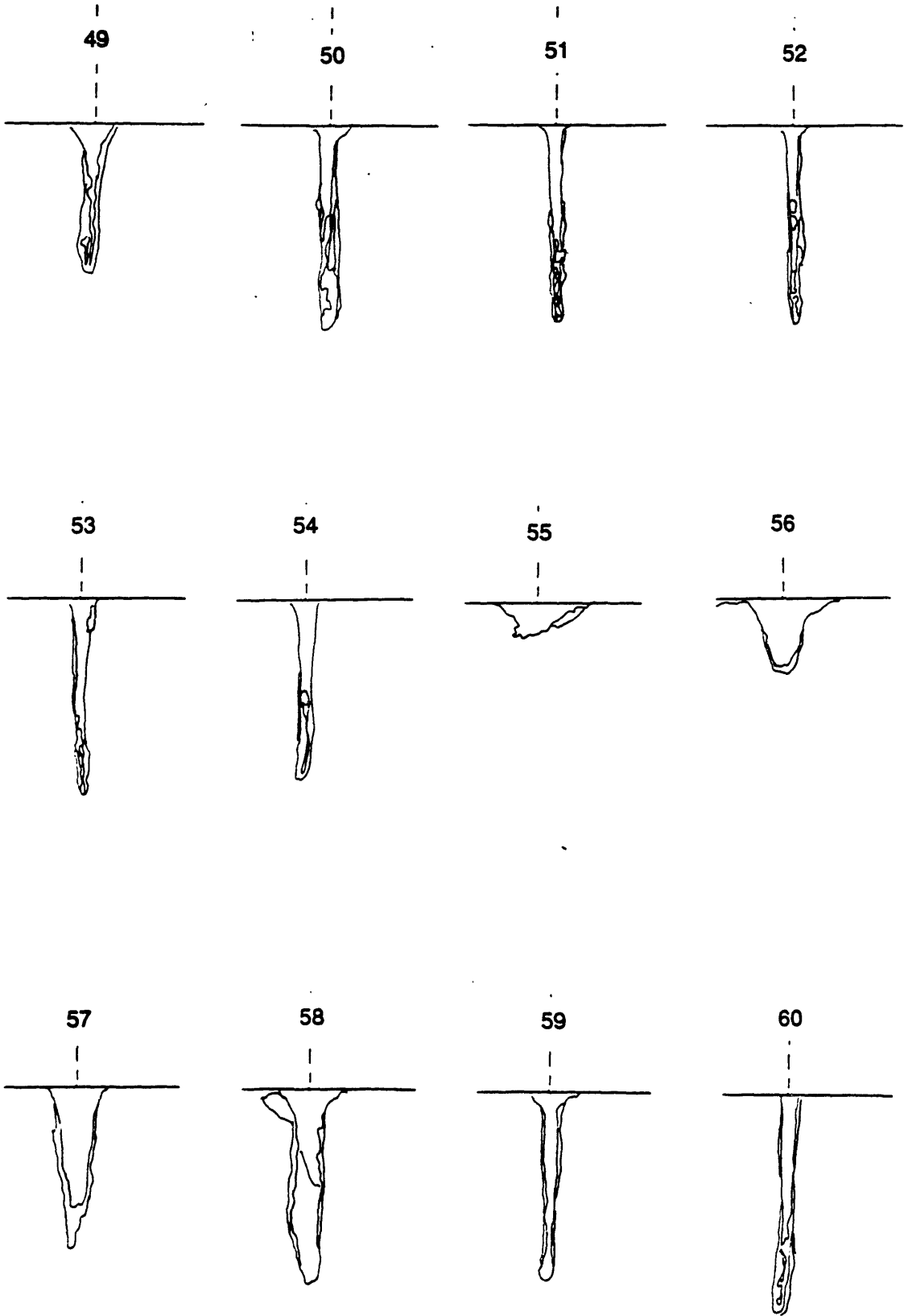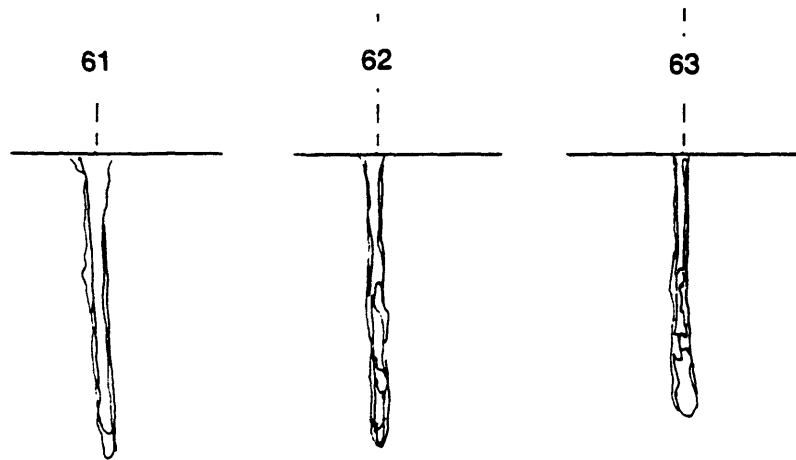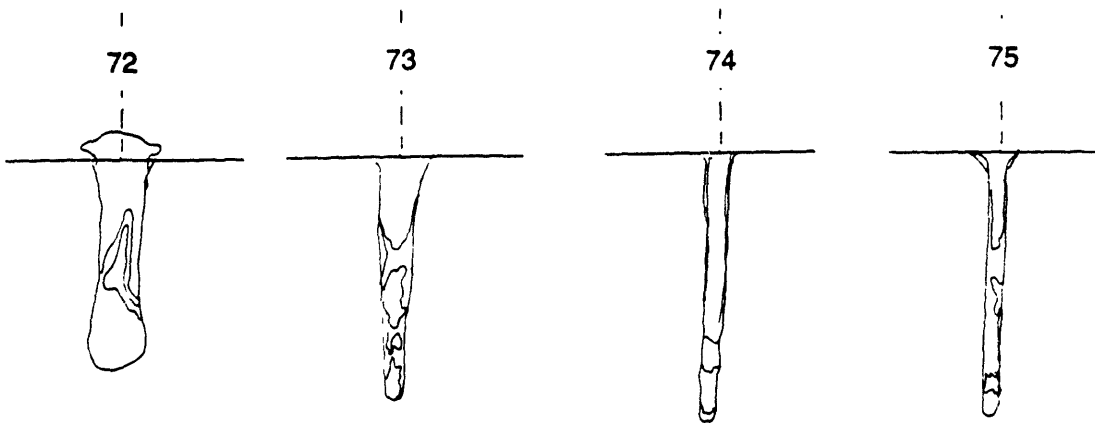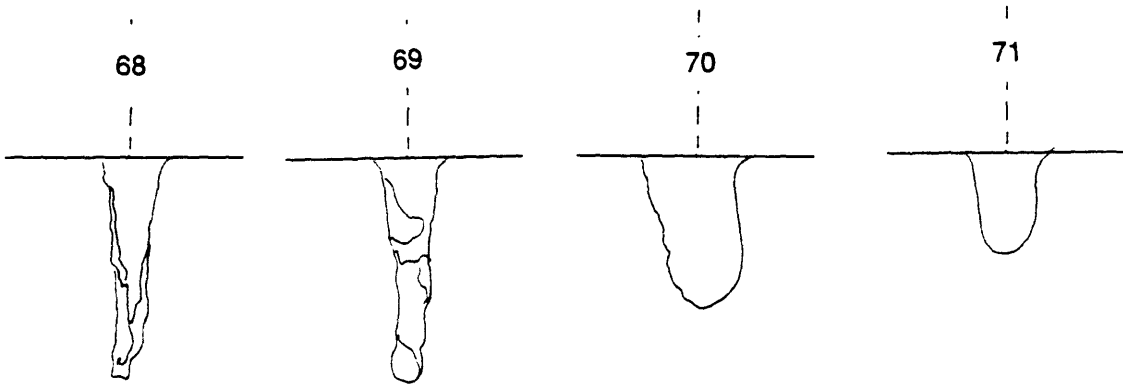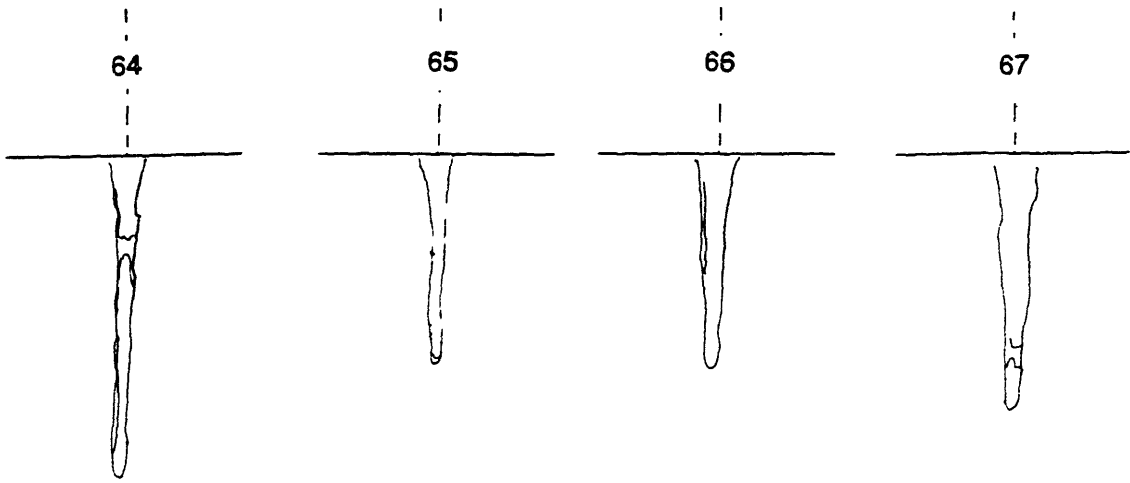
76 77 78 79

80 81 82 83

84 85 86

87

88

89

90

91

92

93

94

95

96

97

98
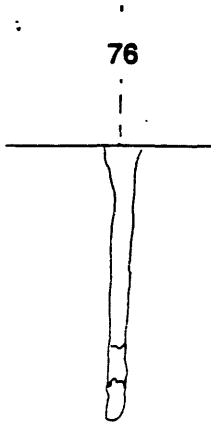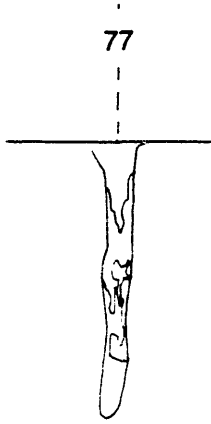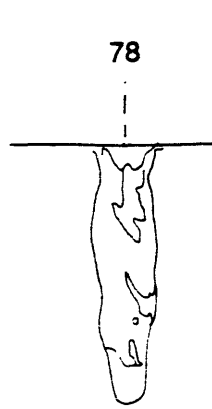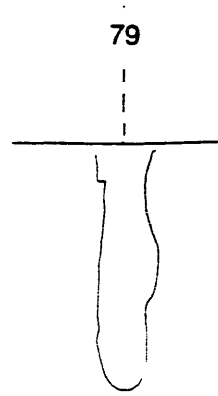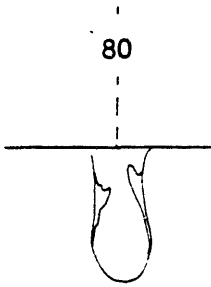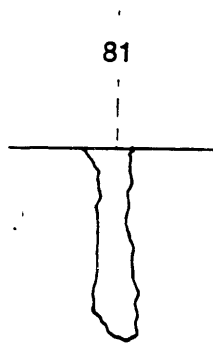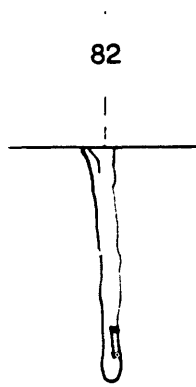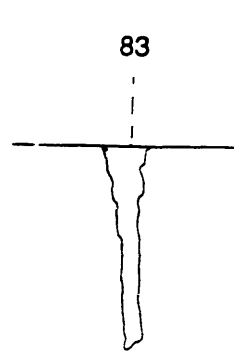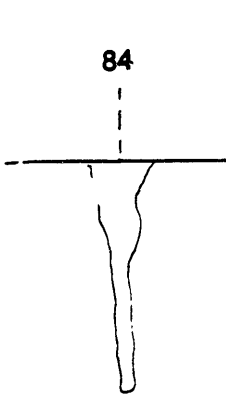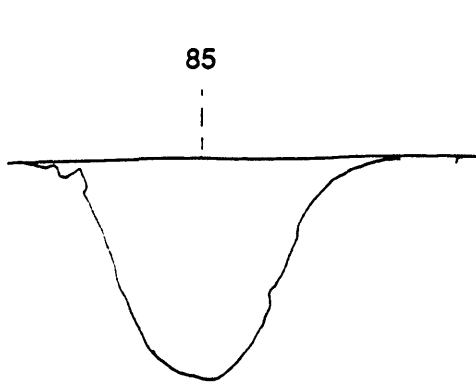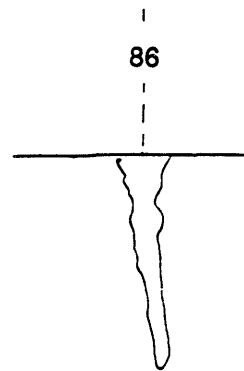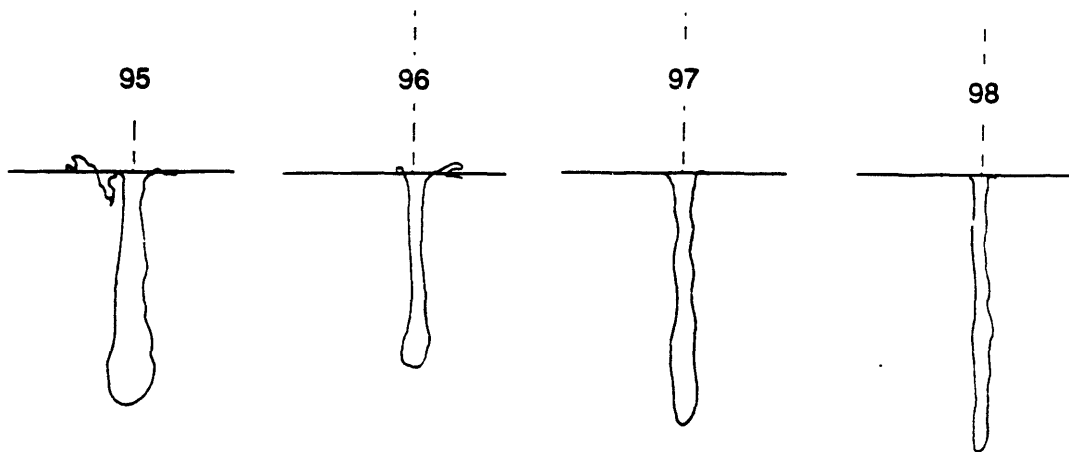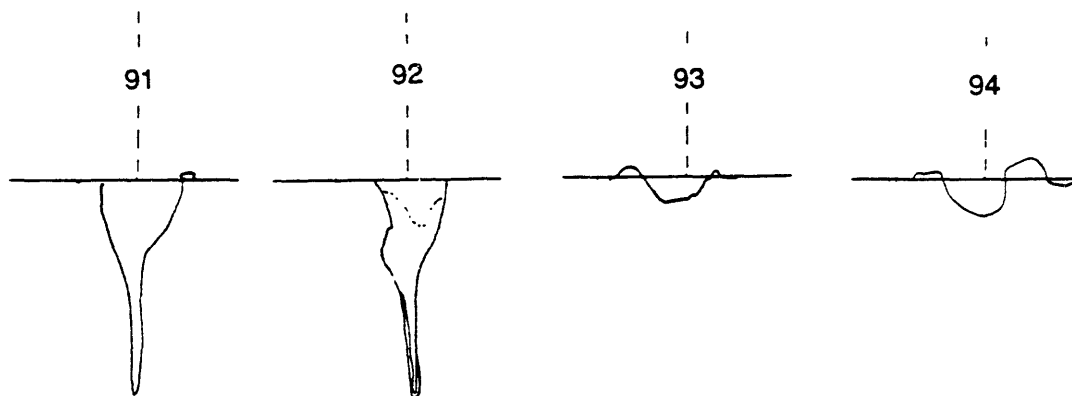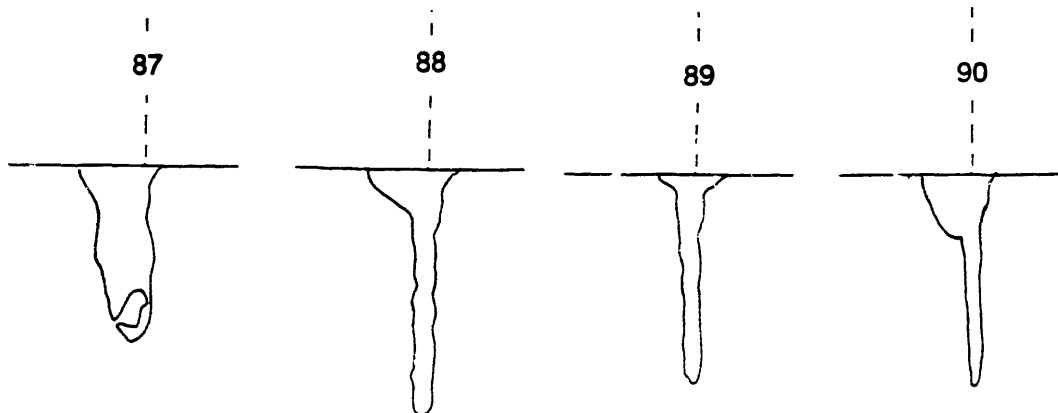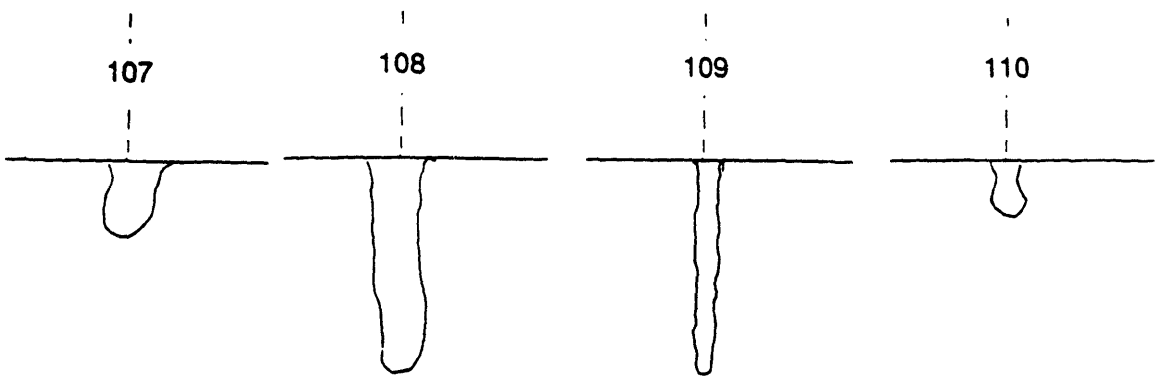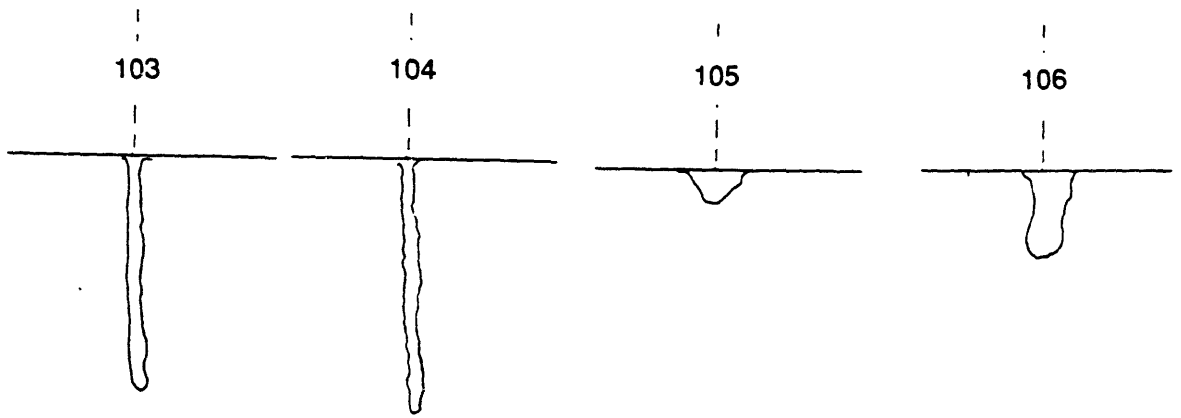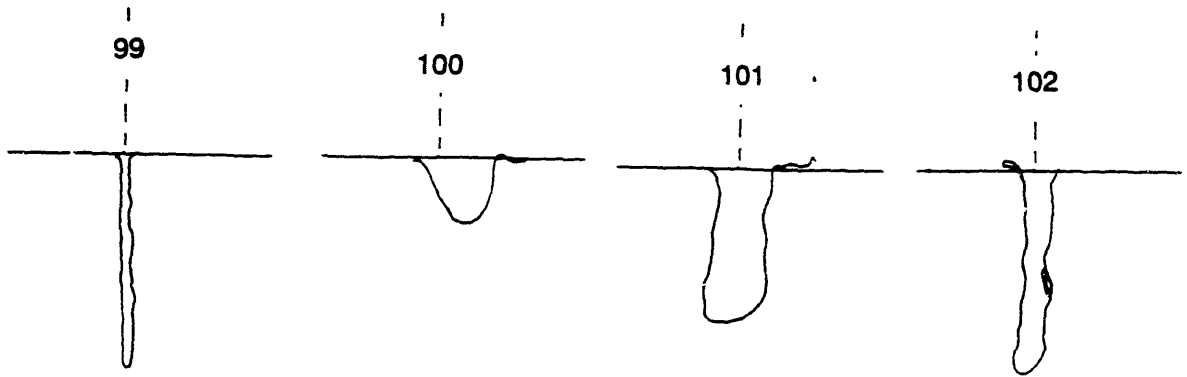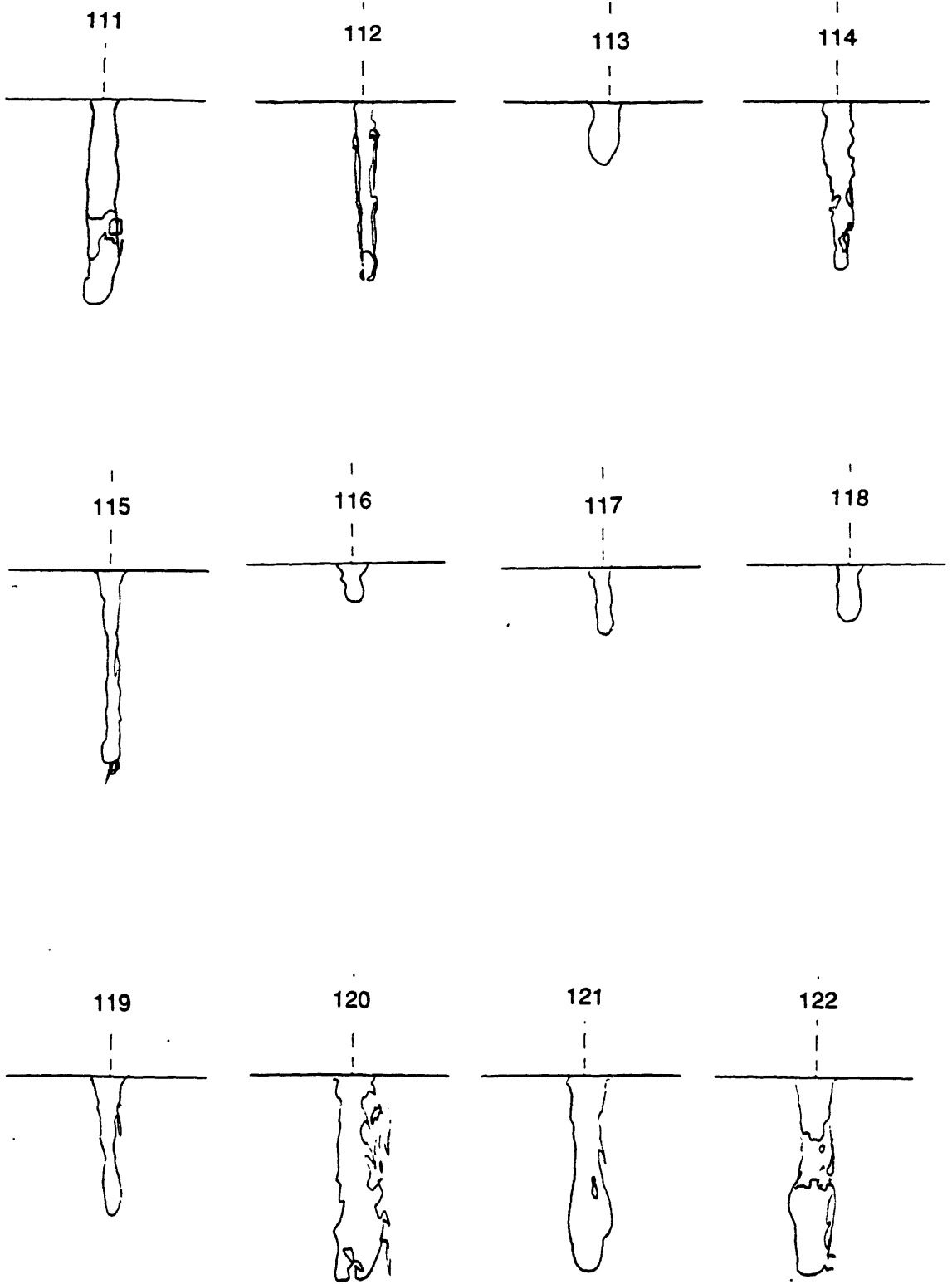
IV. . Finite Difference Program

```
C          THIS DOES A FINITE DIFFERENCE PROPAGATION PROBLEM
C          IN A HORIZONTAL PLATE WITH MOVING HEAT SOURCE.
           DIMENSION Y(53,27)
           DIMENSION Z(53,27)
C
           P = 0.0
           V = 0.0
c
           WRITE (6,9)
           WRITE (8,9)
9          FORMAT ( ' THIS PROGRAM CALCULATES HEAT CONDUCTION ',/,
       +            ' IN A HORIZONTAL PLATE ',/,
       +            ' WITH A MOVING HEAT SOURCE.',//,
       +            ' MAKE SURE ALL YOUR UNITS ARE CONSISTENT!! ',//
C
C          DEFAULT VALUES
C                                                              o
C          FOR AL2O3: UNITS ARE IN JOULES, CM, SEC, AND  K
C
C
           INFLAG=1
           PO = P
           VO = V
           TCO = 0.35
           PCPO = 4.2
           HLMO = 4150.
           HLVO = 3500.
           TAMBO = 275.
           TMO= 2325.
           TRO = 4300.
           TVO = 4300.
           NTO = 10
           NSO = 5
           DO = .0125
           RO = 2.*DO
           T1=300.
           T2=1000.
           T3=2000.
           T5=3000.
           JHLV = 1
           JTV = 1
           JP = 1
           JV = 1
           JTC = 1
           JPCP = 1
           JHLM = 1
           JTAMB = 1
```

```
        JTM= 1
        JTR = 1
        JNT = 1
        JNSO = 1
        JD = 1
        JR = 1.
C
        WRITE (6,10) TAMBO,DO,PCPO,RO,TCO,TMO,TRO,
     +               HLMO,HLVO,TVO,po,VO,NSO,NTO
10      FORMAT ( ' DEFAULT VALUES ARE FOR AL2O3 IN J,CM,SEC,K',/,
     +           ' TAMB=',F10.2,' d=',F10.6,' pCp=',F10.6,/,
     +           ' RADIUS OF CLOSED LOOP = ',F10.6,/,
     +           ' THERMAL COND.=',F10.6,'  TM =',F10.2,/,
     +           ' REML TEMP = ',F10.2,/,
     +           ' LATENT HEAT OF MELTING = ', F10.2,/,
     +           ' LATENT HEAT OF VAPORIZATION = ', F10.2,/,
     +           ' BOILING TEMP = ',F10.2,/,
     +           ' POWER = ', F10.2,
     +           ' VELOCITY = ', F10.4,/,
     +           I4,' ELEMENTS IN SPOT RADIUS',/,
     +           I4,' iterations/output',//)
        WRITE (6,28)
28      FORMAT ( ' ENTER LASER POWER,[ ENERGY/TIME ]: ',$)
        READ (5,42) P
        IF (P.EQ.0.0) JP=0
        IF (P.EQ.0.0) P=PO
        IF (JP.EQ.0) GOTO 52
        WRITE (8,51)  P
51      FORMAT ( ' POWER = ',F10.2,/)
52      WRITE (6,44)
44      FORMAT ( ' ENTER  TRANSLATION SPEED, [LGTH/TIME]: ',$)
        READ (5,45) V
        IF (V.EQ.0.0) JV=0
        IF (V.EQ.0.0) V=VO
        IF (JV.EQ.0) GOTO 73
        WRITE (8,53)  V
53      FORMAT ( ' SPEED = ',F10.6,/)
        READ (5,75) NP
73      WRITE (6,74)
74      FORMAT ( ' NUMBER OF elements in spot radius, [INTEGER]:
        READ (5,75) NSPOT
        IF (NSPOT.EQ.0) JNSO=0
        IF (NSPOT.EQ.0) NSPOT=NSO
        IF (JNSPOT.EQ.0) GOTO 77
        WRITE (8,76)  NSPOT
76      FORMAT ( ' SPOT IS ',I4,' ELEMENTS IN RADIUS',/)
77      WRITE (6,78)
78      FORMAT ( ' NUMBER OF iterations per output, [INTEGER]: ',
        READ (5,75) NT
```

```
        IF (NT.EQ.0) JNT=0
        IF (NT.EQ.0) NT=NTO
        IF (JNT.EQ.0) GOTO 54
        WRITE (8,79)   NT
79      FORMAT ( ' NUMBER OF iterations per output = ',I4,/)
54      WRITE (6,11)
11      FORMAT ( ' ENTER SPOT SIZE, d,[LGTH] : ',$)
        READ (5,49) D
        IF (D.EQ.0.0) JD=0
        IF (D.EQ.0.0) D=DO
        IF (JD.EQ.0) GOTO 81
        WRITE (8,57)   D
57      FORMAT ( ' SPOT SIZE = ',F10.6,/)
81      WRITE (6,12)
12      FORMAT ( ' ENTER RADIUS OF CLOSED LOOP, R G.T. D : ',$)
        READ (5,49) R
        IF (R.EQ.0.0) JR=0
        IF (R.EQ.0.0) R=RO
        IF (JR.EQ.0) GOTO 58
        WRITE (8,13)   R
13      FORMAT ( ' RADIUS OF LOOP = ',F10.6,/)
58      WRITE (6,27)
27      FORMAT ( ' ENTER HEAT CAP,[ ENERGY/VOL*TEMP ]: ',$)
        READ (5,49) PCP
        IF (PCP.EQ.0.0) JPCP=0
        IF (PCP.EQ.0.0) PCP=PCPO
        IF (JPCP.EQ.0) GOTO 60
        WRITE (8,59)   PCP
59      FORMAT ( ' HEAT CAP. = ',F10.6,/)
60      WRITE (6,30)
30      FORMAT ( ' ENTER AMBIENT TEMP: ',$)
        READ (5,42) TAMB
        IF (TAMB.EQ.0.0) JTAMB=0
        IF (TAMB.EQ.0.0) TAMB=TAMBO
        IF (JTAMB.EQ.0) GOTO 56
        WRITE (8,55)   TAMB
55      FORMAT ( ' TAMB = ',F10.2,/)
56      WRITE (6,31)
31      FORMAT ( ' ENTER MELTING TEMP: ',$)
        READ (5,42) TM
        IF (TM.EQ.0.0) JTM=0
        IF (TM.EQ.0.0) TM=TMO
        IF (JTM.EQ.0) GOTO 68
        WRITE (8,67) TM
67      FORMAT ( ' MELTING POINT = ',F10.2,/)
68      WRITE (6,32)
32      FORMAT ( ' ENTER KEYHOLE TEMP: ',$)
        READ (5,42) TR
        IF (TR.EQ.0.0) JTR=0
```

```
           IF (TR.EQ.0.0) TR=TRO
           IF (JTR.EQ.0) GOTO 64
           WRITE (8,63)   TR
63         FORMAT ( ' KEYHOLE TEMP = ',F10.2,/)
64         WRITE (6,15)
15         FORMAT ( ' ENTER BOILING TEMP: ',$)
           READ (5,42) TV
           IF (TV.EQ.0.0) JTV=0
           IF (TV.EQ.0.0) TV=TVO
           IF (JTV.EQ.0) GOTO 70
           WRITE (8,69) TV
69         FORMAT ( ' BOILING POINT = ',F10.2,/)
70         WRITE (6,33)
33         FORMAT ( ' ENTER LATENT HEAT OF MELTING/UNIT VOL.: ',$)
           READ (5,42) HLM
           IF (HLM.EQ.0.0) JHLM=0
           IF (HLM.EQ.0.0) HLM=HLMO
           IF (JHLM.EQ.0) GOTO 66
           WRITE (8,65)   HLM
65         FORMAT ( ' LATENT HEAT OF MELTING = ',F10.2,/)
66         WRITE (6,34)
34         FORMAT ( ' ENTER LATENT HEAT OF VAPORIZATION/UNIT VOL.: '
           READ (5,42) HLV
           IF (HLV.EQ.0.0) JHLV=0
           IF (HLV.EQ.0.0) HLV=HLVO
           IF (JHLV.EQ.0) GOTO 72
           WRITE (8,71)   HLV
71         FORMAT ( ' LATENT HEAT OF VAPORIZATION = ',F10.2,/)
72         WRITE (6,43)
43         FORMAT ( ' ENTER  THERMAL COND.,[ ENERGY/LGTH*TIME*TEMP ]
           READ (5,49) TC
           IF (TC.EQ.0.0) JTC=0
           IF (TC.EQ.0.0) TC=TCO
           IF (JTC.EQ.0) GOTO 48
           WRITE (8,61)   TC
61         FORMAT ( ' THERMAL CONDUCTIVITY = ',F10.6,/)
48         WRITE (6,47) TAMB,D,PCP,R,TC,TM,TV,TR,p,HLM,HLV,V,NSPOT,N
           IF (INFLAG.EQ.1) GOTO 80
           WRITE (8,47) TAMB,D,PCP,R,TC,TM,TV,TR,HLM,HLV,V,NSPOT,NT
47         FORMAT ( ' TAMB=',F10.2,' d=',F10.6,' pCp=',F10.6,/,
         +            ' RADIUS OF CLOSED LOOP = ',F10.6,/,
         +            ' THERMAL COND.=',F10.6,' TM =',F10.2,/,
         +            ' BOILING TEMP = ',F10.2,/,
         +            ' KEYHOLE TEMP = ',F10.2,/,
         +            ' LASER POWER = ',F10.2,/,
         +            ' LATENT HEAT M = ', F10.2,/,
         +            ' LATENT HEAT V = ', F10.2,/,
         +            ' SPEED = ',F10.4,/,
         +            I4,' ELEMENTS IN SPOT RADIUS',/,
```

```
     +                     I4,' iterations per output',//)
C
42         FORMAT (F10.2)
49         FORMAT (F10.6)
45         FORMAT (F10.4)
75         FORMAT (I4)
80         ALPHA = TC/PCP
C
           INFLAG=0
C
           NI = 51
           NJ = 26
C
C    NSPOT IS NUMBER OF ELEMENTS ACROSS SPOT RADIUS
C    NT IS NUMBER OF TIME STEPS TO ADVANCE DIST. H
C
           H = D/(2.*FLOAT(NSPOT))
           WRITE (8,86) H
86         FORMAT ( ' ELEMENT SIZE = ',F10.6,/)
C
           DO 84 I1 = 1, 53
           DO 82 J1 = 1, 27
              Y(I1,J1)=TAMB
              Z(I1,J1)=TAMB
82         CONTINUE
84         CONTINUE
           e = 2.718281828
           RSPOT = FLOAT(NSPOT)
           RINT = R/H
           QCUM = 0.
           PHI = 0.
           XSPOT = 25.
           itime = 0
150        continue
           QINTL = 0.0
           itime = itime+1
           iscal = 1
           jscal = 1
           if (itime.lt.NP) then
C
C          if (itime.lt.int(float(NP)/2.)) then
                  iscal = 5
                  jscal = 5
           endif
           letsgo = 0
           if (itime.eq.np-1) letsgo = 1
              IFLAG = 0
              TINT = INT(((FLOAT(ITIME))/FLOAT(NT)))
              TFIX = ((FLOAT(ITIME))/FLOAT(NT)) - TINT
```

```
      IF ((ABS(TFIX)).LT..001) IFLAG=1
ki = int (float(NI)/iscal)
kj = int (float(NJ)/jscal)
    DO 200 I = 1,ki+1
    DO 100 J = 1,kj+1
        I1=I-1
        J1=J-1
        ISPOT = 1
        iat = (il*iscal)+1
        jat = (j1*jscal)+1
        XI = FLOAT(Iat)
        YJ = FLOAT(Jat)
        RIJ = (((XI-XSPOT)**2.)+(YJ**2.))**0.5
        IF (RIJ.GT.(RSPOT+1.)) ISPOT=0
        FL = 1.0
        FB= 1.0
        FT = 1.0
        FR = 1.0
        IF (Jat.EQ.1) FB = 0.0
        IF (Iat.EQ.1) FL = 0.0
        IF (Jat.EQ.NJ) FT = 0.0
        IF (Iat.EQ.NI) FR = 0.0
        FCOMB = FB+FL+FT+FB
        FEDG = FB*FL*FT*FR
        FOUT = FL*FT*FR
        fcorn = (fb+fl)*(ft+fl)*(fb+fr)*(ft+fr)
        JM1 = jat-jscal
        JP1 = jat+jscal
        IM1 = iat-iscal
        IP1 = iat+iscal
        YDP = y(im1,jm1)+y(ip1,jp1)
        YDN = y(im1,jp1)+y(ip1,jm1)
        YTB = y(iat,jp1)+y(iat,jm1)
        YLR = y(im1,jat)+y(ip1,jat)
        if (fl.eq.0.0) then
                ylr = Y(IP1,JAT)+y(iat,jat)
              YDP = y(iat,jat)+y(ip1,jp1)
              YDN = y(iat,jat)+y(ip1,jm1)
        endif
        if (fr.eq.0.0) then
              ylr = Y(IM1,JAT)+Y(IAT,JAT)
              YDP = y(im1,jm1)+y(iat,jat)
              YDN = y(im1,jp1)+y(iat,jat)
        endif
        if (ft.eq.0.0) then
              ytb = Y(IAT,JM1)+y(iat,jat)
              YDP = y(im1,jm1)+y(iat,jat)
              YDN = y(iat,jat)+y(ip1,jm1)
        endif
```

```
                       if (fb.eq.0.0) then
                              ytb = y(iat,jp1)+Y(IAT,JAT)
                              YDP = y(im1,jat)+y(ip1,jp1)
                              YDN = y(im1,jp1)+y(ip1,jat)
                       endif
                       yavg = (YTB+YLR)/5.+ (YDP+YDN)/20.
                       if (fcorn.eq.0.) yavg = y(iat,jat)
                       DEL2Y = 4.*(YAVG-(Y(IAT,JAT)))
                       DTDX = Y(IAT,JAT)-Y(IM1,JAT)
                       if (fl.eq.0.0) DTDX = Y(IP1,JAT)-Y(Iat,Jat)
                       VDTDX = V*H*(DTDX)*float(iscal)/(4.*ALPHA)
                       Z(IAT,JAT) = yavg-vdtdx
                       IF (ISPOT.EQ.1) Z(IAT,JAT) = TR
                       IF (Z(IAT,JAT).LT.TAMB) Z(IAT,JAT)=TAMB
              if (iat.eq.1) z(iat,jat) =(y(ip1,jat)*2.)-y(ip1+iscal,jat
              if (iat.eq.52) z(iat,jat)=(y(im1,jat)*2.)-y(im1-iscal,jat
              DTDY = Y(IAT,JAT) - Y(IAT,JP1)
              IF(JAT.EQ.RSPOT) QINT=DTDY
              if (ispot.eq.1) qint=0.
              IF(IAT.GT.(XSPOT)) QINT=0.0
              QINTL = QINTL+QINT
              QINT = 0.0
C
C          DTDY is equal to -H times the temp. gradient in y-directi
C          QINTL is equal to 1/H times the integral 0 to infinity DT
C          QINTL times TC is the heat flux/ unit depth from one kerf
C
100           CONTINUE
200        CONTINUE
           qcum = 0.0
           if(letsgo.eq.1) then
                   iscal=1
                   jscal=1
           endif
           ki = int (float(NI)/iscal)+1
           kj = int (float(NJ)/jscal)+1
              DO 320 IK = 1,ki
              DO 310 JK = 1,kj
                   I2=IK-1
                   J2=JK-1
                   I3 = (I2*iscal)+1
                   j3 = (J2* jscal)+1
                   IF (Y(I3,J3).LT.TAMB) Y(I3,J3)=TAMB
                   if (letsgo.eq.0)goto 300
                   ispot=1
                   XI = FLOAT(I3)
                   YJ = FLOAT(J3)
                   RIJ = (((XI-XSPOT)**2.)+(YJ**2.))**0.5
                   IF (RIJ.GT.(RSPOT+1.)) ISPOT=0
```

```
                        ireg = (5*int((float(I3)-.9)/5.))+1
                        jreg = (5*int((float(J3)-.9)/5.))+1
                        wti = float(i3-ireg)/5.
                        wtj = float(j3-jreg)/5.
              yav1 = (y(ireg,jreg)*(1.-wti))+(y(ireg+5,jreg)*wti)
              yav2 = (y(ireg,jreg+5)*(1.-wti))+(y(ireg+5,jreg+5)*wti)
              Z(i3,j3) = (yav1 * (1-wtj)) + (yav2 * wtj)
              if (jreg.eq.0) Z(i3,j3) = yav2
              if(ispot.eq.1) Z(i3,j3) = TR
300                 Y(I3,J3) = Z(I3,J3)
                    IF (IFLAG.EQ.0)GOTO310
                    qij = pcp*(y(i3,j3)-tamb)*H*H*float(iscal*jscal)
                    qcum = qcum+qij
c                   IF (Y(I3,J3).LT.TAMB+25.) GOTO 310
c             WRITE (6,355) I3,J3, Y(I3,J3)
c355          FORMAT ( ' I = ',I2,' J = ',I2' T(X) = ',F10.2,/)
310           CONTINUE
320           CONTINUE
      TL = (TM+TV)/2
      DEPTH = P/((V*D*PCP*(TL-TAMB))+(2*QINTL*TC))
      ETA = (V*D*DEPTH*PCP*(TM-TAMB))/P
      if (iflag.eq.0) goto 401
      qdif =100.*abs(qcum-qcumo)/qcum
      write (6,400) qcum,itime,qdif,DEPTH,ETA
      write (8,400) qcum,itime,qdif
400   format(' heat content = ',F10.4, ' step ',i5,' change ',
     +        f5.1,' %',/,' DEPTH = ', F10.6, ' ETA = ',F6.4,/)
      qcumo = qcum
      qcum= 0.
         INFLAG = 0
             ITIM = INT(FLOAT(ITIME)/100.)
             TINT = (FLOAT(ITIME)/100.)-ITIM
401   if(TINT.GT.0.0001) goto 150
      IF(ITIME.LT.10) GOTO 150
      ki = int (float(NI)/iscal)+1
      do 500 i5=1,KI
      I4 = ((I5-1)*ISCAL)+1
      y1 = (y(i4,1))
      y2 = (y(i4,2))
      y3 = (y(i4,3))
      y4 = (y(i4,4))
      y5 = (y(i4,5))
      y6 = (y(i4,6))
      y7 = (y(i4,7))
      y8 = (y(i4,8))
      write (6,425) i4,y1,y2,y3,y4,y5,y6,y7,y8
      write (8,426) y1
425   format(i4,f8.1,f8.1,f8.1,f8.1,f8.1,f8.1,f8.1,f8.1,/)
426   format(f8.1)
```

```
500      continue
         goto 150
         END.
```